

# **Polymeric capsules for self-healing anticorrosion coatings**

## **Dissertation**

zur Erlangung des akademischen Grades

"doctor rerum naturalium"

(Dr. rer. nat.)

in der Wissenschaftsdisziplin "Physikalische Chemie"

eingereicht an der  
Mathematisch-Naturwissenschaftlichen Fakultät  
der Universität Potsdam

von  
Alexandra Latnikova

This work is licensed under a Creative Commons License:  
Attribution – Noncommercial – No Derivative Works 3.0 Germany  
To view a copy of this license visit  
<http://creativecommons.org/licenses/by-nc-nd/3.0/de/>

Published online at the  
Institutional Repository of the University of Potsdam:  
URL <http://opus.kobv.de/ubp/volltexte/2012/6043/>  
URN <urn:nbn:de:kobv:517-opus-60432>  
<http://nbn-resolving.de/urn:nbn:de:kobv:517-opus-60432>





# Table of contents

Abstract .....	3
List of commonly used abbreviations .....	6
Introduction .....	7
I. An introduction to self-healing coatings .....	8
I.1. Definition of self-healing materials .....	8
I.2. Self-healing coatings .....	8
I.3. Design Strategies .....	9
I.3.1. Mechanical property restoration .....	9
I.3.1.a Materials with intrinsic self-healing .....	9
I.3.1.b Capsule-based sealing approach .....	11
I.3.1.c Vascular self-healing materials .....	13
I.3.2. Active anticorrosion coatings .....	14
II. Corrosion and active anticorrosion coatings .....	16
II.1. Basics of corrosion .....	16
II.1.1. Corrosion of pure metals .....	17
II.1.2. Alloying and multiphase structures .....	19
II.1.3. Inherent reactivity of metals .....	20
II.1.4. How does the corrosion cell appear? .....	21
II.2. Corrosion inhibitors .....	23
II.3. Self-healing anticorrosion coatings based on Nano-/ Microcontainers loaded with corrosion Inhibitors .....	25
III. Motivation of this thesis .....	30
IV. Materials and Methods .....	33
IV.1. Materials .....	33
IV.2. Interfacial polymerization .....	33
IV.3. Methods for characterization .....	35
IV.3.1. Scanning electron microscopy (SEM) .....	35
IV.3.2. Transmission electron microscopy (TEM) .....	36
IV.3.3. Scanning vibrating electrode technique (SVET) .....	36
IV.3.4. Fourier transform infrared spectroscopy (FTIR) .....	37
IV.3.5. Dynamic light scattering (DLS) .....	37
IV.3.6. Contact angle measurements .....	37
IV.3.7. Electrochemical impedance spectroscopy .....	37
IV.3.8. Salt-spray chamber .....	39
IV.4. Swelling behavior of polymers .....	40
V. Control and prediction of capsule morphology .....	41
V.1. Possible morphology of capsules prepared via interfacial polymerization .....	41
V.2. Swelling of polymers .....	42
V.3. Synthesis of capsules with different morphology .....	42
V.3.1. The shape of capsules .....	45
V.3.2. Determination of capsule morphology .....	49
V.3.3. Synthesis of pure polymers .....	55
V.3.4. Swelling behavior of pure polymers and its correlation with capsule morphology .....	56
V.3.4. Flory theory vs. Hildebrand theory .....	64
V.3.5. Hildebrand and Hansen solubility parameters .....	65

V.3.6. HSP solubility spheres for PU, PUa and PA .....	66
VI. Practical application .....	69
VI.1. PU capsules loaded with water- repelling agent .....	69
VI.1.1. Active material .....	69
VI.1.2. The choice of the components .....	71
VI.1.3. Synthesis of capsules .....	74
VI.1.4. Characterization .....	75
VI.1.5 Performance of the coating modified with PU-AlkSi capsules .....	78
VI.1.6 Conclusions .....	83
VI.2. PA capsules loaded with cerium diethylhexyl phosphate .....	83
VI.2.1. Synthesis of the cerium phosphate salt derivation .....	84
VI.2.2. The choice of the components .....	84
VI.2.3. Encapsulation of cerium diethylhexyl phosphate .....	86
VI.2.4. Characterization .....	86
VI.2.5. Performance of the coating modified with PA-Ce capsules .....	87
V.2.6. Conclusions .....	90
VI.3. PU capsules loaded with biocide .....	90
VI.3.1. Active material .....	91
VI.3.2. The coise of the components .....	92
VI.3.3. Synthesis of PU-biocide capsules .....	94
VI.3.4. Characterization .....	94
VI.3.5. Conclusions .....	98
VI.4. Compact and core-shell capsules loaded with MeBT .....	99
VI.4.1. Characterization .....	100
VI.4.2. Performance of the coating modified with PUa-MeBT capsules .....	101
VI.4.3. Conclusions .....	103
VI.5. When in-situ loading is not possible .....	104
VI.5.1. Exploitation of swelling for capsule loading .....	105
VI.5.2. Calculation of loading .....	106
VI.5.3. PUa capsules loaded with BTA and 8HQ .....	107
VI.5.3.a Characterization .....	107
VI.5.3.b Performance of the coating modified with PUa-BTA and PUa-8-HQ capsules .....	108
VI.5.3.c Conclusions .....	110
VII. Conclusions .....	112
VIII. References .....	114

## Abstract

The present work is devoted to establishing of a new generation of self-healing anti-corrosion coatings for protection of metals. The concept of self-healing anticorrosion coatings is based on the combination of the passive part, represented by the matrix of conventional coating, and the active part, represented by micron-sized capsules loaded with corrosion inhibitor.

Polymers were chosen as the class of compounds most suitable for the capsule preparation. The morphology of capsules made of crosslinked polymers, however, was found to be dependent on the nature of the encapsulated liquid. Therefore, a systematic analysis of the morphology of capsules consisting of a crosslinked polymer and a solvent was performed. Three classes of polymers such as polyurethane, polyurea and polyamide were chosen. Capsules made of these polymers and eight solvents of different polarity were synthesized via interfacial polymerization. It was shown that the morphology of the resulting capsules is specific for every polymer-solvent pair. Formation of capsules with three general types of morphology, such as core-shell, compact and multicompartment, was demonstrated by means of Scanning Electron Microscopy. Compact morphology was assumed to be a result of the specific polymer-solvent interactions and be analogues to the process of swelling. In order to verify the hypothesis, pure polyurethane, polyurea and polyamide were synthesized; their swelling behavior in the solvents used as the encapsulated material was investigated. It was shown that the swelling behavior of the polymers in most cases correlates with the capsules morphology. Different morphologies (compact, core-shell and multicompartment) were therefore attributed to the specific polymer-solvent interactions and discussed in terms of “good” and “poor” solvent. Capsules with core-shell morphology are formed when the encapsulated liquid is a “poor” solvent for the chosen polymer while compact morphologies are formed when the solvent is “good”. Multicompartment morphology is explained by the formation of infinite networks or gelation of crosslinked polymers. If gelation occurs after the phase separation in the system is achieved, core-shell morphology is present. If gelation of the polymer occurs far before crosslinking is accomplished, further condensation of the polymer due to the crosslinking may lead to the formation of porous or multicompartment morphologies. It was concluded that in general, the morphology of capsules consisting of certain polymer-solvent pairs can be predicted on the basis of polymer-solvent behavior. In some cases, the swelling behavior and morphology may not match. The reasons for that are discussed in detail in the thesis.

The discussed approach is only capable of predicting capsule morphology for certain polymer-solvent pairs. In practice, the design of the capsules assumes the trial of a great number of polymer-solvent combinations; more complex systems consisting of three, four or even more components are often used. Evaluation of the swelling behavior of each component pair of such systems becomes unreasonable. Therefore, exploitation of the solubility parameter approach was found to be more useful. The latter allows consideration of the properties of each single component instead of the pair of components. In such a manner, the Hansen Solubility Parameter (HSP) approach was used for further analysis. Solubility spheres were constructed for polyurethane, polyurea and polyamide. For this a three-dimensional graph is plotted with dispersion, polar and hydrogen bonding components of solubility parameter, obtained from literature, as the orthogonal axes. The HSP of the solvents are used as the coordinates for the points on the HSP graph. Then a sphere with a certain radius is located on a graph, and the “good” solvents would be located inside the sphere, while the “poor” ones are located outside. Both the location of the sphere center and the sphere radius should be fitted according to the information on polymer swelling behavior in a number of solvents. According to the existing correlation between the capsule morphology and swelling behavior of polymers, the solvents located inside the solubility sphere of a polymer give capsules with compact morphologies. The solvents located outside the solubility sphere of the solvent give either core-shell or multicompartment capsules in combination with the chosen polymer.

Once the solubility sphere of a polymer is found, the solubility/swelling behavior is approximated to all possible substances. HSP theory allows therefore prediction of polymer solubility/swelling behavior and consequently the capsule morphology for any given substance with known HSP parameters on the basis of limited data. The latter makes the theory so attractive for application in chemistry and technology, since the choice of the system components is usually performed on the basis of a large number of different parameters that should mutually match. Even slight change of the technology sometimes leads to the necessity to find the analogue of this or that solvent in a sense of solvency but carrying different chemistry. Usage of the HSP approach in this case is indispensable.

In the second part of the work examples of the HSP application for the fabrication of capsules with on-demand-morphology are presented. Capsules with compact or core-shell morphology containing corrosion inhibitors were synthesized.

Thus, alkoxysilanes possessing long hydrophobic tail, combining passivating and water-repelling properties, were encapsulated in polyurethane shell. The mechanism of action of the active material required core-shell morphology of the capsules.

The new hybrid corrosion inhibitor, cerium diethylhexyl phosphate, was encapsulated in polyamide shells in order to facilitate the dispersion of the substance and improve its adhesion to the coating matrix.

The encapsulation of commercially available antifouling agents in polyurethane shells was carried out in order to control its release behavior and colloidal stability.

Capsules with compact morphology made of polyurea containing the liquid corrosion inhibitor 2-methyl benzothiazole were synthesized in order to improve the colloidal stability of the substance. Capsules with compact morphology allow slower release of the liquid encapsulated material compared to the core-shell ones.

If the “in-situ” encapsulation is not possible due to the reaction of the oil-soluble monomer with the encapsulated material, a solution was proposed: loading of the capsules should be performed after monomer deactivation due to the accomplishment of the polymerization reaction. Capsules of desired morphologies should be preformed followed by the loading step. In this way, compact polyurea capsules containing the highly effective but chemically active corrosion inhibitors 8-hydroxyquinoline and benzotriazole were fabricated.

All the resulting capsules were successfully introduced into model coatings. The efficiency of the resulting “smart” self-healing anticorrosion coatings on steel and aluminium alloy of the AA-2024 series was evaluated using characterization techniques such as Scanning Vibrating Electron Spectroscopy, Electrochemical Impedance Spectroscopy and salt-spray chamber tests.

## List of commonly used abbreviations

8-HQ	8-hydroxyquinoline	<b>Methods</b>	
BTA	benzotriazole	SEM	Scanning Electron Microscopy
CHn	cyclohexanone	EDX	Energy-Dispersive X-ray Spectroscopy
DABCO	1,4-diazabicyclo[2.2.2]octane	TEM	Transmission Electron Microscopy
DBuPh	dibutyl phosphate	SVET	Scanning Vibrating Electrode Technique
DCOIT	4,5-Dichloro-2-octyl-2H-isothiazol-3-one	FTIR	Fourier Transform Infrared Spectroscopy
DEPh	diethyl phthalate	DLS	Dynamic Light Scattering
DETA	diethylenetriamine	EIS	Electrochemical Impedance Spectroscopy
DEtHePh	bis(2-ethylhexyl) phosphate		
DMPH	dimethyl phthalate		
DOPh	dioctyl phthalate	<b>Parameters</b>	
EDA	ethylenediamine	$\delta$	Hildebrand Solubility Parameter
EtOH	ethanol	$\delta_D$	dispersion component of HSP
HSP	Hansen Solubility Parameter	$\delta_P$	polar component of HSP
isocyanate prepolymer	poly[(phenyl isocyanate)-co-formaldehyde]	$\delta_H$	hydrogen-bonding component of HSP
MeBT	2-methyl benzothiazole	c	cohesive energy density
MeOH	methanol	C	concentration in wt. %
PA	polyamide	I	current
PDI	polydispersity index	L	loading efficiency
PEI	poly(ethylemeimine)	R	the gas constant
PU	polyurethane	T	absolute temperature
PUa	polyurea	U	voltage signal
PVA	poly(vinyl alcohol)	$U_m$	molar internal energy
TEPA	tetraethylenepentamine	$V_m$	molar volume
TETA	triethylenetetramine	Z	complex impedance
THF	tetrahydrofuran	$\alpha$	the swelling ability of polymer
TMODS	Trimethoxy(octadecyl)silane	$\Delta H_m$	molar vaporization enthalpy
TMOS	trimethoxy(octyl)silane	$\phi$	phase shift
TPhCl	terephthaloyl chloride	$\omega$	angular frequency

## Introduction

The present work is devoted to establishing of a new generation of self-healing anti-corrosion coatings for protection of metals. The concept of self-healing anticorrosion coatings is based on the combination of the passive part, usually represented by the matrix of a conventional coating, and the active part represented by micron-sized capsules loaded with corrosion inhibitor. As long as the integrity of the coating stays intact, corrosion inhibitor remains entrapped inside the capsules. If the integrity of the coating is damaged due to the mechanical impact (e.g. crack or scratch), capsules introduced into the coating break and release the active encapsulated material. Further, leakage or diffusion of encapsulated material to the metal surface occurs and results in passivation of active corrosion centers on the metal surface and suppression of the corrosion process in the local spot of a coating damage. In contrast to self-healing, damage of the conventional coating integrity, leads to the fast attack of the bare metal substrate by the corrosive species and fast corrosion of the metal as a result. The concept of self-healing was already shown to provide sufficient enhancement of protective performance and durability of the coatings. Up-to-date the concept was mostly applied for comparatively thin sol-gel coatings; the implementation of corrosion inhibitors was done in a form of nano-sized inorganic carriers. The majority of the market nowadays is, however, represented by polymeric coatings with a thickness of 20  $\mu\text{m}$  and higher. Implementation of nano-sized carriers in the case of thick polymeric coating would not be effective due to the small size of the carriers. Therefore, new carriers of appropriate size (for high efficiency) and surface chemistry (for good adhesion to the polymeric matrix of the conventional coatings) should be developed.

# **I. An introduction to self-healing coatings**

## **I.1. Definition of self-healing materials**

All materials that surround us have designed properties in order to fulfill their function in a desired application. As we entered into the twenty-first century, search for advanced materials with crack avoidance and long-term durability gained high priority. The challenge for material scientists is therefore to develop new technologies that can produce novel materials with increased safety, extended lifetime and no aftercare or a much smaller amount of repairing costs. Since creation of a perfect material, which would never break, does not seem to be possible, the idea of self-healing becomes one of the main streams.

In <sup>1</sup> self-healing is defined as “the ability of a material to heal (recover/repair) damages automatically and autonomously, that is, without any external intervention”. This definition does not specify to which extent and which properties of the material are restored/repared. In the broadest sense self-healing materials can be distinguished as materials which are able to autonomously (partially) restore (some of) their properties in such a manner that they can serve longer as compared to similar materials without self-healing capabilities. If after rupture at least one property of the material is restored at least partially without any external intervention, one can speak about self-healing capabilities of the material.

## **I.2. Self-healing coatings**

The main function of coatings is the protection of an underlying substrate against an environment-induced corrosion attack. Application of organic coatings is the most common and cost effective method of improving the corrosion protection and, thereby, the durability of metallic structures. A wide range of engineering structures, from cars to aircrafts, from chemical factories to household equipment, is effectively protected by coatings. The main role of an organic polymer coating in corrosion protection is to provide a dense barrier against corrosive species. Along with these barrier properties, resistance to a flow of charge, electronic and ionic, is also important since corrosion processes involve the transfer of charge. However, defects appear in organic protective coatings during exploitation of the coated structures opening a direct access for corrosive agents to the metallic surface. The corrosion processes develop faster after disruption of the protective barrier. Therefore, an active ”self-healing” of defects in coatings is necessary in order to provide long-term protection.

In the case of corrosion protective coatings the term self-healing can be interpreted in two different ways <sup>1,2</sup>.

From one perspective only full recovery of the coatings functionality including mechanical and barrier properties of the coating is considered as “healing”.

From another perspective the main function of anticorrosion coatings is the protection of an underlying metallic substrate against an environment-induced corrosion attack. Thus, it is not obligatory to recuperate all the properties of the film in this case. The hindering of the corrosion activity in the defect by the coating itself employing any mechanisms can be already considered as self-healing, because the corrosion protective system recovers its main function, namely, the corrosion protection, after being damaged. Both self-healing concepts will be described in the next section.

### **I.3. Design Strategies**

Self-healing coatings can be divided into two big groups:

- coatings that restore their mechanical or barrier properties
- coatings that act actively against corrosion of the underlying substrate by reducing the corrosion activity in the defect

The first approach is analogous to self-healing in bulk, while the second one can be applied for protection of surfaces. This difference in the approaches to self-healing coatings will be used as the basis for the classification of possible designs of self-healing coatings.

#### **I.3.1. Mechanical property restoration**

##### **I.3.1.a Materials with intrinsic self-healing**

Intrinsic self-healing materials (**fig.1**) achieve repair through inherent reversibility of bonding of the polymer matrix. Intrinsic self-healing can be accomplished through thermally reversible reactions, hydrogen bonding, ionic coupling, a dispersed moldable thermoplastic phase, or molecular diffusion <sup>3</sup>. Self-healing materials based on reversible reactions include components that can be reversibly transformed from the monomeric state to the cross-linked polymeric state through the addition of external energy <sup>4</sup>. Generally, a damaged polymer is subjected to heat or intense photo illumination, triggering enhanced mobility in the damage region, bond reformation, and polymer remending. The most widely used reaction scheme for remendable self-healing materials is based on the Diels-Alder (DA) and retro-Diels-Alder (rDA) reactions <sup>4-9</sup> (**Fig. 1.1**).

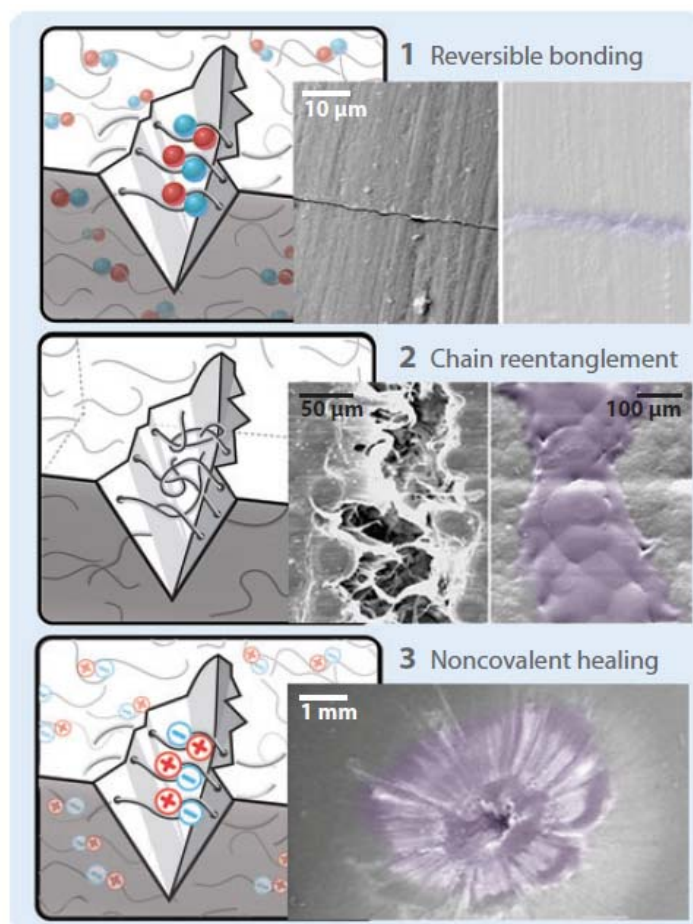


**Fig.1.** Intrinsic self-healing materials **(1)** Reversible bonding schemes make use of the reversible nature of certain chemical reactions **(2)** Chain entanglement approaches utilize the mobility at crack faces to entangle chains that span the crack surfaces **(3)** Noncovalent self-healing systems rely on reversible hydrogen bonding or ionic clustering which manifests as reversible cross-links in polymers. Reprinted from <sup>3</sup>.

Self-healing in thermoset materials can be achieved by incorporating a meltable thermoplastic additive. Self-healing occurs by the melting and subsequent redispersion of the thermoplastic material into the crack plane, filling the crack and mechanically interlocking with the surrounding matrix material <sup>10,11</sup>(**Fig.1.2**).

Ionomeric copolymers are a class of materials with ionic segments that can form clusters acting as reversible crosslinks <sup>12-16</sup> (**Fig. 1.3**). These clusters can be activated by external stimuli such as temperature or ultraviolet irradiation. Because the formation of the clusters is reversible, multiple local healing events are possible. Further details on the historical development and synthesis of many of these polymers are available in an excellent review by Bergman & Wudl <sup>4</sup>.

An intrinsic self-healing in all forms has one groundbreaking advantage: disruption and restoration at the local spot can be done multiple times. However, reversible linkages are not very strong, therefore the number of healing acts is limited, and the efficiency of each successive healing event decreases. Furthermore the intrinsic healing often needs an additional trigger, like elevated temperature or strong irradiation; in absence of a trigger healing does not happen. Another weak point of the concept is that two parts of polymer to be glued together need to come close. In bulk systems the main type of damage is cracking, therefore the distance between surfaces can not become too big. On the surface the damage very often happens in the form of a scratch, when part of the polymeric material is removed. In the case of scratch this approach probably would not be very effective.

### I.3.1.b Capsule-based sealing approach

The idea of a coating suitable for the reflow-healing of defects is an analogue of the bulk capsule-based self-healing approach<sup>17</sup>.

The repair of the coating is achieved through microencapsulated polymerizable agents incorporated into the coating matrix. If the coating is damaged, the microcapsules rupture, leaching the film forming components in the immediate vicinity of the damage (**fig.2**). The fluid flows over exposed areas of the surface and fills any defects or cracks in the coating renewing the protective barrier.

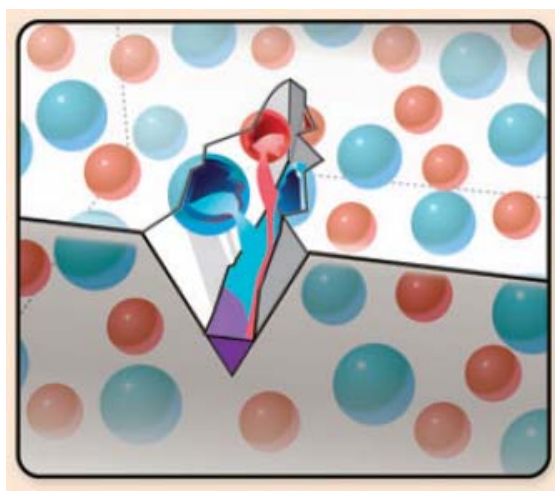


**Fig. 2** Illustration of the capsule-based sealing approach. Reprinted from<sup>3</sup>

Kumar et al.<sup>18</sup> examined commercially synthesized urea-formaldehyde shell microcapsules containing various healing agents to determine their effectiveness when incorporated into paint primer coatings for steel surfaces. Under appropriate preparation conditions, several encapsulated compounds, including camphor and tung oil, exhibited a more than twofold reduction in damage as compared with microcapsule-free controls.

Suryanarayana et al.<sup>19</sup> examined the effectiveness of linseed oil-filled microcapsules in epoxy coatings on steel parts. Rapid film

formation of the oil released from microcapsules in a coating crack plane was observed optically as the oil was activated by exposure to ambient environment. Scratched samples showed no visual evidence of corrosion after exposure to salt spray.

Sauvant-Moynot et al.<sup>20</sup> employed epoxide-based film-forming particles embedded in epoxy-amine coatings to protect steel surfaces under cathodic protection. The healing components were designed to activate only under potential within a film defect; the barrier formation was confirmed by electrical impedance spectroscopic measurements of films before and after in situ scratching in 0.17 M NaCl aqueous solution. The healed films exhibited temperature-dependent recovery of barrier behavior, but impedance values never reached those of undamaged films.

Cho et al.<sup>21</sup> examined multicomponent polydimethylsiloxane-based healing systems in epoxy and vinyl ester coatings on steel. In both a phase-separated version and polyurethane capsule-based systems, polydimethylsiloxane, a catalyst, and an adhesion promoter were distributed in the matrix so that the components would combine and cross-link within the scratch damage. Scribed samples were allowed to heal over 24 h and then examined by optical and scanning electron microscopy and by electrical conduction measurements while immersed in 1 M NaCl aqueous solution. In the phase-separated system, a reduction in conductance of more than an order of magnitude was obtained for healed samples versus scratched controls.

The idea of reflow-healing of protective coatings has already found its commercial realization. Nissan has recently announced the “Scratch Guard Coat” painting system, which contains a newly developed highly elastic resin providing reflow in artificial scratches. The new coating system is effective for about three years and is five times more resistant to abrasions caused by a car-washing machine compared with a conventional clear paint.

Examples of self-healing coatings presented above are based on the polymerization of a healing agent in the defects recovering the barrier properties of the protective coatings. However, the barrier properties of a damaged coating can also be recuperated by a simple blocking of the defects with insoluble precipitates. Sugama et al.<sup>22</sup> developed a poly(phenylenesulfide) (PPS) self-sealing coating containing calcium aluminate (CA) fillers dispersed in the coating matrix. The decalcification–hydration reactions of the  $\text{CaO} \cdot \text{Al}_2\text{O}_3$  and  $\text{CaO} \cdot 2\text{Al}_2\text{O}_3$  fillers, surrounding the defect, lead to a fast growth of boehmite crystals in the cracks. The block-like boehmite crystals fill the cracks effectively sealing them after 24 h. Incorporation of capsules of micrometer size into off the shelf coatings allows to create hybrid systems with healing capabilities without changing much the design circle of the coating, which is a salient advantage of these systems. Nevertheless this approach has

disadvantages too. The main of them is the limited amount of material available inside the capsules which leads to the situation when only relatively small damage volumes can be effectively healed. Another limitation is that the volume of sealant at every local spot is limited and can not be refilled, therefore only singular local healing is possible.

An attempt to overcome this problem was done by using elongated capsules or tubes. Using capsules with larger aspect ratios leads to sufficient increase of the healable damage volumes. Further extension of this idea leads directly to the vascular self-healing materials approach.

### I.3.1.c Vascular self-healing materials

Vascular self-healing materials (**fig.3**) sequester the healing agent in a network in the form of capillaries or hollow channels, which may be interconnected one-dimensionally (1D), two-dimensionally (2D), or three-dimensionally (3D), until damage triggers self-healing.

After the vasculature is damaged and the first delivery of healing agent occurs, the network may be refilled by an external source or from an undamaged but connected region of the vasculature. This refilling action allows for multiple local healing events, but causes other problems like requirement of refilling of the vascular network or appearance of a new defect due to the transport of part of the material from one spot to another.

The literature discusses two main techniques used for the assembly of network structures for self-healing. The first is to employ hollow glass fibers (HGFs) as channels (60  $\mu\text{m}$  in

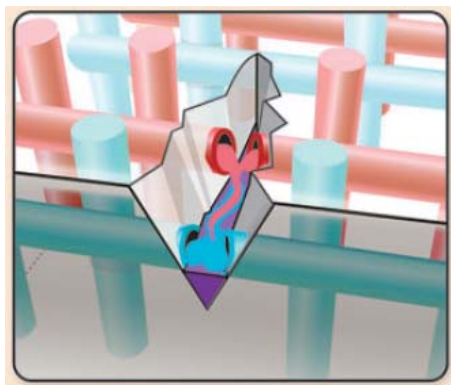


**Fig.3.** Illustration of vascular-based self-healing approach. Reprinted from <sup>3</sup>

diameter), filled with the appropriate healing agent (**fig.3**). HGFs, easily made using existing glass fiber drawing techniques, are compatible with many standard polymer matrices, and are inert to many popular self-healing agents such as two-part epoxy resin systems and cyanoacrylates. Although self-healing networks made from these fibers meet a number of advantages in terms of practicality, they are restricted to 1D connectivity. For vascular

systems, additional connectivity adds numerous performance advantages. Any location in the network has multiple connection points, leading to increased reliability with regard to channel blockages and a larger accessible reservoir for the healing agent(s) <sup>23</sup>. Multiple connections

between channels also allow for easier refilling of the network after depletion. The technique used most commonly for higher-connectivity vascular fabrication is direct-ink writing of a fugitive ink scaffold and subsequent infiltration with an uncured polymeric precursor. The scaffold is subsequently removed after solidification, leaving a hollow channel network embedded with the polymer matrix. This technique provides control over network shape and connectivity but restricts the choice of matrix to materials that can be formed around the fugitive scaffold.

As opposed to capsule-based systems, for vascular materials the healing agents are introduced after the network has been integrated into the matrix. Thus, some properties that determine the choice of healing agents are surface wettability, chemical reactivity, and viscosity. High viscosities and/or unfavorable wetting properties prevent efficient filling of the network, whereas chemical incompatibility endangers long-term stability of the system. These properties also affect vascular network design, especially the channel diameter, because viscosity and wettability affect the release and transport of the healing agent(s). Importantly, for vascular healing systems, access to a large reservoir of healing agent(s) and the ability to replenish the network enable repeated healing of multiple damage events.

### **I.3.2. Active anticorrosion coatings**

The examples reviewed above concern coatings that are able to heal or seal the defects blocking them mechanically via polymerization or precipitation mechanisms. The physical integrity of the coating is partially recovered due to these processes. However, the main function of the protective coatings is to protect the underlying substrate from corrosion processes. The partial blocking of the pathways for corrosive species very often does not mean an effective hindering of the corrosion. Corrosion processes can occur even under the coating in place of the healed or sealed defect if the electrolyte has already penetrated into the substrate when the defect was induced. Being entrapped under the coating, corrosive species can be extremely aggressive, leading to the fast corrosion of the underlying substrate. Therefore, the coating integrity restoration should be combined with active corrosion protection, which would lead to deactivation of corrosion species.

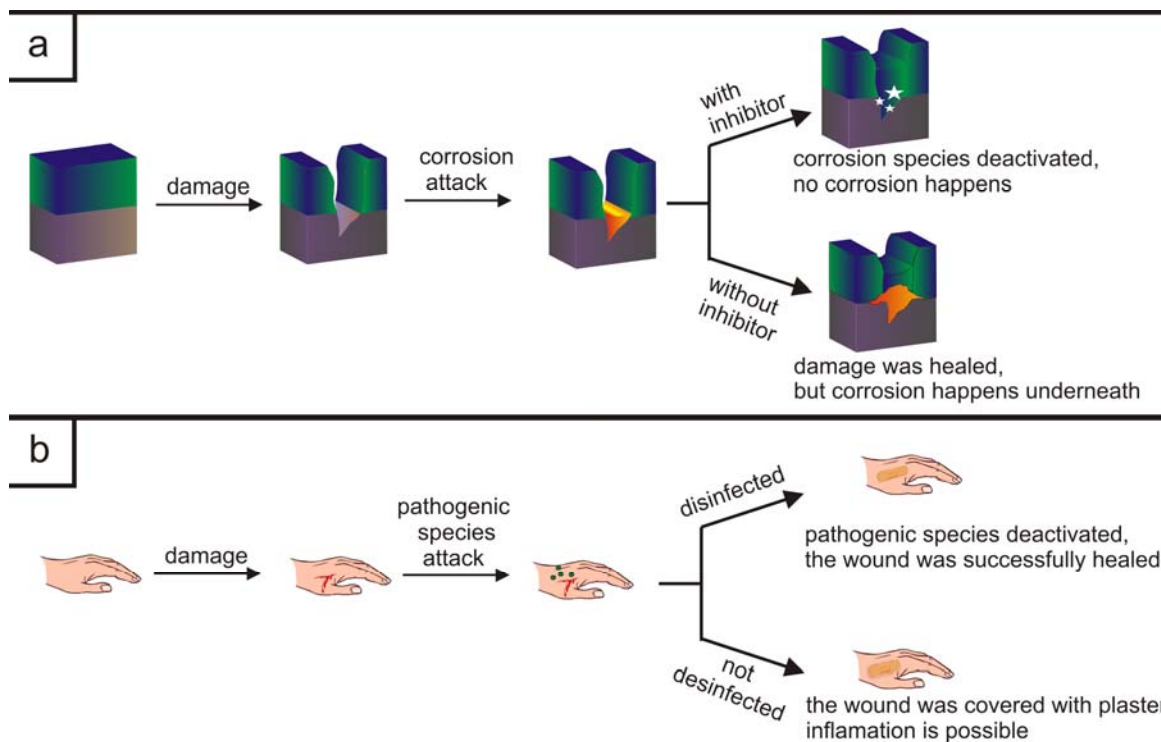


**Fig.4.** Bio-mimetic concept of self-healing process based on the combination of integrity restoration with application of corrosion inhibitors. **(a)** healing of a scratch on the surface of a metal substrate covered with anticorrosion coating. **(b)** healing of a wound

In this sense the whole process can be compared with wound healing (**fig.4**). When an injury happens the open wound should be first disinfected and only then covered with the plaster. Application of the plaster without disinfection can lead to the development of an inflammation. In the same way the surface of the metal substrate should be first “disinfected” by the introduction of corrosion inhibitors and only thereafter covered with the new layer of coating. Otherwise an “inflammation” in the form of underlying corrosion can happen.

The active corrosion protection is realized by application of corrosion inhibitors, which being effective at comparatively low concentrations can sufficiently slow down or totally suppress corrosion. Before discussion of corrosion inhibitors and possible ways to introduce them into a coating the fundamentals of corrosion should be discussed.

## II. Corrosion and active anticorrosion coatings

### II.1. Basics of corrosion

Corrosion is a natural process. Just like water flows to the lowest level, all natural processes tend toward the lowest possible energy states. Thus, for example, iron has a natural tendency to combine with other chemical elements to return to its lowest energy states. In order to return to lower energy states, iron frequently combines with oxygen and water, both of which are present in most natural environments, to form hydrated iron oxides (rust), similar in chemical composition to the original iron ore (**fig.5**).

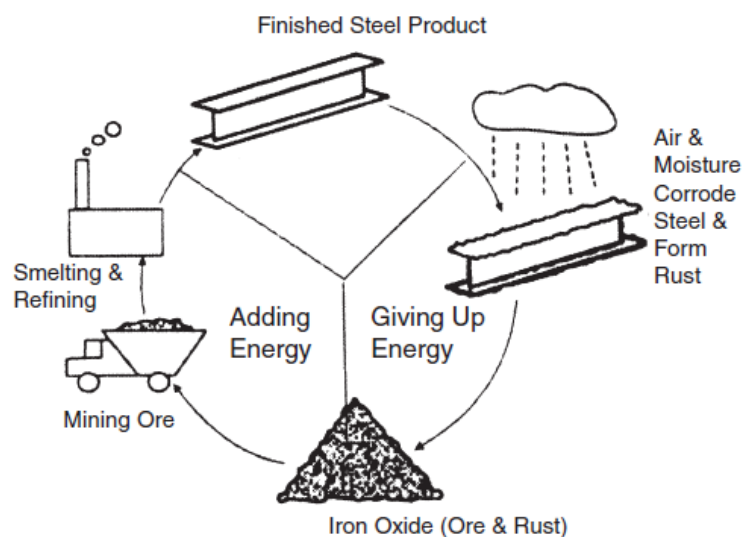


**Fig.5.** The corrosion life cycle of a steel product. Reprinted from <sup>24</sup>

The word “corrode” is derived from the Latin *corrodere*, which means “to gnaw to pieces.” Corrosion can be defined as a chemical or electrochemical reaction between a material, usually a metal, and its environment that produces a deterioration of the material and its properties. Corrosion occurs in several widely differing forms.

Classification is usually based on one of three factors:

**Nature of the corrodent:** Corrosion can be classified as “wet” or “dry.” A liquid or moisture is necessary for the former, and dry corrosion usually involves reaction with high-temperature gases.

**Mechanism of corrosion:** This involves either electrochemical or direct chemical reactions.

**Appearance of the corroded metal:** Corrosion is either uniform and the metal corrodes at the same rate over the entire surface, or it is localized, in which case only small areas are affected. Common forms of wet (or aqueous) corrosion are illustrated in **fig.6**.

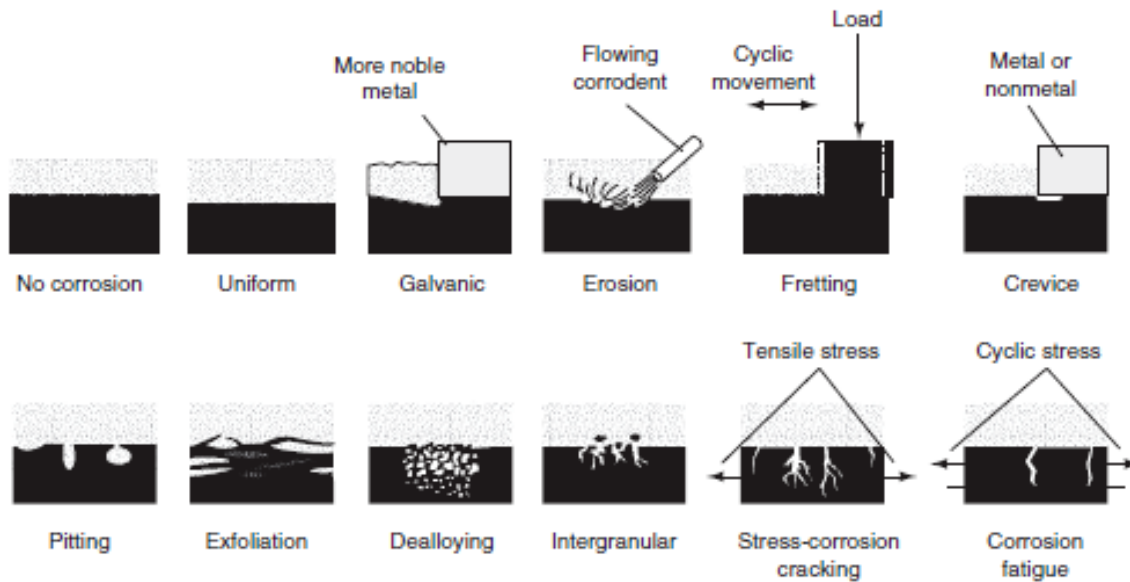


**Fig.6.** Illustration of the common forms of corrosion. Reprinted from <sup>24</sup>

### II.1.1. Corrosion of pure metals

When a metal is immersed in an environment, it can behave in one of three ways. These behaviors are shown schematically in **fig.7**, which represents a metal partially immersed in a corrosive environment.

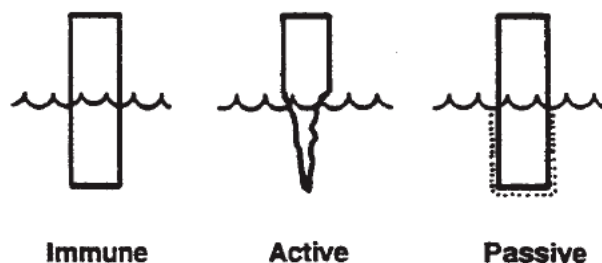


**Fig.7.** Three behaviors of a metal in an environment. Reprinted from <sup>24</sup>

### **- Immune Behavior:**

For a combination of metal and environment resulting in immune behavior, there is no reaction of the metal, and there is no corrosion of the metal. Immune behavior results from the metal being thermodynamically stable in the particular environment; that is, the corrosion reaction does not occur spontaneously. Metals known to display this immunity are called noble metals and include, for example, gold, silver, and platinum.

### **- Active Behavior:**

When active behavior is observed, the metal dissolves in solution and forms soluble corrosion products. Corrosion or dissolution of the metal continues in this solution because the corrosion products do not prevent subsequent corrosion. Active corrosion is characterized by high weight loss of the metal.

### **- Passive Behavior:**

With the third behavior, the metal corrodes but a state of passive behavior is observed. Upon immersion of the metal into the solution there is a corrosion reaction, however, an insoluble, protective corrosion-product film is formed. This thin protective film, also referred to as a passivating film, slows the reaction rate to very low levels. Some examples of metals that exhibit passivity are aluminium, chromium, titanium, nickel, and alloys containing these metals (most notably stainless steels). Passivation is generally associated with oxidizing media. Being very thin, the films are often fragile and not very stable, therefore an additional protection of the metal is needed.

From a corrosion control standpoint, the desired behavior is either immune or passive, while the behavior to be avoided is active. Immune behavior is the most desirable, because corrosion protection does not depend on the stability of protective films. Most engineering alloys, however, are passive in their applications and thus depend on the integrity of the passive film. If the environment becomes more corrosive, passive metals tend to exhibit localized forms of corrosion, that is, pitting, stress-corrosion cracking, and crevice corrosion.

Only the most noble metals exhibit immune behavior in a wide variety of corrosive environments. In most cases, it is not practical to use these materials for engineering applications because of their high costs and strength limitations. While the behavior exhibited by metals is dependent on the corrosive environment to which the metals are exposed, some characteristic behaviors are exhibited. As mentioned above, gold, platinum, and silver typically exhibit noble or immune behavior. Sodium, potassium, and magnesium are active in nearly all aqueous environments. Titanium and tantalum are passive in a wide range of

aqueous environments. Aluminium and zinc are very reactive metals and often exhibit active behavior; however, in some important environments they form stable, passive films.

### II.1.2. Alloying and multiphase structures

Two or more metals mixed together give rise to alloys with a wide variety of properties not available using single metals. The microstructure resulting from the mixture of two elements can vary widely. In some cases the two elements are completely soluble and a homogeneous, single-phase structure is established. Other metals have only limited solubility, and mixtures of these elements result in multiphase materials.

Many alloys are not homogeneous, pure materials, but rather are a mixture of multiple phases. Each phase has its characteristic crystallographic structure and chemical composition. When these structures are then exposed to a corrosive environment, it is not surprising that the different phases exhibit different corrosion behaviors. This leads to preferential corrosion of specific constituents of the alloy.

The effects of inclusions at the metal surface are shown schematically in **Fig. 8**.

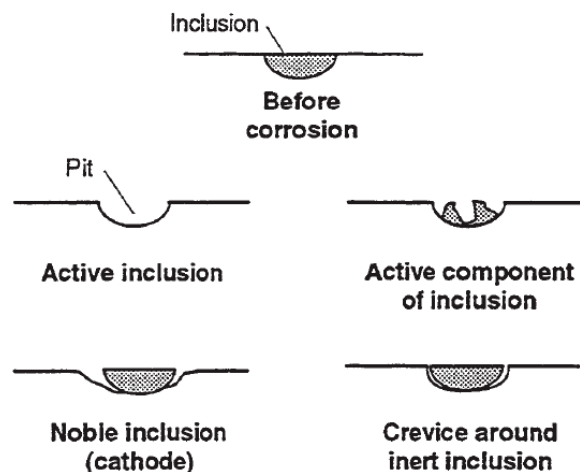


**Fig.8.** The effects of inclusions at the metal surface on the corrosion behavior of alloy. Reprinted from <sup>24</sup>

The uppermost figure represents an inclusion exposed at the metal surface prior to corrosion, and the lower diagrams indicate the behavior under different conditions. If the inclusion is active, that is, less corrosion resistant than the matrix, the inclusion dissolves, leaving a hole or pit in the metal surface. If only portions of the inclusion are active, the exposed portions are

attacked, leaving the other portions intact. If the inclusion is noble (more corrosion resistant than the matrix), then accelerated attack of the matrix adjacent to the noble inclusion can be observed. In other cases where the inclusion is inert to attack, accelerated corrosion adjacent to the inclusion can still occur because of a crevice generated between the inclusion and the matrix.

### II.1.3. Inherent reactivity of metals

Each metal has its own inherent tendency to corrode. Some metals, such as gold and silver, are very noble and have little tendency to corrode. They can be found in the earth in their natural, metallic state. At the other end of the scale of inherent reactivity are metals such as sodium. Sodium is an extremely active metal and corrodes spontaneously in the presence of water with a violent reaction. Iron is a moderately active metal and corrodes spontaneously in the presence of water. The variety of metals available provides a wide range of inherent reactivities, from very noble materials, which do not corrode, to extremely active metals, which corrode quite readily.

Electrode	Electrode reaction	$E^0/V$
Au Gold	$Au^{3+} + 3e^- \rightleftharpoons Au$	+1.43
Ag Silver	$Ag^+ + e^- \rightleftharpoons Ag$	+0.80
Cu Copper	$Cu^{2+} + 2e^- \rightleftharpoons Cu$	+0.34
H Hydrogen	$H^+ + e^- \rightleftharpoons H$	0
Pb Lead	$Pb^{2+} + 2e^- \rightleftharpoons Pb$	-0.13
Sn Tin	$Sn^{2+} + 2e^- \rightleftharpoons Sn$	-0.14
Ni Nickel	$Ni^{2+} + 2e^- \rightleftharpoons Ni$	-0.25
Cd Cadmium	$Cd^{2+} + 2e^- \rightleftharpoons Cd$	-0.40
Fe Iron	$Fe^{2+} + 2e^- \rightleftharpoons Fe$	-0.44
Zn Zinc	$Zn^{2+} + 2e^- \rightleftharpoons Zn$	-0.76
Ti Titanium	$Ti^{2+} + 2e^- \rightleftharpoons Ti$	-1.63
Al Aluminium	$Al^{3+} + 3e^- \rightleftharpoons Al$	-1.66
Mg Magnesium	$Mg^{2+} + 2e^- \rightleftharpoons Mg$	-2.37
Na Sodium	$Na^+ + e^- \rightleftharpoons Na$	-2.71
K Potassium	$K^+ + e^- \rightleftharpoons K$	-2.93
Li Lithium	$Li^+ + e^- \rightleftharpoons Li$	-3.05

**Fig.9.** The electrochemical series of metals

**The electromotive force (emf) series** is a formal ranking of metals with respect to their inherent reactivity (**Fig.9**). The most noble metals are at the top of the emf series and have the highest positive standard electrode potentials. The most active metals are at the bottom of the series and have the most negative standard electrode potentials. The potential for hydrogen is taken as zero by internationally accepted convention. All other standard electrode potentials are referred to this standard hydrogen electrode (SHE) value. Thus, the potential of gold is +1.50 V with respect to the hydrogen reference potential, and the potential of iron is -0.44 V with respect to the hydrogen reference potential. The standard electrode potential values are determined for a special set of conditions; that

is, the standard potential is defined for the equilibrium of the pure metal with its own ions at a specified concentration in the absence of other ions.

Thermodynamic calculations yield the standard electrode potential for each metal under these specified conditions. The emf series is most valuable for indicating the inherent reactivity of metals. Most corrosion applications, however, deal with mixed reactions, that is, not only the reaction of the metal with its own ions but also the reaction of the metal with other species in the solution, such as hydrogen ions or oxygen. Nevertheless, the emf series is quite useful. Metals at the bottom or most negative end of the emf series are active metals. They have less corrosion resistance than metals higher in the series. In order of increasing corrosion resistance, magnesium is the least corrosion resistant, followed by zinc, iron, and copper, with gold being the most corrosion resistant. A metal with a more negative potential in the series will replace from solution the ions of a metal more positive in the series. Iron immersed in a solution containing copper ions, for example, a solution of copper sulfate, reduces the copper ions. The iron goes into solution as iron ions, and the copper ions deposit out of solution onto metal as metallic copper.

The emf series provides an indication of the potential difference between two metals coupled together in a galvanic corrosion cell. If two dissimilar metals are connected, the potential difference is a driving force for corrosion reactions. The farther apart the metals are in the emf series, the greater the driving force for corrosion. For example, copper and aluminium form a strong cell with a potential difference of greater than 2 V. In the case of aluminium-copper alloy aluminium will act as anode, while copper would be cathode (see **fig.10**). Magnesium and aluminium form a weaker cell with a potential difference of less than 1 V. The metal that is more positive in the series is the cathode, and the metal that is more negative in the series is the anode. The anodic member of the galvanic couple is severely corroded. Other considerations for the galvanic corrosion couple exist, and the emf series should only be used as a general indication.

#### **II.1.4. How does the corrosion cell appear?**

Speaking in terms of electrochemistry, depending on its activity an inclusion will demonstrate either cathodic or anodic behavior. The surface of metal can be then represented by the corrosion cell. Analysis of electrochemical characteristics of corrosion cell parts is in many cases useful for the prediction of the corrosion behavior of an alloy.

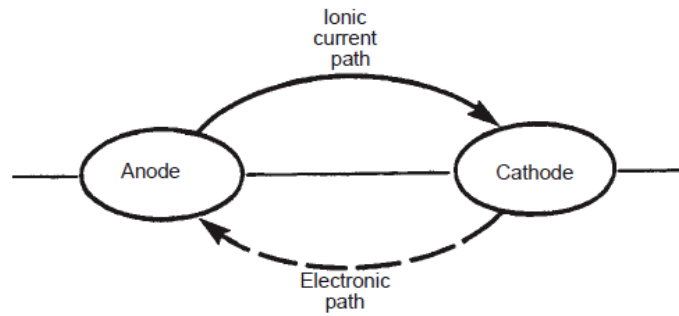


**Fig.10.** Scheme of a corrosion cell.. Arrows show the direction of the current flow. Reprinted from <sup>24</sup>

The scheme of a corrosion cell is shown in **fig.10**, where an anode and a cathode on the metal surface in contact with the solution are indicated.

The anode and cathode are connected through the solution by an ionic current path, and they are connected through the metal by an electronic path. An electrochemical reaction involves the transfer of electrons from one species to another, causing direct current flow through the corrosion cell. The anode is generally where the corrosion occurs. This is the location on the metal surface where metal atoms go into solution as metal ions and weight loss occurs. The direct current passing through the corrosion cell enters the solution at the anode. The reactions at the anode are referred to as anodic and are oxidation reactions; that is, electrons are generated.

At the cathode, no corrosion occurs and no weight loss occurs. There are, however, reactions occurring that are just as important to the operation of the corrosion cell as the anodic reactions. These reactions are cathodic or reduction reactions; that is, electrons are consumed. The direct current flowing through the corrosion cell enters the metal at the cathode. The direct current of the corrosion cell moves through the solution by an ionic path. Current flows from the anode to the cathode by the movement of charged ions in the solution.

The movement of charged ions in the solution is the vehicle for current flow through this portion of the corrosion cell. The direct current moves through the metal of the corrosion cell by an electronic path. Electrons generated at the anode by oxidation reactions move to the cathode, where they are consumed by reduction reactions.

The dissolution (oxidation) at the anode can only proceed as quickly as the electrons generated there can be consumed by reduction reactions at the cathode. If the reduction reactions are slowed down, this in turn slows down the dissolution reactions. Resistance in the ionic current path or the electronic current path will slow down the corrosion reaction by limiting the amount of current that can flow through the corrosion cell.

If the anodes are removed or made inactive, no metal dissolution can occur. An effective control of corrosion is realized by the elimination of the cathodes. If there is no place for the consumption of electrons generated by the corrosion reaction, there is no corrosion reaction. Elimination of the ionic current path also stops corrosion. There is no means for the transfer of electrical charge from the anodes to the cathodes. A practical example of this form of corrosion control is the removal of the electrolyte in a corrosion cell. This can be done by completely drying the metal surface. If there is no moisture on the surface for the formation of an ionic current path, there is no corrosion. Similarly, elimination of the electronic path between anode and cathode also eliminates corrosion. If we are dealing with galvanic corrosion, a corrosion reaction driven by two dissimilar metals, the galvanic corrosion can be eliminated by electrically isolating the two metals. There then is no path by which electrons can be transferred from the anode to the cathode, and the two metals do not affect each other.

## **II.2. Corrosion inhibitors**

An inhibitor is a chemical substance or combination of substances that, when present in the environment, prevents or reduces corrosion without significant reaction with the components of the environment. The application of inhibitors must be viewed with caution by the user because inhibitors may afford excellent protection for one metal in a specific system but can aggravate corrosion for other metals in the same system.

Inhibitors can be organic or inorganic compounds, and they are usually dissolved in aqueous environments. Some of the most effective inorganic inhibitors are chromates, nitrites, silicates, carbonates, phosphates, and arsenates. It should be noted that environmental concerns have significantly impacted the use of chromates. The organic inhibitors are many and include amines, heterocyclic nitrogen compounds, sulfur compounds (such as thioethers, thioalcohols, thioamides, thiourea), some natural compounds (such as proteins), and mixtures of two or more compounds.

### **Types of Inhibitors**

Various types of inhibitors commonly used include the following: anodic, cathodic, ohmic, precipitation and in some cases biocides.

The protection afforded by these inhibitor types can result from several different mechanisms: the presence of adsorbed films, the formation of bulky precipitates, or the promotion of passivity of the metal to be protected.

**Anodic (passivating) inhibitors** function by selectively covering anodic sites on the metal surface. Anodic inhibitors are considered dangerous, because insufficient concentrations can

lead to accelerated localized attack at unprotected sites. Generally, a critical concentration for anodic inhibitors must be maintained. Typical anodic inhibitors include oxidizing chemicals, such as chromates<sup>25-29</sup>, , and nitrates<sup>30,31</sup>, and nonoxidizing chemicals, such as nitrites<sup>26-28</sup>, phosphates<sup>29,31-33</sup>, tungstates<sup>31,34-36</sup>, and molybdates<sup>29,34-36</sup>. The nonoxidizing chemicals require the presence of other oxidizing species (e.g., oxygen) in the environment to be effective.

**Cathodic inhibitors** reduce corrosion by slowing the reduction reaction rate of the electrochemical corrosion cell. This is done by blocking the cathodic sites by precipitation. For example, calcium, magnesium, and zinc ions will precipitate hydroxides on cathodic sites as the local environment becomes more alkaline due to the reduction reaction at these sites. As the pH increases, hydroxide precipitation occurs. Cathodic inhibitors are effective when they slow down the cathodic reaction rate. Arsenic, bismuth, and antimony<sup>37</sup>, which are referred to as cathodic poisons, reduce the hydrogen reduction reaction rate and, thus, lower the overall corrosion rate. Other cathodic inhibitors remove reducible species from the environment. Lanthanide ions are well known to form insoluble hydroxides which enable them to be used as cathodic inhibitors<sup>38</sup>. Benzotriazole being able to form insoluble complexes with copper<sup>39</sup> works as a cathodic inhibitor for aluminium alloys.

**Ohmic inhibitors**, also referred to as general filming inhibitors, reduce the corrosion rate by decreasing the mobility of ionic species between anodes and cathodes on the corroding metal surface. By decreasing the ionic conductivity of the solution, the corrosion rate is reduced. These inhibitors function through strong adsorption to the metal surface. Ohmic inhibitors include amines, which are cationic, and sulfonates, which are anionic.

**Precipitation inhibitors** promote the formation of a bulky precipitation film over the entire surface. Silicates<sup>29,40</sup> and phosphates<sup>40</sup> are examples of such inhibitors.

**Biocides** Microbiologically induced corrosion (MIC) is a recognized problem in the gas and oil industries, pipelines, municipal sewage treatment systems, the pulp and paper industry, and a variety of industrial applications. Sulfate-reducing bacteria can convert noncorrosive water into highly corrosive water through the conversion of sulfate to sulfide<sup>41</sup>. Other microorganisms can also increase the corrosivity of the environment by a variety of mechanisms.

### II.3. Self-healing anticorrosion coatings based on Nano-/ Microcontainers loaded with corrosion Inhibitors

In order to provide active protection of the substrate, corrosion inhibitors should be introduced into a coating. The easiest way to introduce a corrosion inhibitor to a coating is just a simple mixing with the coating formulation. However, the simple mixing, in fact, is not so simple because it can raise many problems if some important factors are not taken into account. At first, the inhibiting species are effective only if their solubility in the corrosive environment is in the right range. Very low solubility leads to a lack of active agent at the substrate interface and, consequently, to a weak self-healing activity. If the solubility is too high the substrate will be protected but only for a relatively short period since the inhibitor will be rapidly leached out from the coating. Another disadvantage, which can appear due to the high solubility, is the osmotic pressure that forces water permeation leading to blistering and delamination of the protective coating. **Fig.11** clearly shows how the solubility of the corrosion inhibitor influences the adhesion of the coating on the metal surface. A high solubility of the inhibiting species dispersed in the matrix causes very fast complete stripping of the polymer film from the substrate <sup>29</sup>.

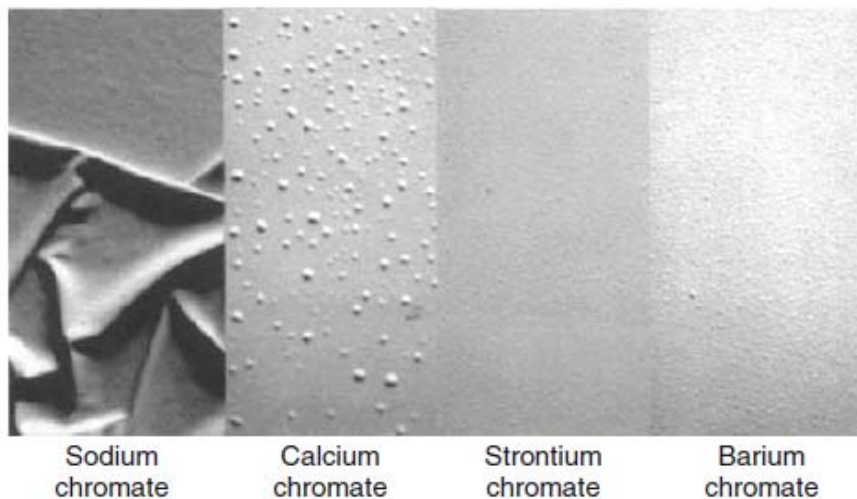


**Fig.11.** Osmotic blistering of organic coatings as a function of corrosion inhibitor pigment solubility. The solubility of chromate salts decreases from left to right. Reprinted from <sup>29</sup>

Another important problem can appear when the corrosion inhibitor can chemically interact with the components of the coating formulations weakening the barrier properties of the final coating. Degradation of the barrier properties resulting from the addition of an inhibitor to the coating system is the main problem hampering the development of active corrosion protection

systems. Moreover, interactions between the inhibitor and the components of the coating can lead to a complete deactivation of its inhibiting activity. Therefore, a direct doping of organic coatings with inhibitors can be problematic.

The solution to this problem is fabrication of self-healing coatings through integration of nano-, microscale containers (carriers) loaded with active inhibiting compounds into existing conventional coatings. Encapsulated active species are uniformly distributed in the passive matrix and stay in a “trapped state” as long as the coating is intact. When the coating is damaged, containers respond either to the mechanical impact or to the change of local environment and release the immobilized active material <sup>42,43</sup>.

One of the first attempts of a corrosion inhibitor entrapment was based on complexation of organic molecules by cyclodextrin <sup>44,45</sup>. Several organic compounds, such as mercaptobenzothiazole, mercaptobenzimidazole, mercaptobenzimidazolesulfonate, and thiosalicylic acid, have been selected by Khramov et al. to add to a hybrid sol-gel film used for corrosion protection of AA2024 aluminium alloy. The hybrid films doped with corrosion inhibitors in entrapped form provide superior corrosion protection when compared with the undoped ones. Moreover, the coatings doped with inhibitors in entrapped form outperform those made by a simple addition. The formulations that contain  $\beta$ -cyclodextrin demonstrate superior corrosion protection properties due to the slowed release of the inhibitor and its continuing delivery to the corrosion sites followed by self-healing of corrosion defects. However, the complexation with cyclodextrin confers only a prolonged release of the inhibitor without a delivery of it on demand as a response to any external stimuli.

Another entrapment concept is based on the use of nanoparticles, which can play a role of nanocarriers for corrosion inhibitors absorbed on their surface. The high surface area of the carriers, which results from the small size of the nanoparticles, provides sufficient loading capacity for the inhibitor. The prolonged release of inhibitor from the surface of nanoparticles provides an enhanced long-term corrosion protection compared to the case when the inhibitor is directly added to the sol-gel matrix. Examples of this approach are zirconia nanoparticles with immobilized  $Ce^{3+}$  <sup>30,46</sup> ions for AA2024 aluminium alloy protection. Silica and ceria-based nanocarriers were introduced to organosilane coating applied to galvanized steel <sup>47</sup>. Chemical anchoring of an organic inhibitor to aluminium oxyhydroxide nanoparticles through carboxylic bonds was employed in protective coatings for aluminium, copper, nickel, brass, and bronze substrates <sup>48</sup>. In the latter case hydroxide ions generated from the corrosion of a metal trigger the release of the corrosion inhibitors from the particles at pH 9. Thus the release

of the inhibitor starts only by the corrosion process, which prevents undesirable leakage of the inhibitor from an intact coating during exploitation.

Usage of hollow cellular structure loaded with organic and/or inorganic inhibitors<sup>49</sup> allows achieving much higher loading capacities of the carriers. Zeolite particles are very attractive carriers because the cations in their structure can readily be exchanged for the inhibiting cations in the contact solution<sup>50</sup>. Inhibiting inorganic cations can also be incorporated as exchangeable ions associated with cation-exchange solids<sup>51,52</sup>. A different situation appears when anion-exchange pigments are used to immobilize anionic inhibitors<sup>53-55</sup>. The release of inhibitor anions can be provoked in this case by aggressive corrosive chloride ions. The anion-exchange pigment can play a double role, absorbing the harmful chlorides and releasing the inhibiting ions in response.

Immobilization of the corrosion inhibitor discussed above was shown to be a useful technique for corrosion protection. However, the described approach can be used only to provide prolonged release of inhibitor, but not to protect it from the interaction with the coating formulation. Another strategy is based on the use of different encapsulation techniques when a protective shell on a core containing inhibitor is created.

A corrosion inhibitor can be encapsulated together with a polymerizable healing agent<sup>18</sup>. Yang et al. encapsulated triazole inhibitor using plasma polymerization (PP) to produce PP-perfluorohexane and PP-pyrol layers employing radio frequency plasma discharge<sup>56</sup>. The plasma-treated triazole was used as a pigment in a water-based epoxy coating slowly releasing the inhibitor and providing a long-term corrosion protection. In both cases, the release of the inhibitor from the capsule is possible only when it is mechanically damaged. The damaged capsule releases the entire active agent very fast in an uncontrollable way.

A very interesting alternative that allows a controllable leaching triggered by a corrosion-related stimulus is the use of layer-by-layer (LbL) assembled shells. Nanocontainers with regulated storage/release of the inhibitor can be constructed with nanometer-scale precision employing the LbL deposition approach<sup>57</sup>. With such a step-by-step deposition of oppositely charged substances (e.g. polyelectrolytes, nanoparticles, and biomaterials) from the aqueous and nonaqueous media on the surface of a template material, the LbL shells were assembled and investigated as perspective materials for different applications. LbL films containing one or several polyelectrolyte monolayers assembled on a surface of a sacrificial template possess the control of the shell permeability toward ions and small organic molecules. The storage of corrosion inhibitors in the polyelectrolyte multilayers has two advantages: isolation of the inhibitor avoiding its negative effect on the integrity of the coating and providing an

intelligent release of the corrosion inhibitor regulating the permeability of polyelectrolyte assemblies by changing local pH and humidity <sup>42,43,58-62</sup>. The samples coated with LbL nanocontainer-doped hybrid film demonstrate sufficiently enhanced performance in corrosion tests in comparison to an undoped sol-gel film or a film doped directly with free nonimmobilized benzotriazole. The promising results obtained on the LbL nanocontainers described above show the feasibility to use this approach for intelligent self-healing coatings. However, the nanocontainers with silica core do not provide high inhibitor loading capacity. Porous cores are more promising in this sense.

In <sup>63,64</sup> mesoporous silica nanoparticles loaded with corrosion inhibitor (1H-benzotriazole) were embedded in hybrid sol-gel coating for the corrosion protection of aluminium alloy. A sufficiently high uptake and storage of the corrosion inhibitor in the mesoporous nanocontainers was achieved. Ceria, cerium molybdate and mesoporous nanoparticles were loaded with 8-HQ and 2-mercaptobenzothiazole correspondingly <sup>65-69</sup> and incorporated into epoxy coatings on aluminium alloys 2024-T3 and investigated with respect to the corrosion protection of the metallic surfaces. The coatings with the loaded containers exhibited improved corrosion resistance.

Inhibitor-doped hydroxyapatite microparticles (HAP) <sup>70</sup> have high surface area and, consequently, a high loading capacity and were also used as reservoirs, storing corrosion inhibitor to be released on demand. Release of the entrapped inhibitor was triggered by red-ox reactions associated with the corrosion process. HAP were used as reservoirs for several species: cerium (III), lanthanum (III), salicylaldehyde, and 8-hydroxyquinoline inhibiting 2024 aluminium alloy. The protective properties of the sol-gel films were improved by the addition of HAP, proving their applicability as submicrometer-sized reservoirs of corrosion inhibitors for active anticorrosion coatings.

One of the prospective future containers can be industrially mined halloysite nanotubes. Halloysite was found to be a viable and inexpensive hollow nanoscale container for the encapsulation of biologically active molecules. A strong surface charge on the halloysite tubules has been utilized for designing nano-organized multilayers using the LbL method <sup>71-76</sup>. Halloysite nanotubes are capable of entrapping a range of active agents (within the inner lumen, as well as within void spaces in the multilayered aluminosilicate shell) followed by their retention and release. Both hydrophobic and hydrophilic agents can be embedded after an appropriate pretreatment of the halloysite <sup>77</sup>. Cheap halloysite nanotubes as perspective nanocontainers for anticorrosion coatings with active corrosion protection were recently demonstrated in <sup>42,71,72</sup>. Halloysite nanotubes were loaded with the corrosion inhibitor 2-

mercaptobenzothiazole and then incorporated into a hybrid sol–gel coating. To prevent undesirable leakage of the loaded inhibitor from the halloysite interior, the outer surface of the 2-mercaptobenzothiazole-loaded halloysite nanotubes was modified by deposition of several alternating polyelectrolyte multilayers. Another functionality of the polyelectrolyte shell is to provide the release of the encapsulated inhibitor in a way controlled by pH changes in the environment surrounding the halloysite nanotube <sup>42</sup>. Halloysite nanocontainers showed very good upkeep characteristics—almost complete suppression of the inhibitor release with more than 90% of the initial loading retained inside the inner cavity. The results of long-term corrosion tests demonstrated superior corrosion protection performance of halloysite-doped hybrid sol–gel films compared to that of undoped coatings <sup>78</sup>.

In <sup>79</sup>, thiourea as a liquid corrosion inhibitor for Q235 carbon steel was encapsulated using glutin. The releasing times of the thiourea microcapsule corrosion inhibitors were prolonged from 18 to 48 h by re-sealing and using PVA as a protective agent. Evaluation of the carrier efficiency as part of an active anticorrosion coating was not performed.

In <sup>80</sup>, the emulsion polymerization was used for fabricating structured polymer particles which can store active materials. The hollow polymer particles were synthesized by multi-stage emulsion polymerization consisting of four main stages. The specific target material of encapsulation were the phosphoric acid partial esters (PAPes), which are known to form a stable anticorrosive protective film on metallic substrates. The morphology of polymer capsules was manipulated by varying the process parameters of the core polymer expansion stage. The surface area and pore size could be significantly changed at a certain synthesis condition. Further introduction of the containers into a coating was not performed.

Pickering emulsions stabilized by silica nanoparticles were utilized <sup>81</sup> as carriers for 8-hydroxyquinoline (8-HQ). Such emulsions are stable in a narrow pH region. Drastic changes of pH happening due to corrosion can lead to destabilization of the emulsion and to the immediate release of encapsulated material.

In <sup>82</sup> corrosion inhibitor and antifouling agent were encapsulated in urea-formaldehyde resin. Positive influence of microcapsule embedment on the performance of anticorrosion coatings was demonstrated.

The analysis of the literature shows that encapsulation of corrosion inhibitors in all cases allowed to enhance sufficiently the corrosion protection properties of coatings. In all cases described in this chapter better performance of coating with encapsulated corrosion inhibitor in comparison to either unmodified or directly doped coatings was demonstrated.

### III. Motivation of this thesis

Incorporation of capsules carrying corrosion inhibitors into conventional coatings was shown to be a very promising approach. A wide use of self-healing coatings for different commercial applications is, however, limited because of the extremely high costs of the suggested technologies. These emerge from the costs of the initial chemicals and those of the manufacturing process (synthesis of the carriers, washing, drying, loading step etc). A possible direction for further evolution of the field would be development of new technologies that would use less expensive chemicals for production and involve minimal number of manufacturing steps.

Encapsulation in polymers would offer a great advantage, since polymers are cheap. The exploitation of the “in situ” loading mechanism would decrease the number of manufacturing steps, which would also lead to the reduction of final costs. Furthermore ceramic or oxide carriers discussed above were mostly applied for sol-gel coatings, while integration of them into polymeric coatings (which nowadays constitute the majority on the market) can cause problems related to the bad adhesion of such carriers to the polymeric matrix. Good adhesion of capsules to the coating matrix is one of the basic requirements for effective self-healing coating fabrication. Usage of polymeric capsules, surface properties of which can be comparatively easily tuned, would solve the problem of adhesive compatibility with the polymeric coating matrix.

Another issue that should be taken into account is the size of the capsules. It was shown in <sup>83</sup> that the efficiency of capsules is proportional to their size. This is due to the fact that the amount of material available for healing is equal (or in some cases somewhat higher) to the volume of capsules located on the way of the damage propagation. Therefore the bigger the size of capsules introduced into the coating the higher the efficiency of the final “smart” coating. From the other hand, too big capsules being introduced into a coating would disturb its barrier properties. Therefore the size of the capsules should be adjusted according to the coating thickness in every particular case and is a compromise between efficiency and coating matrix tolerance. For comparatively thin (2-5  $\mu\text{m}$ ) sol-gel coatings described in Chapter II. 2 usage of nano-sized capsules was dictated by the comparatively low coating thickness.

The thickness of most of the polymeric coatings used nowadays is 20  $\mu\text{m}$  and higher (can reach few millimeters for marine applications). Therefore usage of nanometer sized capsules is in this case not reasonable. Capsules of micron or submicron size should be applied as the

active part of the active anticorrosion coating. Characterization and handling of micron-sized objects is sufficiently easier compared to nano-sized ones. This factor would also lead to the decrease of the cost of the final product.

The big advantage of inorganic carriers is their inertness, which allows using them in coatings containing aggressive organic solvents and mixtures of solvents (like in sol-gel formulation). Such species would not be dissolved or damaged in most organic solvents, which makes them (in the sense of inertness) compatible with any kind of coatings including solvent-based ones. The challenge would be to use polymers as building block of the capsules, but keep the inertness specific for inorganic substances. Given these limitations the usage of crosslinked polymers is the only choice, since it is the only class of polymers that can not be dissolved in any kind of solvents. This property makes it possible to use this class of compounds in combination with any kinds of coatings, no matter if water- or solvent-based.

Crosslinked polymers, once formed, can not be redissolved or melted; the shape of the polymer can not be changed neither. Therefore when one aims to synthesize capsules made of crosslinked polymer of certain size and structure, the process of capsule formation should happen simultaneously with the polymerization reaction. Interfacial polymerization is therefore the best choice for the capsule fabrication process. Moreover, interfacial polymerization allows “in situ” loading of the capsules. The latter would allow fabrication of capsules with high loading efficiency (up to 90%wt.) in a one-pot process.

Along with the listed undeniable advantages interfacial polymerization has one heavy complication: the morphology of the resulting capsules is hard to predict and to control. The morphology of capsules was shown<sup>84-91</sup> to influence strongly the release properties, therefore morphology control is one of the main preconditions for the successful capsule design. The possibility of fabrication of capsules with both compact and core-shell morphology via interfacial polymerization was demonstrated in the literature. Systematic investigation of the parameters leading to the formation of different morphology especially for the case of crosslinked polymers is, however, still missing.

In the present work, an attempt has been made to fill up this gap. The influence of the “chemistry”, namely the nature of the polymer and the encapsulated material, on the morphology of the resulting capsules was investigated. The morphology of capsules prepared by interfacial polymerization was shown to be strongly affected by the capsule composition. The way to control and even predict capsule morphology on the basis of the independent properties of capsule components is suggested and discussed in details in Chapter V.

Further discussion of the present work concerns preparation of capsules of micrometer size for further application as the active part of “smart” self-healing anticorrosion coatings. The synthesis conditions and performance of capsules containing different kinds of corrosion inhibitors with on-demand morphology is discussed in Chapters VI. The latter can be also considered as the illustration of successful application of the approach presented in chapter V.

## IV. Materials and Methods

### IV.1. Materials

Aluminium alloy AA2024 and steel specimens were supplied by EADS Deutschland GmbH. Poly[(phenyl isocyanate)-co-formaldehyde] (isocyanate prepolymer, number of reactive groups per molecule~3.0, MW~375), terephthaloyl chloride (TPhCl), glycerol, ethylenediamine (EDA), tetraethylenepentamine (TEPA), diethylenetriamine (DETA), triethylenetetramine(TETA),poly(ethylenemeimine) (PEI, 50%wt. water solution, average  $M_w$  ~1.200), poly(vinyl alcohol) (PVA, MW~9,000-10,000, 80% hydrolyzed), 1,4-diazabicyclo[2.2.2]octane (DABCO), ethanol (EtOH), methanol (MeOH), acetone, toluene, chloroform, cyclohexanone (CHn), dimethyl phthalate (DMPH), diethyl phthalate (DEPh), dioctyl phthalate (DOPH), anisaldehyde, tetrahydrofuran (THF), styrene, N-methyl-2-pyrrolidone, dimethyl sulfoxide, 1-dodecanethiol, 2,2,2-trifluoro ethanol, 1-hexanol, diaminocyclohexane, trimethoxy(octadecyl)silane (TMODS, technical grade), trimethoxy(octyl)silane (TMOS, 96%), dibutyl phosphate (DBuPh), Bis(2-ethylhexyl) phosphate (DEtHePh), benzotriazole (BTA) and 8-hydroxyquinoline (8-HQ) were purchased from Sigma–Aldrich and used without further purification.

The Millipore Milli-Q Plus 185 purified water with a resistivity higher than  $18 \text{ M}\Omega\cdot\text{cm}^{-1}$  was used in all experiments.

The model coating is water-based two-component epoxy coating. The two components are mixed immediately before the coating application. The application was carried with spiral blade. After application coating was left for curing at ambient conditions for 24 hours.

### IV.2. Interfacial polymerization

Interfacial polymerization is a conventionally used method for encapsulation in polymeric shells <sup>92</sup>. The reaction of polymerization happens on the boundary between two immiscible liquid phases (**fig.12a**). First reactive monomer is dissolved in a solvent 1. An emulsion of this solution in a solvent 2 using a stabilizer is then formed. After the emulsification step, the second reactive monomer is added to the continuous phase. The polymerization reaction between two monomers on the surface of emulsion droplets leads then to the formation of capsules.

Solvent 1 corresponds to the liquid substance to be encapsulated or to a solution of solid active material in inert solvent. Solvent 2 is usually water (however inverse and oil-in-oil emulsions may be used). Monomer 1 corresponds to isocyanate prepolymer in case of polyurethane (PU) and polyurea (PUa) capsules and to TPhCl in case of polyamide (PA). Monomer 2 is glycerol in case of PU and a mixture of bifunctional and pentafunctional amine in case of PUa and PA. The stabilizer is PVA.

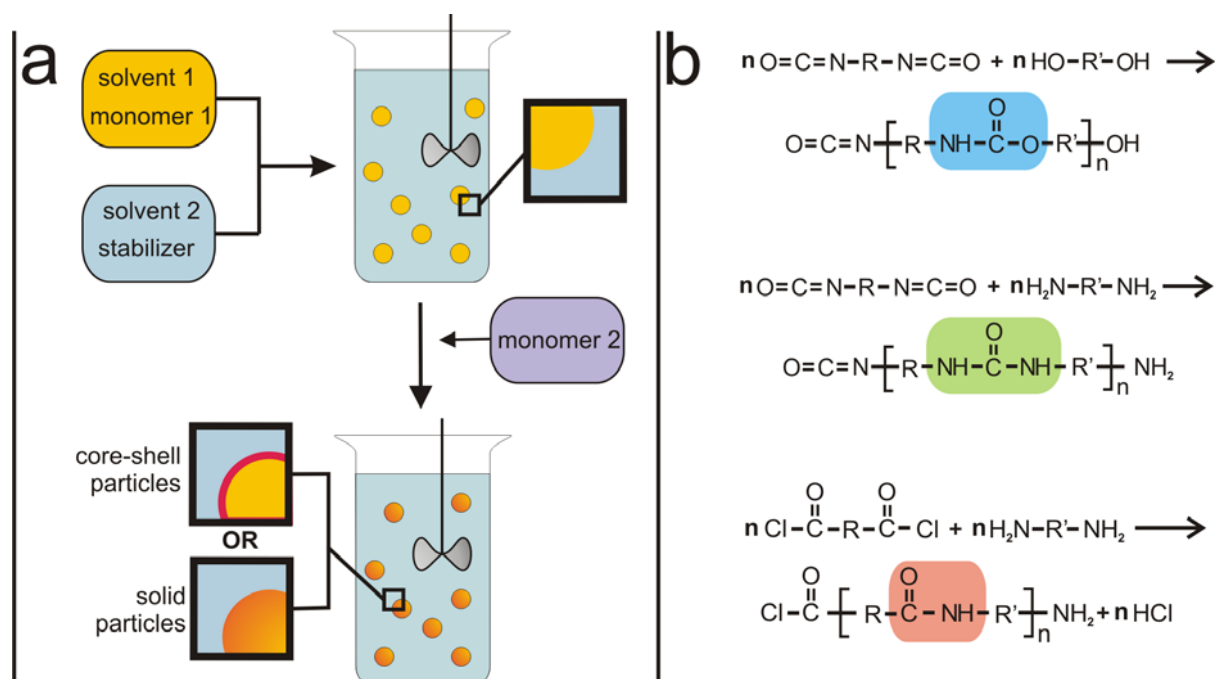


**Fig. 12.** Synthesis of the containers by interfacial polymerization **(a)** general scheme of the process and possible capsule morphologies **(b)** schemes of polymerization reactions for polyurethane, polyurea and polyamide. The PU, PUa and PA bonds are marked by a blue, green and red box, correspondingly.

The schemes of the polymerization reactions are represented in **fig. 12b**. The nature of the oil-soluble monomer was aromatic for all three classes of polymers; the nature of the water-soluble one was aliphatic.

For preparation of capsules with different morphology, eight solvents were used: toluene, chloroform, DMPH, DPh, DOPH, CHn, anisaldehyde and MeBT. In such a manner 24 (3 polymers×8 solvents) different polymer-solvent combinations were realized.

Isocyanate prepolymer for polyurethane and polyurea microcapsules or TPhCl for polyamide microcapsules was dissolved in 1 ml of solvent (the weight fraction of the monomer was kept 30%). This amount of oil was emulsified in 10 ml of 2wt.% aqueous PVA solution using an

ULTRA-TURRAX® high-speed homogenizer (IKA® Werke, Staufen, Germany) for 3 minutes at 16000 rpm if not other specified.

For preparation of PU microcapsules, a solution of glycerine (4 ml) and DABCO (200 mg) in water (6 ml) was added slowly to the emulsion. This mixture was left for one hour at 65°C under stirring. Then, heating was stopped and the solution was left without stirring overnight. A suspension of containers was dialyzed in order to remove residual glycerol and PVA (membrane with pore size of 12-18 kDa was used). Heat and DABCO as polymerization reaction catalyst are needed due to the low reactivity of alcohols compared to amines.

For the preparation of PUa microcapsules, a mixture of EDA (1.1g) and TEPA (2.8 g) was used. The amount of components was adjusted in such a way that the total functionality of the amine would be equal to 3. The mixture of amines was dissolved in 10 ml of water and added slowly to the emulsion under stirring without heating. After 10 minutes stirring was stopped and the mixture was left for reaction completion overnight.

For the preparation of PA microcapsules, a mixture of EDA (0.91 g) and TEPA (3.4 g) was used. The amount of components was adjusted in such a way that total functionality of the amine would be equal to 4. The mixture of amines was dissolved in 10 ml of water and added slowly to the emulsion under stirring without heating. After 10 minutes stirring was stopped and the mixture was left for the reaction completion overnight.

### **IV.3. Methods for characterization**

#### **IV.3.1. Scanning electron microscopy (SEM)**

For characterization of particles by SEM a sample (10 µl) of the particle suspension was placed at the sample holder and left overnight to dry at atmospheric pressure.

If needed, the resulting sample was crushed with a razor blade. A new razor blade was taken for every new experiment in order to avoid sample contamination.

An alternative procedure was applied in some cases. For that capsules were introduced into the polymeric matrix and after the matrix was dry, small slices were cut and directed on the sample holder in such a way, that the cut edge of the sample is parallel to the sample holder surface.

(SEM) measurements were performed using a Gemini 1550 instrument at an operation voltage of 3 keV. All samples were gold-sputtered. Elemental analysis was carried out by energy-dispersive X-ray spectroscopy (EDX).

When an operation voltage of 6 keV was used the analysis was limited by specimen charging and specimen damaging under the electron beam.

### **IV.3.2. Transmission electron microscopy (TEM)**

In the TEM analysis, strong deformation of the particles was observed, which is an indicator that the material is not stable under the high-energetic electron beam (200 kV). Further analysis with TEM was not possible.

### **IV.3.3. Scanning vibrating electrode technique (SVET)**

SVET operates with a non-invasive scanning, vibrating probe measuring and mapping the electrical potential generated in a plane above the surface of an electrochemically active sample. This enables the user to map and quantify local electrochemical and corrosion events in real time. In the present work, the current 300  $\mu\text{m}$  above the scratched metal substrate covered with a coating was investigated. For unmodified coatings, the bare surface of metal starts to corrode, once it is in contact with electrolyte solution; the increase of the current density in the local area of the scratch can be detected in dependence of time. Introduction of corrosion inhibitor into the coating is supposed to reduce corrosion activity of the metal substrate at the scratched site. The current density of the scratched modified sample is therefore measured to verify the inhibitor activity.

SVET experiments were performed by using the equipment supplied by Applicable Electronics (Forestdale, MA, USA). Samples were prepared for SVET measurement by cutting into  $1 \times 2 \text{ cm}^2$  plates,  $3 \times 3 \text{ mm}^2$  areas were opened for the measurements, other parts of the samples were protected by an adhesive tape. The anticorrosion coating of each sample was scratched to introduce a defect extending to the metal surface; the area of the defect ranged from 0.1 to 0.3  $\text{mm}^2$ . After scratching the samples containing capsules loaded with water-repelling agent were allowed to heal for 12 hours at room temperature and 100% humidity. The immersion solution was 0,1 M NaCl aqueous solution. Scans started 5 min after immersion and were collected every 15 min for the duration of the experiment, typically 12 h. The current density was detected with a resolution of 150  $\mu\text{m}$ . A complete surface scan required ca. 5 min. The analysis of the SVET data was carried out via homemade software examining the time development of minimal and maximal current densities.

The normal or -z component of the measured current density in the plane of the vibrating electrode was plotted in 3D format over the scan area, with positive and negative current densities representing anodic and cathodic regions, respectively.

#### **IV.3.4. Fourier transform infrared spectroscopy (FTIR)**

FTIR measurements were carried out with a Bruker Hyperion 2000 IR spectrometer equipped with a 158 IR objective and DTGS detector at room temperature in KBr pellets. The pellets were fabricated from a mixture of containers and potassium bromide using a manual pellet press (Specac, Orpington, UK) and mounted on a QuickLock base plate. Spectra between 400 and 2000  $\text{cm}^{-1}$  were recorded with 2  $\text{cm}^{-1}$  resolution in the transmission mode.

#### **IV.3.5. Dynamic light scattering (DLS)**

A Zeta Sizer Nano ZS (Malvern Instruments, UK) was utilized to determine the size distribution of the containers. Before the measurement, all samples were appropriately diluted to obtain slightly turbid dispersions. Measurements were done in backscattering mode at a detector position of 173°. At least three measurements of 15 runs each were averaged. The scattering data analysis was done with the CONTIN algorithm.

#### **IV.3.6. Contact angle measurements**

Drops of the corresponding liquid ( $\sim 2 \mu\text{l}$ ) were deposited on the AA 2024 plate surface with a micro syringe, and their advancing contact angles were measured on a Kruss contact angle goniometer G10, equipped with a CCD video camera (Zoom 1:6.5). At least 10 drops per sample were measured for statistical reasons. The contact angles were evaluated with the Kruss software.

#### **IV.3.7. Electrochemical impedance spectroscopy**

The electrical impedance is the complex ratio of the voltage to the current in an alternating current (AC) circuit. Impedance extends the concept of resistance to AC circuits, and possesses both magnitude and phase, unlike resistance which has only magnitude. In the present work electrical impedance is measured for the layer of coating spread on the surface of a metal. Impedance or resistance is therefore a measure of barrier properties of the coating. Appearance of inhomogeneities in the coating leads to the formation of pores and paths for water and electrolyte species into the coating. Decrease of impedance values in this case is observed.

During an electrochemical impedance spectroscopy (EIS) <sup>93</sup> measurement, the sample (e.g. an aluminium or steel plate covered with polymer film) is subjected to a sinusoidal voltage signal ( $U = U_0 \sin(\omega t)$ ). The system answer is a phase shifted oscillating current signal ( $I =$

$I_0 \sin(\omega t + \phi)$ ). Both  $U$  and  $I$  can be represented vectorially and by dividing the absolute values of these vectors the systems impedance is obtained.

$$|\vec{Z}| = \frac{|\vec{U}|}{|\vec{I}|}$$

The representation of the impedance by complex numbers combines the ratio of the voltage and current amplitudes  $U_0/I_0$  with the phase shift  $\phi$  in one mathematical expression. In its Cartesian form, the complex impedance writes  $Z = Z' + iZ''$ . An EIS test is performed for a set of different frequencies of the sinusoidal voltage signal (usually in the range  $10^{-2} - 10^5$  Hz). The measurements in the frequency domain are performed with a frequency response analyzer (FRA). A typical experimental setup is shown in **fig.13**.

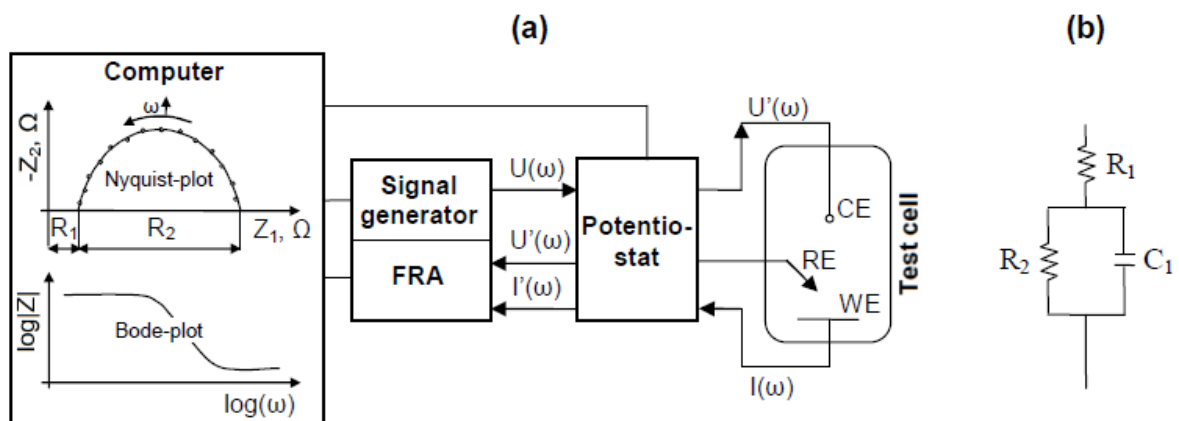


**Fig.13.** Electrochemical impedance spectroscopy (a) Impedance setup using a frequency response analyzer (FRA), calomel electrode (CE), reference electrode (RE), working electrode (WE) (b) electrical circuit of a resistor ( $R_1$ ) in a series with a parallel circuit of another resistor ( $R_2$ ) and a capacitor ( $C_1$ ).

In the signal generator, a sinusoidal voltage  $U(\omega)$  is generated and transmitted via a potentiostat through the calomel electrode to the test cell. The test cell is filled with an electrolyte solution and contains the immersed sample, which is connected to the working electrode (WE). Measurement of the electrical current  $I(\omega)$  takes place in the potentiostat, which also transfers the ( $U'(\omega)$ ) and output ( $I'(\omega)$ ) signal to the FRA. In the FRA, the impedance  $Z(\omega) = U'(\omega)/I'(\omega)$  is calculated and transferred to a computer for data processing. The real and imaginary parts of the impedance for each frequency can then be plotted in a Nyquist- or Bode- plot. Depending on the shape of the data representation in these plots

different physical models can be used for the analytical representation of the data. The models can be obtained by fitting the data numerically to an equivalent electrical circuit, which consists of parallel- or serial circuits of elementary electrical modules (resistor, capacitor and inductor). The appearance of the impedance data in the Nyquist- or Bode- plot allows for the selection of an appropriate electrical circuit. In the scheme in **fig.13** a qualitative example is shown, which corresponds to a series circuit of a resistor with a parallel circuit of a second resistor and a capacitor  $R_1(R_2/C_1)$  as depicted in Scheme (b). Herein  $R_1$  can be physically interpreted as the resistance of the electrolyte solution. For a sample consisting of e.g. a blank aluminium plate  $C_1$  can be interpreted as the electrical double layer capacitance and  $R_2$  as the resistance of the oxide layer on the surface. For the case of a polymer-film on the aluminium substrate  $C_1$  and  $R_2$  can be assigned to the properties of this polymer-film. The analytical expression of the complex impedance for this circuit is given in the equation

$$Z = R_1 + \frac{R_2}{1 + \omega^2 C_1^2 R_2^2} - i \frac{\omega R_2^2}{1 + \omega^2 C_1^2 R_2^2}$$

This model is applied to measured EIS data by numerically fitting the data with the last equation by means of the software IviumSoft. All measurements were performed at constant voltage amplitude of 10 mV in a frequency range of  $65 \times 10^3 - 10^{-2}$  Hz. Before the measurement the open cell potential was detected, and measured impedances were corrected by the obtained value. The potentiostat-microprocessor combination used for the measurements was a Compact Stat instrument from Ivium Technologies.

#### **IV.3.8. Salt-spray chamber**

The salt spray test is a standardized test method used to check corrosion resistance of coated samples. Since coatings can provide a high corrosion resistance through the intended life of the part in use, it is necessary to check corrosion resistance by other means. Salt spray test is an artificially accelerated corrosion test that produces a corrosive attack to the coated samples in order to predict its suitability in use as a protective coating. The appearance of corrosion products (oxides) is evaluated after a period of time. Test duration depends on the corrosion resistance of the coating; the more corrosion resistant the coating, the longer the period of testing without showing signs of corrosion.

Salt spray testing is popular because it is cheap, quick, well standardized and reasonably repeatable. The salt spray test is widely used in the industrial sector for the evaluation of corrosion resistance of finished surfaces or parts.

The apparatus for testing, used in this work (ISO 9227), consists of a closed testing chamber, where an aqueous solution of 5% sodium chloride is atomized by means of a nozzle at 35°. This produces a corrosive environment of dense saline fog in the chamber so that parts exposed in it are subjected to severely corrosive conditions.

#### **IV.4. Swelling behavior of polymers**

To determine the extent of swelling approximately 200mg of pure PU, PUa or PA powder was dispersed in 2 ml of solvent by shaking. After one week shaking was stopped, the dispersion was centrifuged in order to precipitate the swollen polymer grains. The free solvent was removed by decantation. The mass of the solvent absorbed by polymer was calculated as the mass of the solid part of the suspension subtracted by the mass of initial polymer particles.

## V. Control and prediction of capsule morphology

### V.1. Possible morphology of capsules prepared via interfacial polymerization

Interfacial polymerization (see **fig.12**) is conventionally used for encapsulation in polymeric shells. The reaction of polymerization happens on the boundary between two immiscible (usually) liquid phases. One reactive monomer is dissolved in one phase, another reactive monomer - in another. When monomers meet on the interface the polymerization reaction takes place. The whole process is divided into two steps. On the first step an emulsion is formed. The first reactive monomer is dissolved in the dispersed phase, while the continuous phase usually contains emulsion stabilizer. On the second step the second reactive monomer is added to the continuous phase, leading to the polymeric shell formation on the surface of the emulsion droplets. The liquid content of the dispersed phase turns to be entrapped inside the polymer after the polymerization reaction is finished. The size and the shape of the final capsules are expected<sup>94</sup> to be equal to the ones of the original emulsion droplets, which serve as liquid templates for the capsules. Different kinds of emulsions can be used for interfacial polymerization. The most common way is to use conventional oil-in-water emulsions<sup>95-125</sup>, while inverse water-in-oil<sup>103,126-128</sup> and oil-in-oil<sup>129-134</sup> emulsions also have been used.

A polymeric solid shell around the liquid droplet is formed due to phase separation of the polymer. The composition of the core is usually chosen to ensure the phase separation<sup>135</sup>, which means that the resulting polymer should be soluble neither in the core material (nor in continuous phase). The insolubility should be established in advance; otherwise one can not ensure the formation of the capsules.

Both linear and crosslinked polymers can be used as a shell material. In practice the choice of linear or crosslinked polymer is usually determined by the beneficial properties of the resulting polymer: mechanical strength, elasticity, chemical inertness, permeability etc. The processes leading to the formation of capsules are considered by experimentalists to be principally the same for both types of polymers. At the same time, the difference in physical chemistry and phase separation phenomena for two classes of polymers is dramatic. The difference is in the ability of crosslinked polymers to swell in the solvent in stead of dissolution typical for linear polymers.

## **V.2. Swelling of polymers**

“Swelling” involves an increase of the polymer volume due to absorption of solvent (or mixture of solvents). In this sense, both linear and crosslinked polymers are swellable. Infinite increase of the amount of solvent in case of linear polymer will lead to the dissolution of the polymer in the solvent (if the polymer is swellable in this solvent) and formation of one homogeneous phase instead of two initial phases. Therefore “swelling” of linear polymers is a direct analogue of dissolution. In the case of crosslinked polymer the dissolution is not possible; polymer can swell only to a certain extent. After the saturation point is reached, one will find two phases in equilibrium: solvent and gel (polymer swollen in solvent). The content of a solvent in gel can be comparatively high and reach 99.9% wt. From now on the term “swelling” will be used only in relation to crosslinked polymers.

Since the formation of the capsules is a direct consequence of the phase separation in the oil droplets, the difference in the phase behavior of two types of polymers should lead to differences in the process of capsule formation. When linear polymers are under consideration polymer insolubility (or precipitation) is a precondition of the core-shell capsule formation. Crosslinked polymers are not soluble, but they can swell. The latter means that crosslinked polymer can coexist with the solvent in form of a single solid-like phase. The insolubility of crosslinked polymer therefore is not a precondition of core-shell structure formation. The formation of compact structures with the core material homogeneously distributed inside the polymer matrix is theoretically possible. The conditions leading to the formation of this or that structure have never been systematically investigated even for the simple case of a binary system consisting of one crosslinked polymer and one solvent.

At the same time morphology is an extremely important parameter, since it influences the release behavior as well as mechanical properties and colloidal stability of capsules. The control of the capsule morphology is therefore one of the most essential preconditions for the successful capsule design.

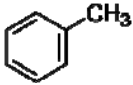
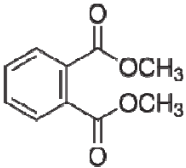
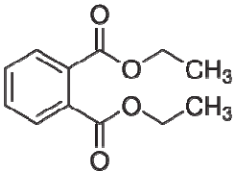
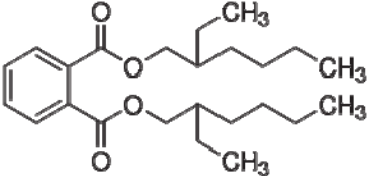
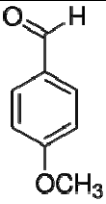
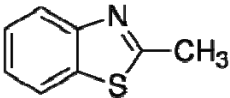
## **V.3. Synthesis of capsules with different morphology**

Three classes of polymers - polyurethane, polyurea and polyamide were chosen. The choice of polymers was determined by practical interest: their outstanding mechanical properties and chemical resistivity were of high interest for the further application as carriers for corrosion inhibitors.

Since these three polymers carry groups with different structure and polarity, one could expect that the swelling behavior and consequently the morphology of capsules made of different polymers may differ significantly.

As an encapsulated material and oil phase for interfacial polymerization eight solvents were chosen: toluene, chloroform, DMPH, DEPh, DOPh, CHn, anisaldehyde and MeBT. With these 24 (3 polymers×8 solvents) different polymer-solvent combinations were realized. The solvents were encapsulated via interfacial polymerization according to the procedure described in the experimental section. The structural formulas, boiling points and Hansen solubility parameters (see further in the text) of the solvents are summarized in **Table 1**. Twenty four types of containers were fabricated in form of a powder (after the washing and drying procedure). Already from the external appearance of the resulting powders one could guess that the solvents were encapsulated with different success. Some powders were dry and free-flowing while others were sticky. The redispersion of the sticky powder in water was sometimes problematic, while redispersion of the dry ones was effortless. The stickiness of the resulting powder was attributed to partial leaking of encapsulated solvent leading to the appearance of capillary forces holding the particles together.

The size of synthesized capsules was analyzed by DLS. The size distribution and the mean size of the capsules prepared at the same stirring speed, oil phase content and stabilizer concentration varied only slightly. This was expected, since the size of the containers is equal (or very similar) to the size of the initial oil droplets<sup>94,136</sup>, which at high enough concentrations of the stabilizer is mainly determined by the stirring speed. The size distribution of the capsules was comparatively broad (PDI=0.6) and bimodal. Irrespective of the stirring speed there were two populations of capsules: with the average size of 1 μm and 8 μm. A comparatively broad size distribution of the emulsion droplets and consequently of the resulting containers is common when mechanical stirring is used and mainly attributed to Ostwald ripening of the oil droplets on the emulsification step before the second reactive monomer addition. Addition of a superhydrophobe would probably<sup>94,136</sup> lead to less polydispersity, but would significantly complicate the morphology analysis since the system would become three-component. Therefore an attempt to increase the monodispersity of the system was not made; the morphology of capsules was assumed to be independent of the capsules size in the micron-submicron region.

Name	formula	boiling point	Hansen solubility parameters		
			$\delta_D$	$\delta_P$	$\delta_H$
Toluene		110.6 °C	18	1.4	2
Chloroform	<chem>CHCl3</chem>	61 °C	17.8	3.1	5.7
Cyclohexanone		155.6 °C	17.8	8.4	5.1
Dimethyl phthalate		283 °C	18.6	10.8	4.9
Diethyl phthalate		295 °C	17.6	9.6	4.5
Dioctyl phthalate		384 °C	16.6	7	3.1
Anisaldehyde		248 °C	19.4	11.9	8.3
2-methyl benzothiazole		237 °C	20.2	7.1	6.4

**Table 1.** Chemical structure, boiling points and Hansen solubility parameters of the encapsulated solvents

### V.3.1. The shape of capsules

The analysis of the appearance of the capsules was made on the basis of SEM images (fig.14-17). Different capsule shapes were observed, depending on the polymer-solvent combination: spherical, spheroidal with concavities and/or folds and collapsed.

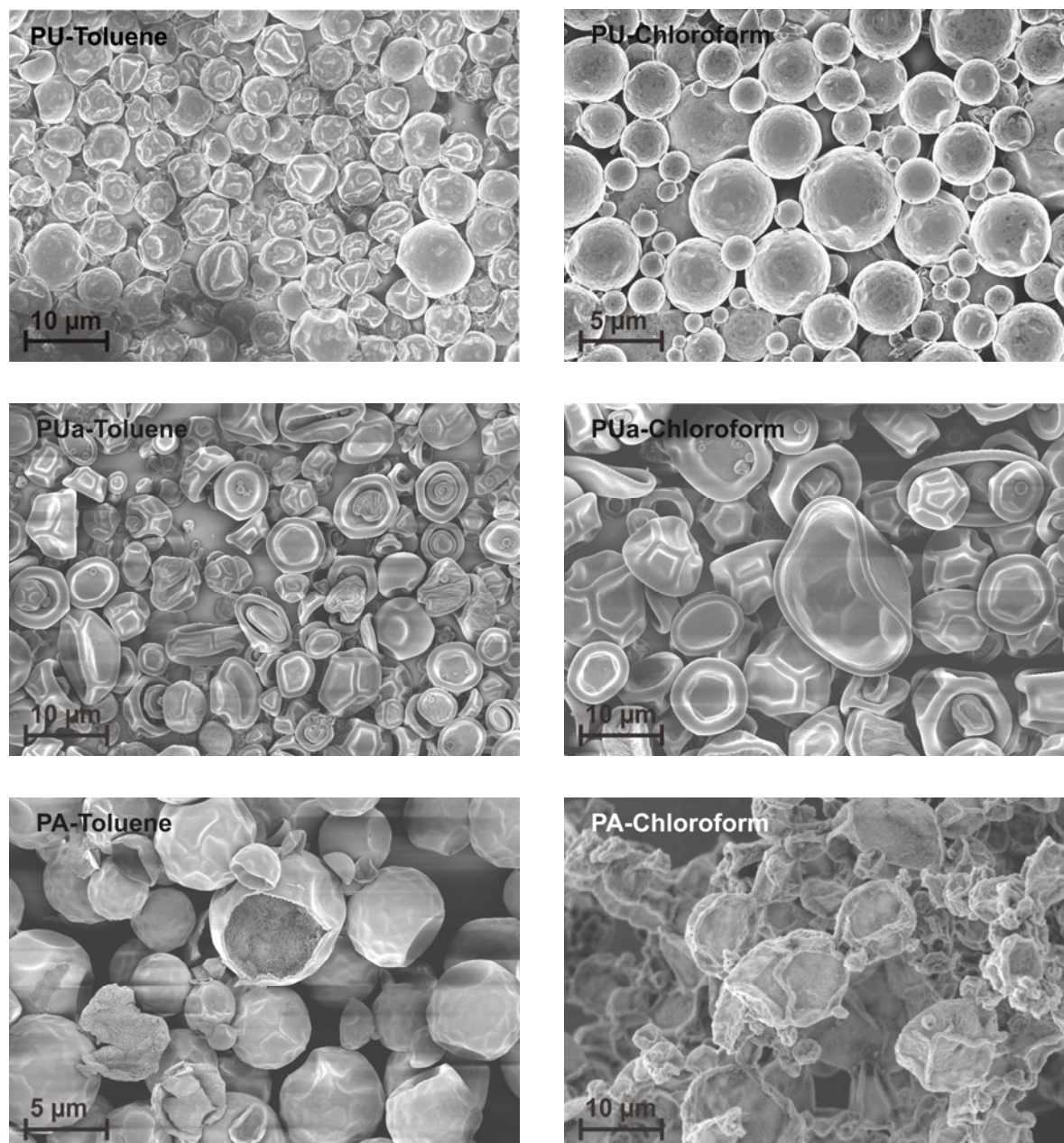


**Fig.14.** SEM images of capsules made of PU, PUa and PA (from top to down) with toluene (left) and chloroform (right) encapsulated.

Appearance of small concavities is attributed to collision of capsules on the first steps of the polymerization reaction when the capsule walls are still soft. Folding and even collapse of capsules can happen due to the high vacuum used in SEM leading to the evaporation of the solvent or partial extraction of the capsule liquid content during the washing procedure.

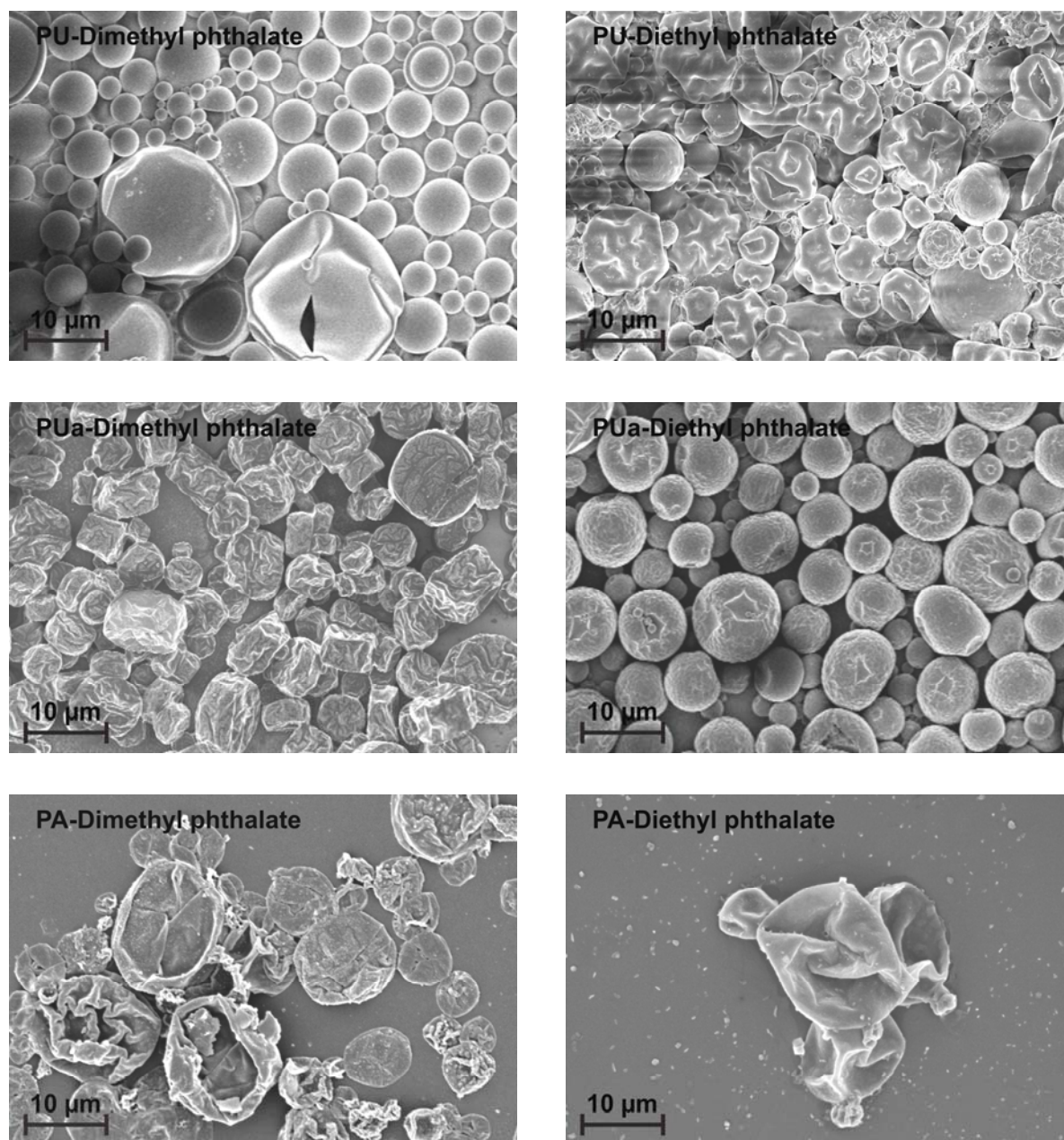


**Fig.15.** SEM images of capsules made of PU, PUa and PA (from top to down) with dimethyl phthalate (left) and diethyl phthalate (right) encapsulated.

Another reason for irregular shape formation can be compression or shrinkage of the polymer due to crosslinking. Capsules are considered as “collapsed” when there is no or a very small amount of liquid material inside the capsule left (see for example PA-DMPH or PA-DEPh capsules). For such capsules further analysis is not necessary, the core-shell structure can be concluded from the capsule appearance (if the rest of the capsule walls can be distinguished). Spherical, bumped and folded capsules should be analyzed further in order to find out how the polymer material is distributed inside the capsule.

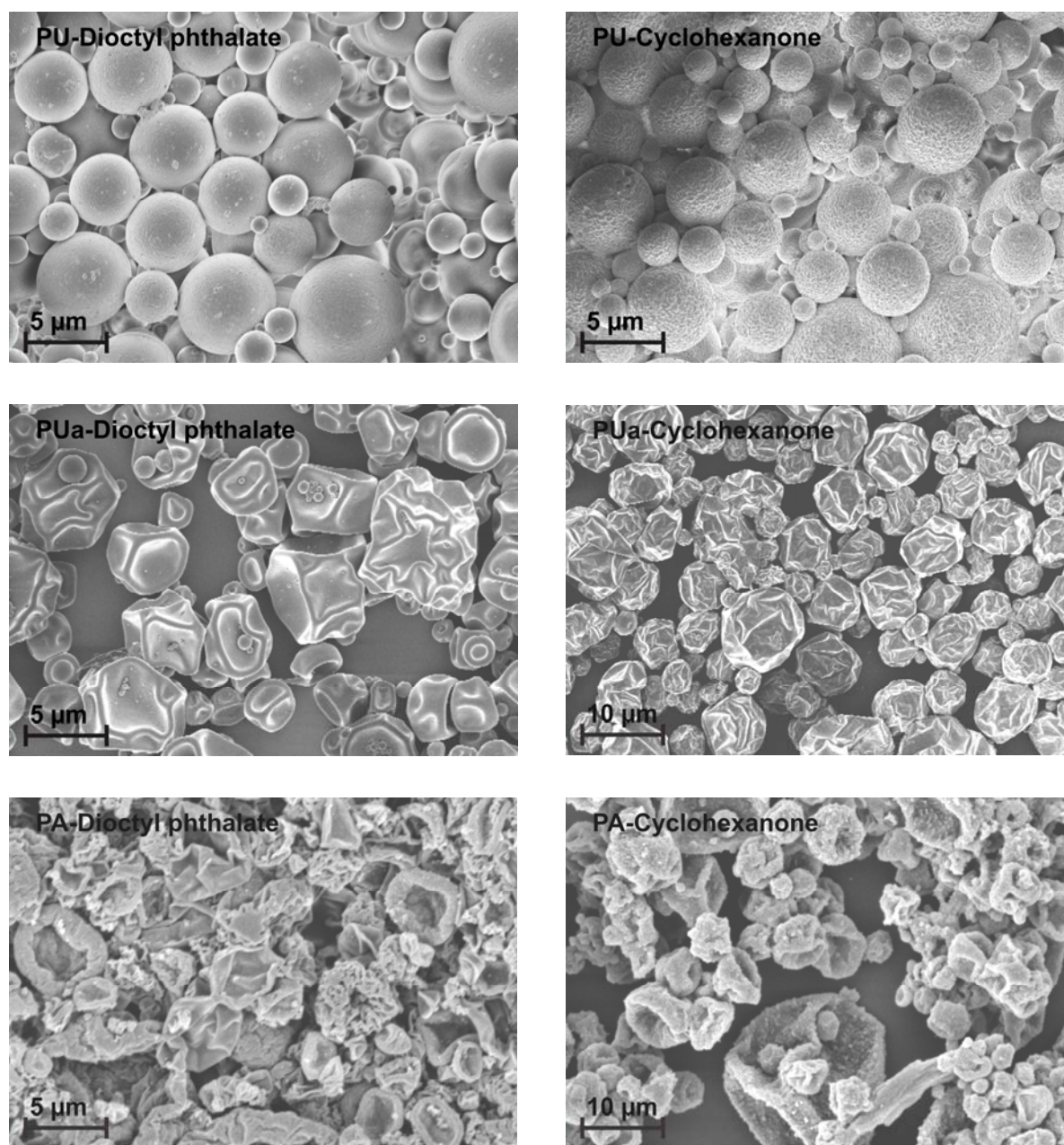


**Fig.16.** SEM images of capsules made of PU, PUa and PA (from top to down) with diethyl phthalate (left) and cyclohexanone (right) encapsulated.

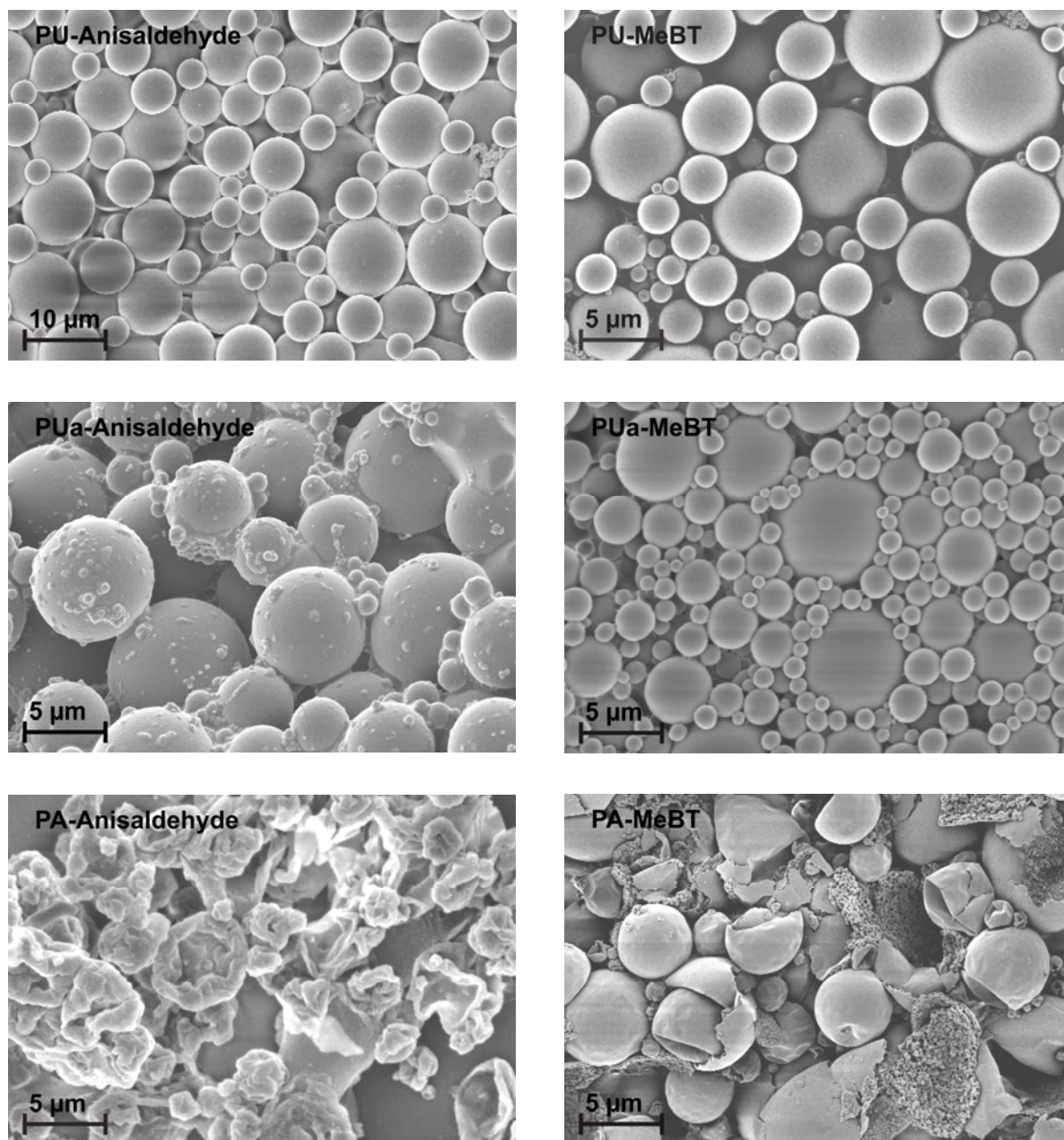


**Fig.17.** SEM images of capsules made of PU, PUa and PA (from top to down) with anisaldehyde (left) and MeBT (right) encapsulated.

Each type of capsules was synthesized at least three times. The shape of the PU and PUa capsules is reproducible, only slight variation of the shape from batch to batch was observed (like the size and number of concavities and folds). For PA capsules, the shape of the capsules varied significantly from batch to batch. Some capsules have generally spherical shape, like for toluene and MeBT capsules on the SEM image, some are collapsed (like for other

solvent). In one batch capsules are either mainly spherical or collapsed. This effect is not solvent – specific; both types of capsules were observed for most solvents in different batches. The shape was found to be influenced by the drying procedure. Freeze-dried capsules exhibit spherical shape more often than those dried in air, though not always. The effect of the drying procedure on the final shape of polyamide capsules was already discussed in the literature<sup>137</sup>. The phenomena can be explained by a plasticizing effect of water on PA. In water suspension the walls of capsules are soft and elastic due to the swelling of the polymer in water; dried in air capsules collapse, because the walls are too soft to keep the spherical shape of the capsules. Freeze-drying leads to the preservation of the spherical shape during drying. This hypothesis is supported by the fact that in the suspension most of the PA capsules have spherical shape with minor amount of concavities or folds (the data is not presented here). Even though examination of the parameters influencing mechanical properties of the PA capsules would be useful for their further application, it was not performed here. The main goal here was to investigate the morphology of capsules. Appearance of collapsed capsules in this sense is advantageous, since it is the direct evidence of the core-shell morphology. For determination of morphology of capsules with spherical shape other methods should be used.

### **V.3.2. Determination of capsule morphology**

As it was already mentioned, crushing of PA capsules is not necessary since appearance of the collapsed capsules is clear evidence of core-shell structure. Images of toluene-containing and MeBT-containing capsules show generally spherical capsules, but some of them are broken, clearly demonstrating core-shell morphology. Toluene-containing and MeBT-containing capsules were not crushed, but broke on one of the steps of the sample preparation due to the fragility of the PA shells. Therefore it is concluded that all synthesized PA capsules presented here possess core-shell structure.

Analysis of PU and PUa capsule morphology was made on the basis of SEM of crushed capsules. Application of TEM was not appropriate because of the comparatively big size of the capsules and low contrast between polymeric shell and capsule core (see an example in Chapter VI.3.3). It is extremely time-consuming to find crushed capsules between uncrushed ones on the SEM sample due to the great total number of capsules in one sample and a comparatively small number of crushed ones. Therefore, an alternative procedure was applied in some cases. For that, capsules were introduced into the polymeric matrix and after the matrix was dry, small slices were cut and directed on the sample holder in such a way, that the cut edge of the sample is perpendicular to the electron beam. By this, it was somewhat easier

to estimate the morphology (since in contrast to capsules crushed in the powder the cut edge is always perpendicular to the line of sight). However, in some cases, the adhesion of capsules to the polymer matrix was too low, which led to falling of capsules out of the coating matrix during the cutting procedure. For the presentation here the variant with better demonstrability was chosen to illustrate the morphology of the resulting capsules for every polymer-solvent pair.

For the sake of distinctness only the capsules having clear separation of the solid and liquid parts will be called “core-shell”. If the separation of polymer and oil material happens, but the distribution of the building material is not in the form of core-shell (polymeric parts are present close to the capsule center), such morphologies will not be considered as “core-shell”.

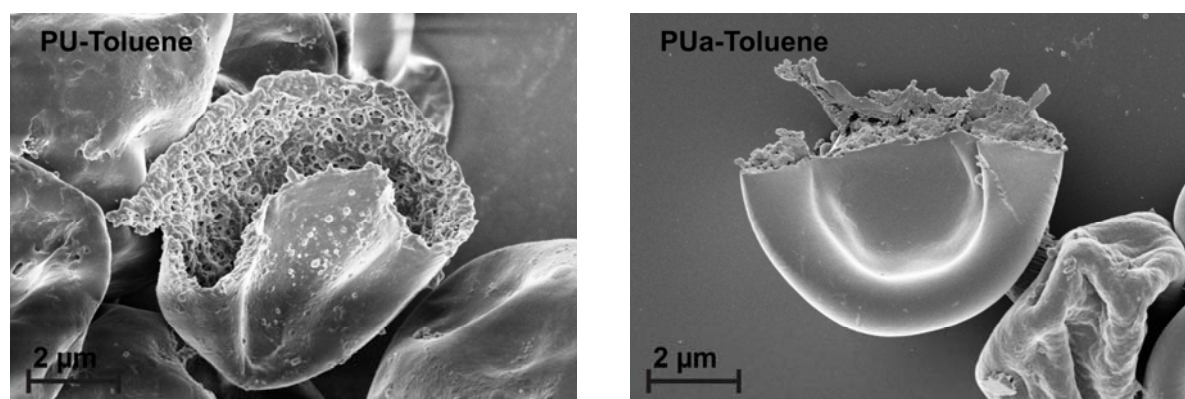


**Fig.18.** SEM images of crushed PU and PUa capsules containing toluene.

Capsules containing toluene (**fig.18**) exhibit core-shell structure in both PU and PUa cases. For PUa-toluene capsules crushing (or cutting as more appropriate term here) was not necessary, the core-shell morphology can be deduced from the outer appearance, since the capsules are collapsed. The PU capsules possess a lot of folds, but do not collapse even if they have a cavity inside. From the latter fact one can draw a conclusion about mechanical properties of capsules: PUa capsules have softer (and as it seems from the image thicker) walls than PU ones.

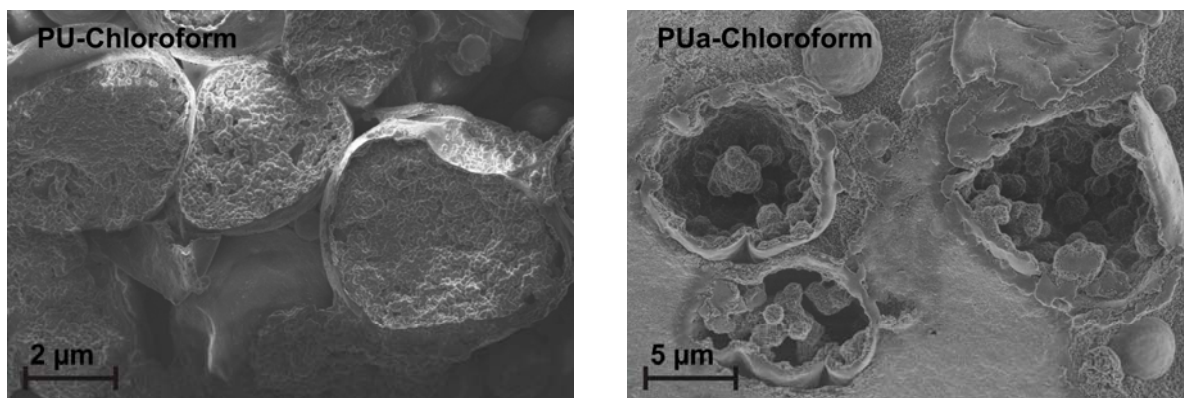


**Fig.19.** SEM images of crushed PU and PUa capsules containing chloroform.

PU and PUa capsules containing chloroform (**fig.19**) have different morphology. PU-chloroform capsules consist of dense outer shell and “lumpy” core. Even though the core and the shell parts can be distinguished in this case, this type of morphology will be considered as “compact”, since a significant part of the polymer is distributed inside the capsule. PUa-chloroform capsules also have some parts of polymer inside the cavity, but in this case the grains of polymers are easy to distinguish and the majority of the polymer is localized on the periphery of the capsule, therefore the morphology of PUa-chloroform capsules is considered as core-shell.

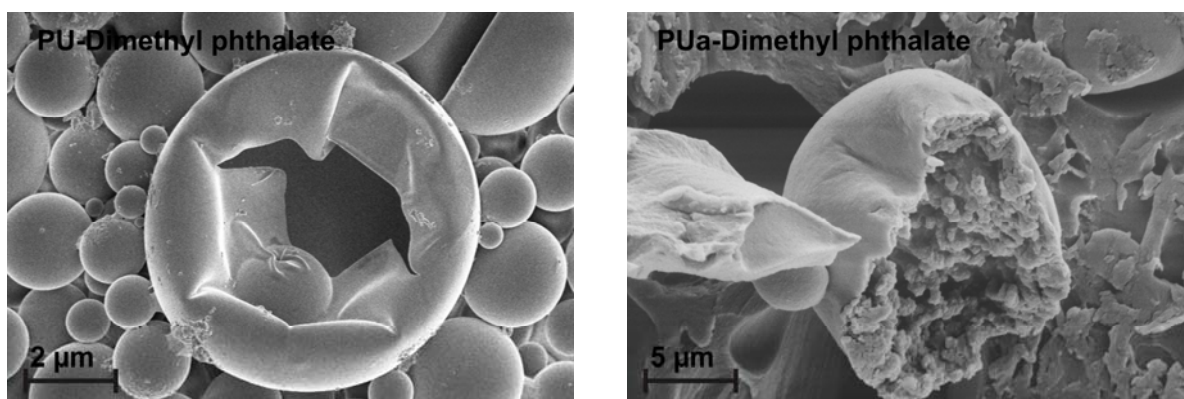


**Fig.20.** SEM images of crushed PU and PUa capsules containing dimethyl phthalate.

DMPH-containing capsules (**fig.20**) made of PU and PUa also differ significantly. PU-DMPH capsules are mostly spherical, some (the biggest) have folds. PUa-DMPH capsules are not collapsed, but have very irregular non-spherical shape with many folds on the surface. PU-DMPH capsules have core-shell morphology with thin and elastic shell. PUa-DMPH capsules possess morphology similar to the PU-chloroform case. According to our terminology these capsules are compact, even distinction between the core and shell parts is possible.

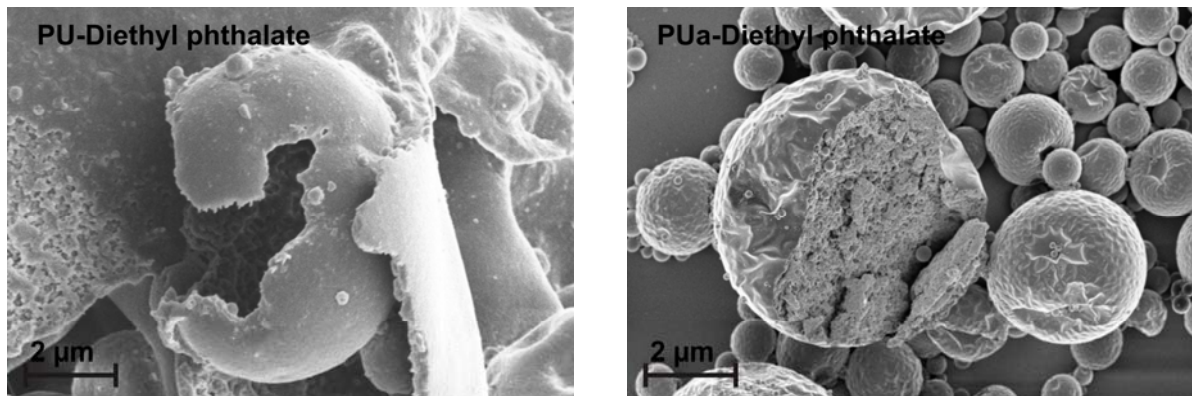


**Fig.21.** SEM images of crushed PU and PUa capsules containing diethyl phthalate.

PU-DEPh and PUa-DEPh capsules (**fig.21**) look similar: generally spherical shape with many concavities and folds. The topography of the capsule surface is somewhat different, but not significantly. The morphology, however, differs: PU-DEPh capsules are core-shell, while PUa-DEPh are compact. In contrast to PUa-DMPH capsules, PUa-DEPh ones do not have any cavity inside, the polymer is homogeneously distributed.

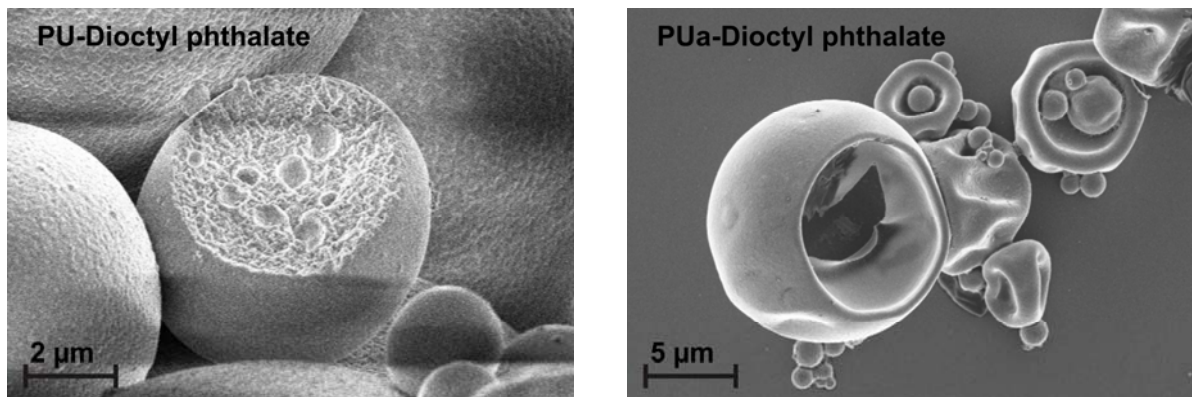


**Fig.22.** SEM images of crushed PU and PUa capsules containing dioctyl phthalate.

DOPh-containing capsules (**fig.22**) have different appearance. The surface of the PUa-DOPh capsules is very smooth, many deep folds can be seen; some capsules are collapsed. The surface of the PU-DOPh is rough. Capsules differ in morphology as well: PU-DOPh are compact, the difference between core and shell can not be distinguished. PUa-DOPh capsules demonstrate core-shell morphology with thin highly elastic shells, very similar to the PU-DMPH capsules.

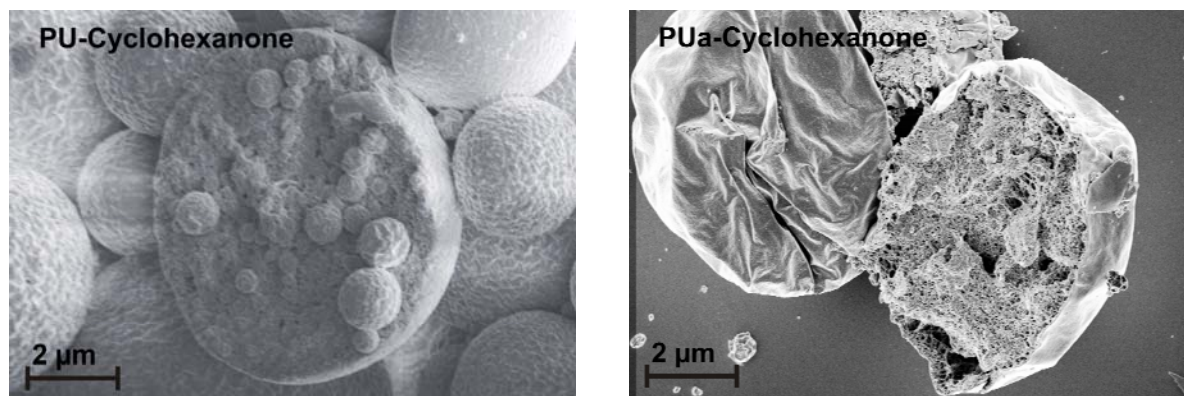


**Fig.23.** SEM images of crushed PU and PUa capsules containing cyclohexanone.

Although the outer appearance of CHn-containing capsules (**fig.23**) is different, both PU-and PUa-CHn capsules have compact morphology. PU-CHn capsules are from both outer and inner appearance very similar to PU-DOPh capsules, while PUa-CHn capsules are very similar to PUa-DMPH ones.

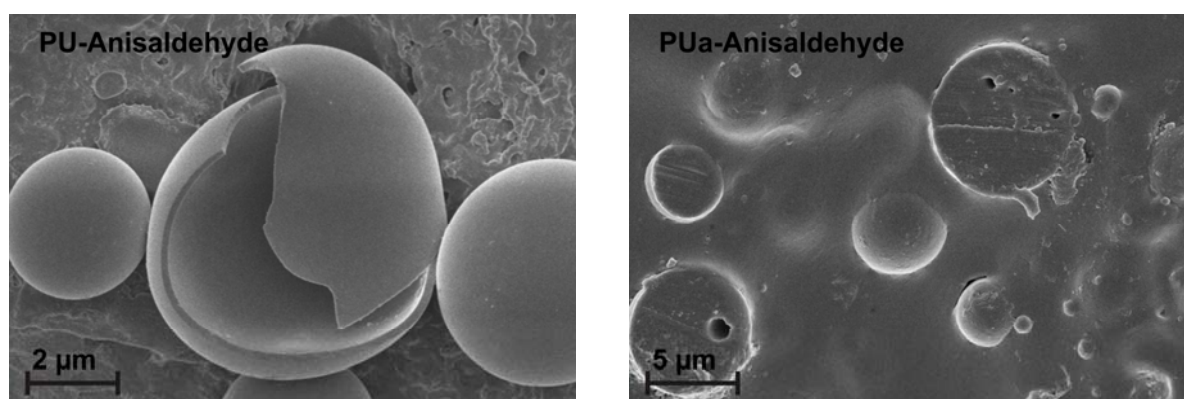


**Fig.24.** SEM images of crushed PU and PUa capsules containing anisaldehyde.

Anisaldehyde-containing (**fig.24**) capsules look similar: the shape is spherical, the surface is smooth. Nevertheless the morphology is different: PU-anisaldehyde capsules have well-defined core-shell structure, whereas PUa-anisaldehyde capsules are compact with some spherical cavities. The cavities can be either the result of phase separation between the solvent and polymer or inclusions of CO<sub>2</sub> gas formed due to the side reaction of isocyanate prepolymer with water.

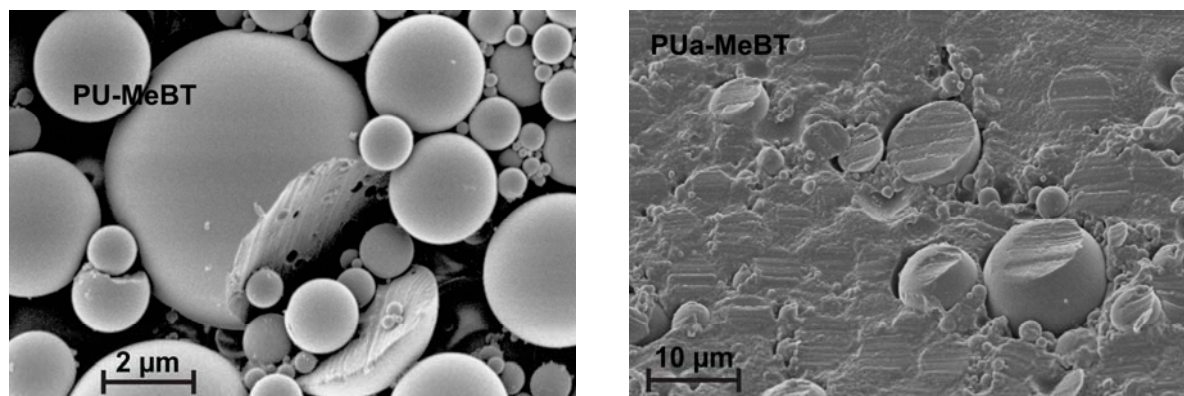


**Fig.25.** SEM images of crushed PU and PUa capsules containing MeBT.

Capsules containing MeBT (**fig.25**) also look similar: the shape is spherical, the surface is smooth. Both types of capsules are compact.

From the analysis of outer appearance and morphology of the capsules made of different solvent-polymer combination one can conclude the following: neither spherical nor irregular shape (with folds and concavities) of capsules can be attributed to certain morphology of capsules. Additional analysis such as TEM (when possible) or SEM of crushed capsules is always needed to draw conclusions on capsule morphology. Only appearance of completely collapsed capsules can be an evidence for core-shell morphology of the polymeric capsules.

For the 24 polymer-solvent combinations presented here three general types of capsule morphologies were observed: core-shell morphology with well defined solid polymeric shell and core consisting of solvent; compact morphology with polymer distributed homogeneously over the capsule volume; multicompartiment morphology somehow in between the ones described before: polymer is separated from the solvent in the form of grains, polymer grains are homogeneously distributed over the capsule volume. The polymer grains can vary in size: for PUa-chloroform or PUa-DMPH capsules the grains are easy to distinguish, while in some cases distinguishing between compact and multicompartiment morphologies is problematic (PU-chloroform and PUa-CHn capsules).

The morphology of capsules is not solvent or polymer specific, but it is specific for every polymer-solvent combination. The morphology is therefore the result of the specific polymer-solvent interactions, which are specific for every polymer-solvent pair. The summary effect of these interactions leads either to the separation of two components or to their mixing. When the solvent-polymer interactions are thermodynamically favorable solvent molecules will distribute homogeneously inside the polymer matrix. Formation of compact morphology is therefore an analogue of the swelling process. In order to find the correlation between capsule

morphology and swelling behavior of polymer, pure PU, PUa and PA polymers were additionally synthesized.

### **V.3.3. Synthesis of pure polymers**

The synthesis of pure polymers is not a trivial task, since the properties (which reflect both the composition and the structure) of pure polymers should be equal (or at least similar) to the properties of polymers present in the synthesized capsules. One should keep in mind that the way of polymer matrix development and arrangement depends on the quality of the media, where the development happens. Therefore polymers formed in different media (solvents) can in principle vary in their properties due to the different arrangement of the polymer chains<sup>138</sup>. The chemical composition is nevertheless very similar, since the polymers are synthesized from the same building blocks. The aim is therefore to synthesize pure polymer that would be at least chemically equal to the polymer from the capsules.

The straightforward solution would be to synthesize polymers from bulk. But in the present case this is problematic due to two reasons:

--the ratio of the reactive monomers is not known, because the reaction happens on the interface; the monomers ratio in this case is determined by the penetration speed of water-soluble monomer into an oil phase.

--both isocyanate prepolymer<sup>139</sup> and TPhCl<sup>140</sup> may undergo side reaction with water, giving side products which would change the chemical composition of the polymers.

Therefore it was decided that the synthesis of the pure polymers should be heterophase; the composition of the oil and water phase should be kept the same as for the synthesis of capsules. The usage of any additional solvents for synthesis was avoided, since even slight contamination of the polymer with solvent could change the polymer properties dramatically.

The pure PU and PUa were synthesized in the same manner as solvent-containing capsules with the only difference: no solvent was added to the oil phase (isocyanate prepolymer is liquid and served as the oil phase itself). For PA this approach can not be applied, since TPhCl is a solid substance. The synthesis of PA polymer was performed on the toluene-water interface (planar). TPhCl was dissolved in toluene (inert solvent), the composition of the water phase was the same as for the capsules synthesis. The film forming between two phases was collected.

#### V.3.4. Swelling behavior of pure polymers and its correlation with capsule morphology

The swelling behavior of the three synthesized pure polymers in 18 different solvents was investigated. The solvents were: EtOH, MeOH, acetone, toluene, chloroform, CH<sub>n</sub>, DMPH, DEPh, DOPh, anise aldehyde, MeBT, THF, styrene, N-methyl-2-Pyrrolidone, dimethyl sulfoxide, 1-dodecanethiol, 2,2,2-trifluoro ethanol, 1-hexanol, diaminocyclohexane. The solvents were chosen in such a manner as to cover a broad variety of solvency properties, which were estimated on the basis of the Hansen solubility parameter values. The values of HSP were taken from the HSP database available at <sup>141</sup>. The HSP solubility parameters of the chosen solvents are listed in **Table 1**. The results of the swelling experiment are schematically represented in **fig. 26-28**.

The threshold value of the swelling was evaluated in order to divide the solvents into two groups. If one considers the formation of compact morphology as an analogue of swelling, the threshold value of swelling should be determined as the extent of swelling, that polymer should be able to achieve in order to absorb all solvent presented in the capsule. In this case all solvent will be homogeneously distributed over the polymer matrix volume and compact structures would be formed. The threshold value of swelling depends on the polymer content in the capsule and is determined as the ratio of the amount of solvent to the amount of polymer. According to the initial composition of oil droplets the threshold value of swelling was estimated as  $70/40=1.75 \text{ cm}^3/\text{g}$ . In other words if one gram of polymer was able to absorb more than 1.75 ml of solvent, the solvent was considered as a “good” solvent, otherwise the solvent was considered as “poor”.

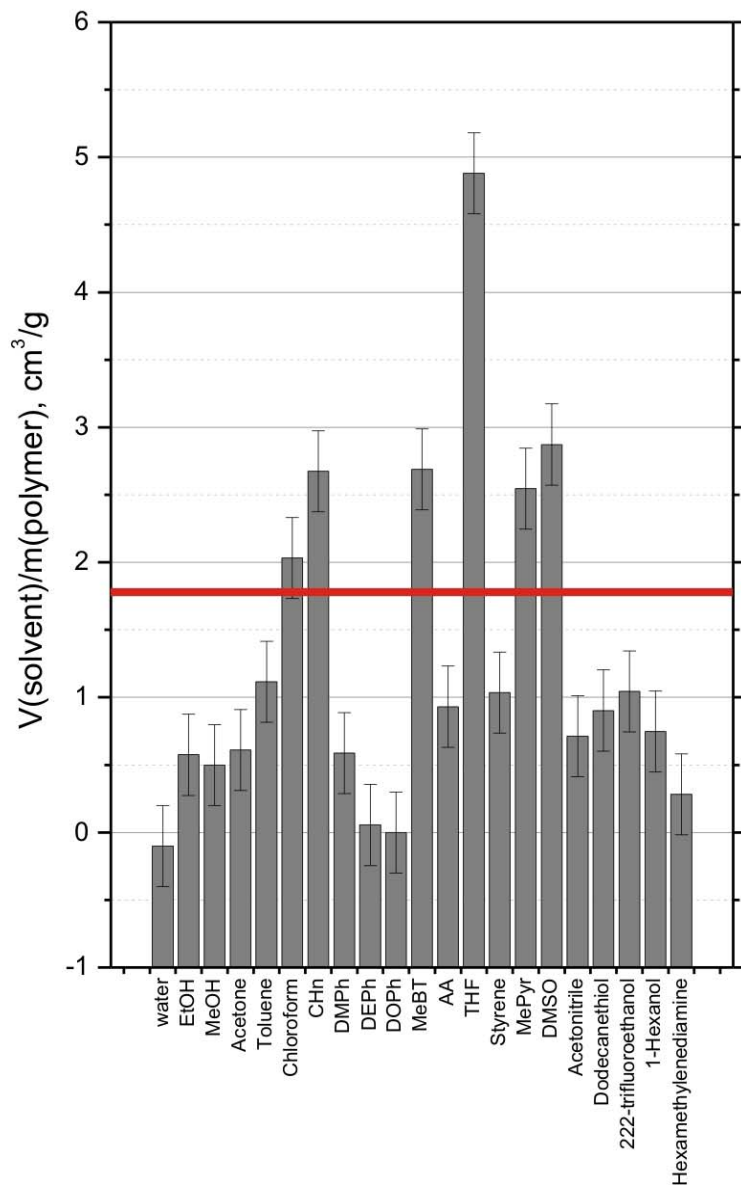


**Fig.26.** Swelling behavior of PU in chosen solvents. The red horizontal line represents the threshold value of swelling. All solvents with swelling ability more than (or close to) the threshold value are considered as “good” solvents for PU and will be located inside the solubility sphere (see further discussion).

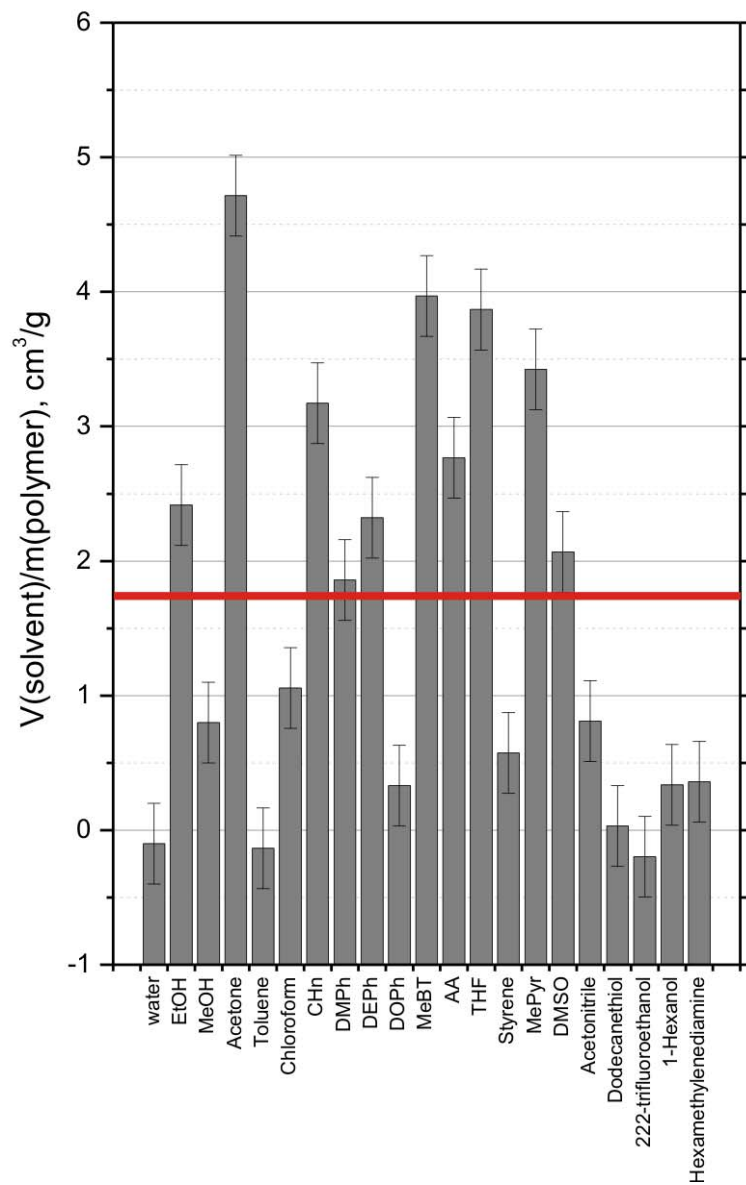


**Fig.27.** Swelling behavior of PUa in chosen solvents. The red horizontal line represents the threshold value of swelling. All solvents with swelling ability more than (or close to) the threshold value are considered as “good” solvents for PUa and will be located inside the solubility sphere (see further discussion).

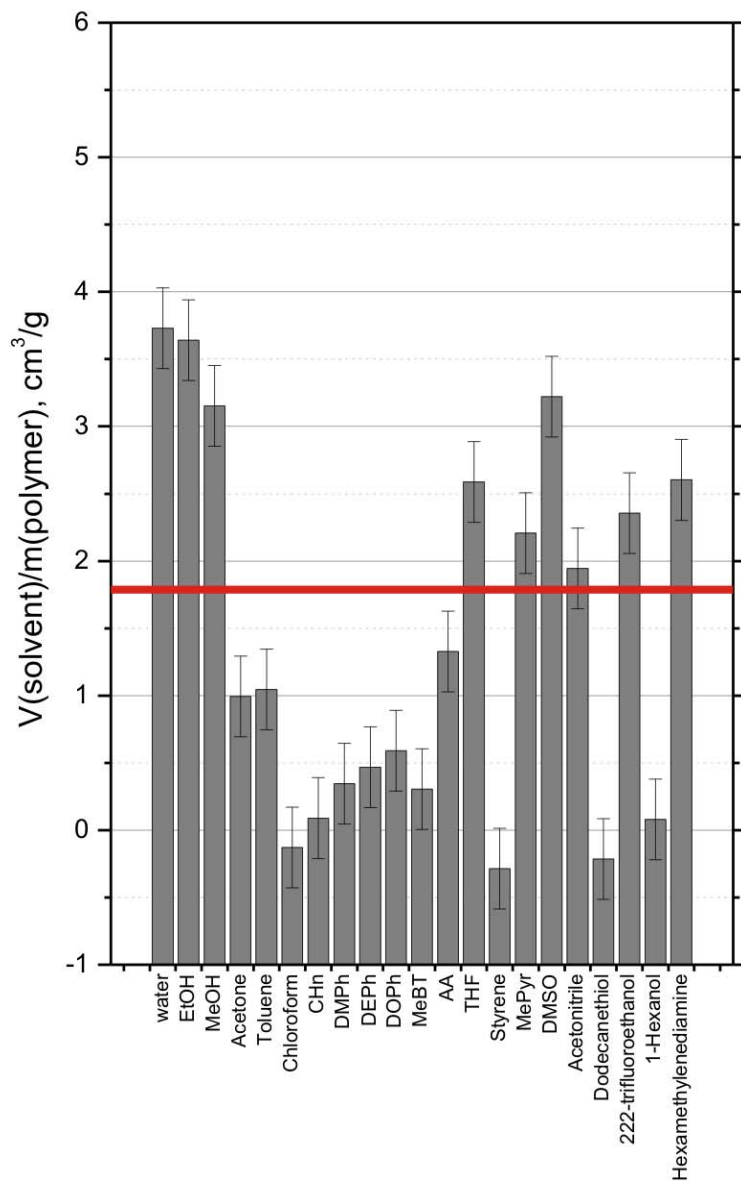


**Fig.28.** Swelling behavior of PA in chosen solvents. The red horizontal line represents the threshold value of swelling. All solvents with swelling ability more than (or close to) the threshold value are considered as “good” solvents for PA and will be located inside the solubility sphere (see further discussion).

It is of high importance to note here, that the terms “good solvent” and “poor solvent” are not used in classical meaning. That means that they are not attributed to the classical Flory  $\chi$  solubility parameter<sup>142</sup>. Here the term “good solvent” is attributed to certain swelling ability of a polymer (more than threshold value); for the “poor solvent” the swelling ability is less than threshold, determined above.

Polymer/ solvent	PU		PUa		PA	
	Core-shell?	„poor“ solvent?	Core-shell?	„poor“ solvent?	Core-shell?	„poor“ solvent?
Toluene	+	+	+	+	+	+
Chloroform	-	-	+	+	+	+
Cyclohexanone	-	-	-	-	+	+
Dimethylphthalate	+	+	-	+	+	+
Diethylphthalate	+	+	-	-	+	+
Diethylphthalate	-	+	+	+	+	+
Anisaldehyde	+	+	-	-	+	+
2-methyl benzothiazole	-	-	-	-	+	+

**Table 2.** Correlation between swelling behavior of polymers and morphology of the resulting capsules. The “+” and “-” are positive and negative answers to the questions about capsule morphology and solvent property. If the both answers are either positive (or negative) correlation between the swelling behavior and capsule morphology is concluded; the pair of table cells corresponding to a certain polymer-solvent combination marked green. If the answers do not coincide the pair of cells is marked red.

Swelling behavior of pure polymers in most cases correlated with the morphology of the resulting capsules. The capsules, containing “good” solvent, exhibit compact structures, while when the poor solvent is encapsulated the core-shell morphology is observed (**Table 2**).

Only in two cases the morphology of capsules and the swelling behavior of the pure polymers do not correlate: PU-DOPh capsules have compact morphology, while the pure polymer does not swell in DOPh; the same holds in the case of PUa-DMPH capsules.

The correlation between the swelling behavior of polymer with the structure of capsules was expected, since the morphology reflects the polymer-solvent phase behavior. The final state of

the polymer-solvent mixture can be achieved from two different directions or by two different pathways:

-- preformed polymer brought to the contact with a solvent. This pathway describes the swelling experiment.

-- formation of the polymer happens in the solvent. This pathway reflects the process of capsules formation.

If the process of swelling is reversible, the equilibrium state of a system of certain composition does not depend on the way it was achieved. Therefore the final state of the polymer-solvent mixture should be independent of the pathway. The latter would mean the existence of correlation between the swelling experiment and the capsule morphology.

The mismatch in case of PU-DOPh and PUa-DMPH can be explained in a few ways. One way to explain the mismatch is to assume that the equilibrium was not achieved in the swelling experiment. It is known that the kinetics of polymer dissolution and/or swelling can be very slow due to extremely low mobility of the polymeric chains, especially for the crosslinked polymers. Some polymers being formally soluble need an extremely long time in contact with the solvent to achieve equilibrium.

Other reason can be incomplete identity of the pure polymer and polymer from the capsule due to the difference in the media of synthesis. The difference in synthesis media can lead to the formation of polymers with different crosslinking density and conformation<sup>138</sup>. Both of these parameters can influence the swelling ability of polymers.

Another reason is attributed to the difficulty of distinguishing between the structures. In the present work three possible morphologies are considered: core-shell, compact and multicompartiment. The distinction between the two latter ones is not trivial due to possible microphase separation. In this case polymer would form a sponge-like structure with solvent distributed inside the pores. When the size of the pores is small enough they are not visible by SEM; the morphology can be attributed to the compact one, even formally phase separation is happened. Such phase separation is possible due to the gelation of crosslinked polymers. If phase separation happens before the gelation point is reached, the forming polymeric (or oligomeric) species are mobile and form a macrophase. If phase separation happens after gelation, the polymer conformation at the point of gelation gets “frozen”, the polymer chains loose their mobility. The continuation of the polymerization process leads to the formation of cavities filled with the solvent, which is pushed away from the polymer matrix after the moment of phase separation.

Most probably none of the factors described above can be excluded, in reality they all would interplay leading to appearance of mismatches similar to the ones described here. Nevertheless according to the present analysis in 22 cases of 24 the swelling behavior correlates with the morphology of the resulting capsules. The result would be the explanation of the capsule formation processes leading to the formation of different morphologies in terms of “good” and “poor” solvent.

One can imagine the whole process of capsule formation as follows. Let us consider one single droplet (see **fig.29a**) of solvent with dissolved monomer 1. This droplet is immersed into water solution of monomer 2. At the moment when these two phases come into contact, the polymerization reaction starts. Until a certain moment of time (the point of gelation <sup>143</sup>) the system keeps a certain extent of mobility. The oligomers of relatively low molecular mass do not stick to each other and consequently can move; the molecules of the solvent are mobile, too.

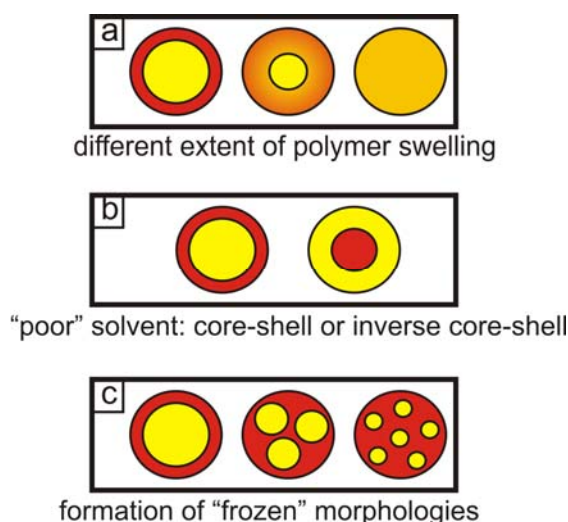


**Fig.29.** Possible capsule morphologies for two-component system solvent-crosslinked polymer (see the description in the text)

In case the solvent is a “good” one, on the step of the formation of oligomers the gradient of chemical potential of the solvent will appear between the center of the droplet (where the concentration of the polymer is zero) and the sphere surface (where the concentration of polymer or oligomers is relatively high). Due to this gradient a flow of “good” solvent towards the sphere surface will appear. An opposite gradient for the oligomers will be directed towards the center of the droplet and will cause the flow of oligomers into this direction. Consequently, the dilution of the polymer molecules on the surface and an increase of polymer concentration in the center of the sphere occur. As a result, after reaching the

gelation point one will find an infinite network with solvent homogeneously distributed in the network, or a gel (**fig.29a, right**).

In the case of a “poor” solvent the driving force of mixing of two types of molecules inside the sphere is absent; the oligomers will stay at the place they were formed, close to the droplet interface. The latter will lead to the formation of well-defined core-shell morphology (**fig.29a, left**).

If the polymer can absorb just a certain part of the solvent, one will obtain a core-shell particle, but the thickness of the shell will be higher compared to the case when the polymer does not swell at all (**fig.29a**). The higher the swelling ability of the polymer, the thicker a shell will be formed, leading in the limit case to a shell thickness equal to the particle radius, or “compact” particle.

In the case of a “poor” solvent the driving force of mixing of two types of molecules inside the sphere is absent. Nevertheless the presence of solvent on the surface of the droplet can be energetically favorable (solvent is more surface active than the oligomers formed). In this case solvent molecules will tend to concentrate on the droplet surface replacing the oligomers and leading to the formation of inverse core-shell structure (**fig. 29b**).

Usually the swelling ability of the polymer decreases with the increase of polymer molecular mass and degree of crosslinking. Therefore theoretically a situation can appear where a certain solvent is a “good enough” solvent for oligomers but a “poor” solvent for the polymer. In this case the oligomers will diffuse to the droplet interior and undergo crosslinking there. After the gelation point is reached the mobility of these polymer networks will be “frozen”. The following increase of molar mass or/and degree of crosslinking can lead to the situation where the formed polymer is not “compatible” with the solvent anymore. The latter will induce shrinkage of the polymer network and release of the solvent in the existing cavities leading to the formation of porous or multicompartment structures (**fig.29c**). The size and the number of pores will depend on the difference of the swelling abilities of the polymers with different molecular mass and degree of crosslinking.

The dependence of the capsule wall thickness on swelling ability of the polymer was predicted. According to this polymers with higher swelling abilities should lead to the formation of capsules with thicker walls. The latter, however, was not found, which can be explained by the high vacuum used for the SEM analysis. Application of high vacuum leads to the evaporation of solvent, resulting in shrinkage of the polymer. The conventional SEM used here is therefore not appropriate for the estimation of capsule wall thickness. The conclusions about capsule wall thickness can not be made on the basis of data presented here.

Analysis of capsule wall thickness should be performed either by means of cryo SEM or environmental SEM in order to avoid the evaporation of the solvent.

Formation of inverse core-shell structures was not detected neither. In order to achieve inverse core-shell structure the oligomers forming on the surface of the droplet should be first detached from the interface. For the big species with a certain surface activity the latter can be problematic. The inverse core-shell structure therefore being energetically favorable can be restricted kinetically due to the high activation energy of the process.

#### **V.3.4. Flory theory vs. Hildebrand theory**

In the previous section the process of capsule formation was explained; the resulting capsule morphology was attributed to the mixing behavior of the polymer-solvent pair. This approach allows predicting the morphology of capsules made of certain polymer-solvent pairs on the basis of swelling behavior of the polymer in this system. This approach is very similar to the Flory approach; the term “good” and “poor” solvents originally come from Flory theory<sup>142</sup>. The definitions of “good” and “poor” here, however, differ from the original meanings. The Flory theory is one of the classical approaches used nowadays in the polymer solubility characterization particularly due to its elegance and strong mathematical background. Having a great qualitative predictive power, it did not allow quantitative prediction of phase behavior of polymer solutions, especially in the case of polar substances. Therefore various attempts to modify the theory were made. To discuss all of them here does not seem to be possible due to the size limitation of the present work. Main attempts of Flory-Huggins theory modifications are described for example in<sup>144</sup> and assume introduction of additional terms into the equation for the free energy of mixing. The main disadvantage of the Flory approach and also the approach presented above from the point of application is that one should deal with a pair of components and estimate their affinity to each other. In practice the design of the capsules assumes the trial of a great number of polymer-solvent combinations; more complex systems consisting of three, four or even more components are often used. Evaluation of the swelling behavior of each component pair of such systems becomes unreasonable.

The solubility parameter approach<sup>145</sup> is more advantageous in this sense, since the properties of each single component instead of the pair of components are considered. The solubility parameter approach was developed by Hildebrand and is based on the “*similia similibus solvuntur*” principle. The principles of Hildebrand solubility parameter theory and its modification in the form of Hansen Solubility Parameters theory will be discussed in the next section.

### V.3.5. Hildebrand and Hansen solubility parameters

Molecular materials exist as liquids and solids over certain ranges of temperature and pressure because in some circumstances the liquid and solid states are more stable than the gaseous state; that is, there are energetic advantages in having the molecules arranged in either random or ordered close-packed configurations. In condensed phases, the strong attractive or cohesive forces existing between the molecules give rise to considerable negative potential energies relative to vapor phase molecules which have negligible potential energy arising in this way. Ionic liquids and crystals have even stronger attractive forces arising from coulombic interactions. The stabilizing or cohesive effect in condensed phases can be expressed in terms of cohesive energy density (cohesive energy per unit volume),

$$c = -\frac{U_m}{V_m}$$

where  $U_m$  is the molar internal energy and  $V_m$  is the molar volume.

Cohesive energy density was the basis of the original definition by Hildebrand in 1936<sup>145</sup> of what is now generally called the Hildebrand solubility parameter,

$$\delta = \sqrt{c} = \sqrt{-\frac{U_m}{V_m}} = \sqrt{\frac{(\Delta H_m - RT)}{V_m}},$$

where  $\Delta H_m$  is the molar vaporization enthalpy.

This parameter was intended for nonpolar, nonassociating systems, but later the concept was extended to all types of systems.

The basis of the cohesion parameter approach to interactions may be stated as follows<sup>146</sup>: A material with a high  $\delta$  value requires more energy for dispersal than is gained by mixing it with a material of low cohesion parameter, so immiscibility results. On the other hand, two materials with similar  $\delta$  values gain sufficient energy on mutual dispersion to permit mixing. In conclusion the closer the  $\delta$  values of two substances, the more the possibility that they will be miscible. This concept is attractive for practical applications because it aims to predict the properties of a system using only the properties of its individual components: in principle no information on the mixed system is required.

Hansen<sup>147-151</sup> proposed a practical extension of the Hildebrand parameter method to polar and hydrogen bonding systems, primarily for use in polymer-liquid interactions. It was assumed that dispersion, polar and hydrogen-bonding parameters were valid simultaneously, related by:

$$\delta^2 = \delta_D^2 + \delta_P^2 + \delta_H^2$$

The values of each component are determined empirically on the basis of many experimental observations. The essential improvement of the Hansen approach compared to the Hildebrand's one is that in the former all three parameters for two substances under consideration should simultaneously "fit", making Hansen's approach much more precise in prediction of polymer swelling/solubility behavior <sup>151</sup>.

For the practical procedure, the three Hansen solubility parameters (HSP) are used as coordinates on the three orthogonal axes for a 3D solubility graph. A point with these coordinates on the graph represents a chosen substance with the corresponding values of Hansen solubility parameters. The closer the points corresponding to solubility parameters of two components on a graph, the higher the possibility, that two components will show good solubility behavior. The HSP approach is very versatile and can be applied also to crosslinked polymers, when the measure of affinity of a certain solvent to a polymer matrix would be the ability to swell <sup>151</sup>.

### **V.3.6. HSP solubility spheres for PU, PUa and PA**

To construct HSP solubility spheres in general cases a three-dimensional graph is plotted in the coordinate system with  $\delta_D$ ,  $\delta_P$  and  $\delta_H$  as the orthogonal axes. The HSP of the solvents are used as the coordinates for the points on the HSP graph. Then, for a given polymer, the sphere with the certain radius should be located on a graph in such a way that the "good" solvents for this polymer are located inside the sphere, while the "poor" ones are located outside. Both the location of the sphere center and the sphere radius should be fitted. According to Hansen's handbook <sup>151</sup> in most of the cases it is impossible to find such a sphere that would fit 100%; that means that often some "poor" solvents can be found inside the sphere, while some "good" ones can be found outside. The aim is therefore to find such a sphere that will fit the majority of the points. This discrepancy or "inaccuracy" of the solubility sphere determination can be either attributed to inadequate calculation of the HSP of the chosen solvents or can point out the fact that more than three types of interactions are involved in the system. According to this discrepancy the location and the radius of the solubility sphere can vary from experiment to experiment, since they both depend on the set of solvents used and the method used for the sphere fitting. Nevertheless HSP theory at the moment is one of the most widely applied ones, since in contrast to the classical Flory-Huggins theory it accounts for the specific interactions.

The resulting three-dimensional graph is hard to present, therefore usually three projections are used. For polymers very often only the  $\delta_P(\delta_H)$  projection is used, since it is considered

that the specific interactions are responsible for the polymer separation. Here, only the  $\delta_H(\delta_P)$  projection of the 3-D HSP graph is presented (**fig.30**). The other two projections ( $\delta_H(\delta_D)$  and  $\delta_P(\delta_D)$ ) are in agreement with the one presented here.

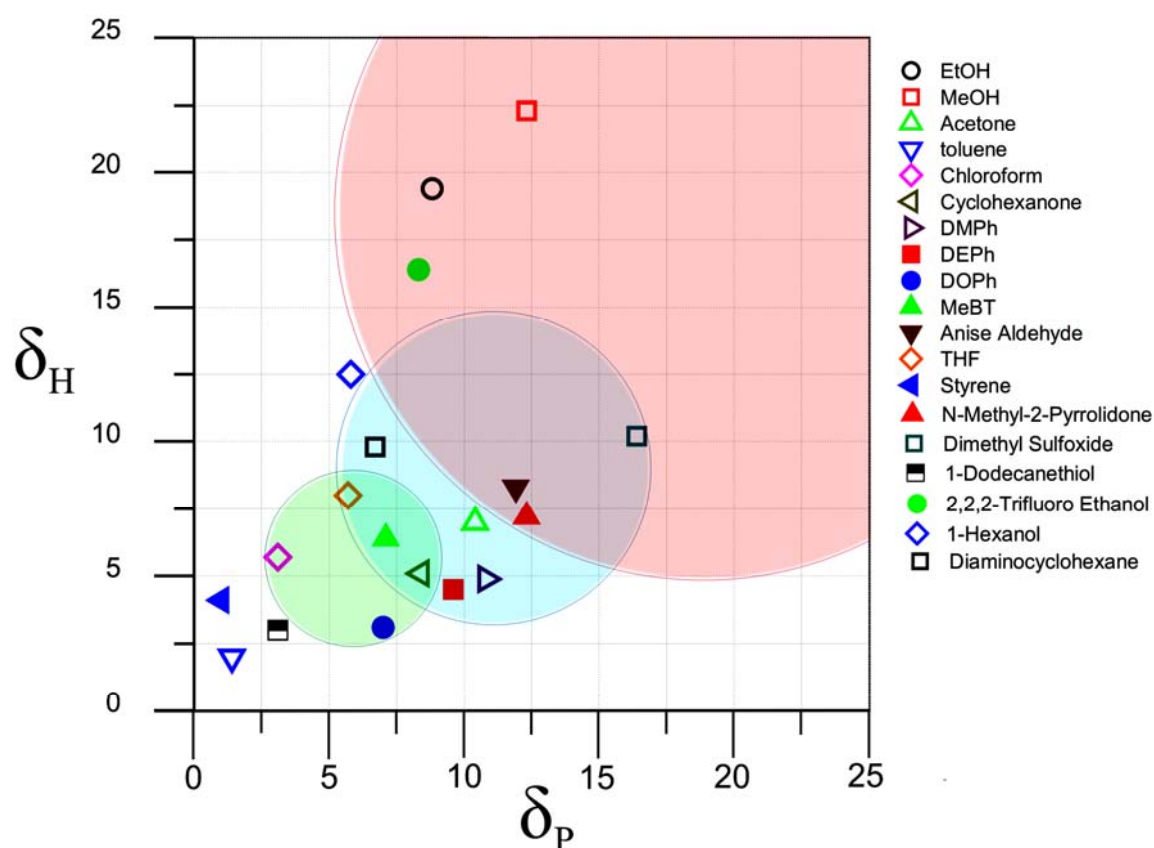


**Fig. 30.** The  $\delta_H/\delta_P$  projection of HSP spheres for PU (green circle), PUa (blue circle) and PA (red circle) constructed on the basis of the polymer swelling behavior in different solvents.

The solubility sphere is basically another way to represent graphically the solubility/swelling behavior of polymers. For every given polymer solvents located inside the solubility sphere are considered as “good” solvents, while the ones outside are “poor”. Once the solubility spheres of a polymer is found the solubility/swelling behavior is approximated to all possible substances. HSP theory allows therefore prediction of polymers solubility/swelling for any given substance with known HSP parameters on the basis of limited data set<sup>151</sup>. The latter makes the theory so attractive for applied chemistry and technology, since the choice of the system components is usually performed on the basis of big number of different parameters that should mutually match. Even slight change of the technology sometimes leads to the

necessity to find the analogue of this or that solvent in a sense of solvency but carrying different chemistry. The HSP approach is in this case indispensable.

Keeping in mind the correlation between capsule morphology and swelling one would expect that the solvents located inside the solubility sphere of a given polymer should give compact particles, while the ones located outside should yield core-shell structures. To underline one more time, the latter is valid for all substances and not only for the ones where the swelling behavior was already tested. Usage of the approach presented here opens a wide range of new possibilities for the design of capsules with desired properties. When certain morphology of capsules is required, the choice of the core material should be made according to the solubility sphere of a polymer. Or the other way around – the polymer with a certain solubility sphere should be chosen when the core material is known. All the possible substances from the appropriate region of the solubility graph (inside or outside the sphere) can be expected to give desired morphology.

Some examples of HSP application for the design of capsules with desired morphology will be given in the next sections. The benefits of the HSP approach will be demonstrated for every given system separately. The discussion of the approach in general terms does not give an appropriate perception, since the variation of possible systems is countless.

Construction of a solubility sphere can be made either on the basis of swelling behavior of polymers or of available data on the capsules morphology. As it was already shown earlier the two latter do not always coincide. When the final goal is the prediction of the capsule morphology the construction of the solubility sphere on the basis of the data on the capsule morphology (when available) is more reliable. This would help to achieve maximum similarity of the experimental conditions and avoid consideration of non-equilibrium states (discussed in Chapter V.3.4).

The weak spot of the HSP approach to prediction of capsule morphology is the construction of the solubility sphere. As it was already pointed out, the HSP approach itself is not strict, since precise determination of the solubility sphere location and radius is ambiguous and pretty much depends on the set of parameters used for the dissolution/swelling experiments. Usage of any other appropriate theory similar to the HSP one, that would be able to predict solubility on the basis of limited number of experiments, is possible. There are other modifications of the Hildebrand theory that account for different kinds of interactions and use different scales of solubility. All these theories, however, to the best knowledge of the author, are not so well-known and widely applied. Development of a theory with stronger predictive power is one of the possible ways to improve the whole approach.

## VI. Practical application

### VI.1. PU capsules loaded with water- repelling agent

Most of the attempts to create a coating with active feedback on an external mechanical impact are related to the incorporation of micro- or nanocontainers filled with various active agents. All these attempts, however, impart a single special protective feature to the substrate – either passivation of a metal surface or creating a new physical barrier in the local area of the coating integrity damage.

Here another type of active agent is proposed for incorporation in “smart” corrosion-protective coatings that principally differs from the ones mentioned above. Appropriate protection of the substrate at the damaged site is achieved by the synergetic combination of the passivation effect of the resulting film with its water-repelling properties. Passivation of the metal surface protects the latter from the reaction with corrosive species. Simultaneous creation of non-wetting conditions prevents the contact of water (and dissolved ionic species). As potential candidates for the encapsulation as the water-repelling agent organofunctional silanes, possessing a long hydrophobic tail, were chosen.

#### VI.1.1. Active material

The general formula for an organosilane typically shows the two classes of functionality<sup>152</sup>.

X is a hydrolyzable group, typically alkoxy, acyloxy, halogen or amine. Following hydrolysis, a reactive silanol group is formed, which can condense with other silanol groups leading to

the formation of three-dimensional networks.

Stable condensation products are also formed with other oxides such as those of aluminium, zirconium, tin, titanium, and nickel. Less stable bonds are formed with oxides of boron, iron, and carbon. Metals and their alloys usually have a thin layer of metal oxide on their surface. Due to the ability to form covalent bonds with the oxides

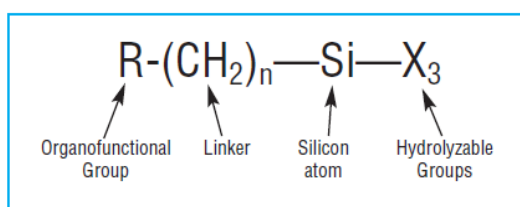


**Fig.30.** Organofunctional silane.

Reprinted from <sup>153</sup>

organofunctional silanes are conventionally used for surface treatment of metals. The R group is a nonhydrolyzable organic radical that may possess a functionality that imparts desired characteristics of the modified surfaces.

Most of the widely used alkoxy silanes have one organic substituent and three hydrolyzable substituents. In the vast majority of surface treatments, the alkoxy groups of the trialkoxy silanes are hydrolyzed to form silanol-containing species.

Reaction of these silanes involves four steps (**fig.31**). Initially, hydrolysis of the three labile groups occurs. Condensation to oligomers follows. The oligomers then hydrogen bond with OH groups of the substrate. Finally, during drying or curing, a covalent linkage is formed with the substrate with concomitant loss of water. Although described sequentially, these reactions can occur simultaneously after the initial hydrolysis step. At the interface, there is

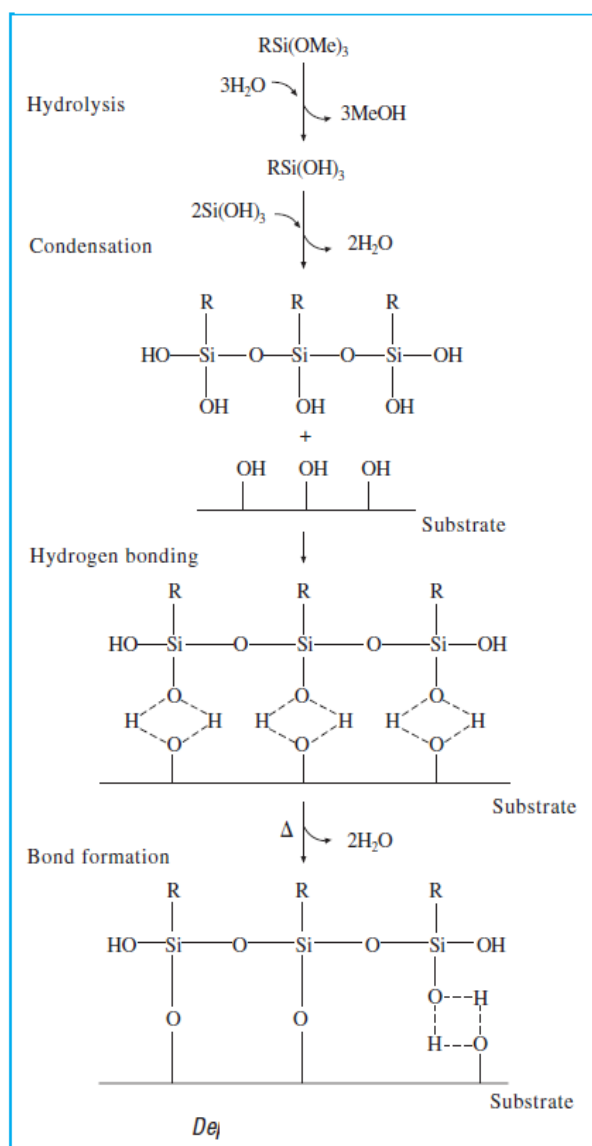


**Fig.31.** Scheme of a trimethoxysilane attachment to a substrate surface followed by hydrolysis and condensation reactions. Reprinted from <sup>153</sup>

usually only one bond from each silicon of the organosilane to the substrate surface. The two remaining silanol groups are present either in condensed or free form. The R group remains available for covalent reaction or physical interaction with other phases. Of the alkoxy silanes, only methoxy silanes are effective without catalysis.

Depending on the nature of organofunctional radical, alkoxy silanes can possess different functionality. Very often alkoxy silanes are used as coupling agent, being able to form a durable bond between organic and inorganic materials. Here, the alkoxy silanes possessing a long hydrophobic tail, responsible for the water-repelling properties of the formed film, were used. It was shown that alkoxy silanes with the hydrophobic tail containing eight or more carbon atoms are very effective for the surface hydrophobization of the surface of steel, aluminium, magnesium and their alloys <sup>154-162</sup>. In general if all other relevant things, factors, or elements remain unaltered, alkoxy silanes with longer hydrocarbon tail possess better surface hydrophobization than the ones with the shorter hydrocarbon tail.

The usage of C<sub>18</sub> substituent allows achieving the best results. Trialkoxysilanes usually perform better than bifunctional and monofunctional analogues.

In the present work the mixture of two alkoxysilanes with eight and eighteen carbon atoms in the hydrocarbon tail were encapsulated in a polymeric shell (MTOS and MTODS, correspondingly). The resulting containers loaded with a mixture of alkoxysilanes were introduced into a model coating. When the integrity of the coating is damaged, containers open and their content flows into the crack and spreads on the substrate surface. Exposure to aggressive ambient medium with high humidity initiates the reaction of the alkoxysilanes with hydroxyl groups on the substrate surface. Finally a highly hydrophobic film is created resulting in a passivation of the substrate surface and water-repelling properties of the damaged area (**fig.32**).

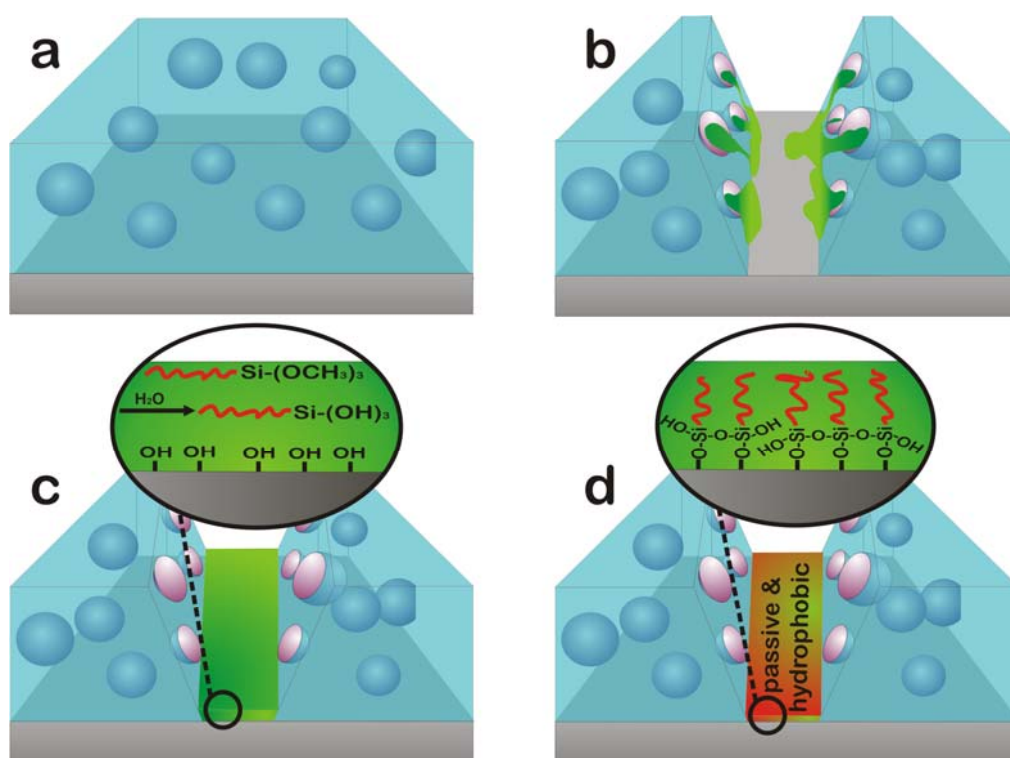


**Fig.32.** Scheme of self-healing process. **(a)** Self-healing coating containing microcontainers filled with an alkoxysilane mixture on a metallic substrate **(b)** Damage of the coating; release of encapsulated material and spreading on the metal surface **(c)** Reaction of alkoxysilanes with water from ambient medium **(d)** The surface of the damage becomes passive and hydrophobic due to the binding of silanes with long hydrophobic tail. Reprinted from <sup>163</sup>

### VI.1.2. The choice of the components

In order to achieve high efficiency of the resulting capsules a list of requirements should

be satisfied:

--The content of the active agent material should be as high as possible. The content of the component with C<sub>18</sub> substituent should be maximal in order to ensure higher efficiency of the active agent.

--The morphology of capsules should be core-shell in order to ensure as fast as possible release and spreading of the encapsulated material once the disruption of the capsule happens.

--The core of the capsules should be liquid in order to achieve the spreading of the core component over the metal surface.

--The 3-phase contact angle between liquid core component, metal surface and air (or water if the coating is designed for application in wet conditions) should allow spontaneous spreading of the liquid material over the metal surface.

The shell material should be water-impermeable in order to protect the core material from possible hydrolysis and consequent condensation leading to the deactivation of the active agent. According to the HSP map (**fig.30**) from three polymers PU has the lowest values of the  $\delta_P$  and  $\delta_H$  parameters. Water, in contrast, has very high polar and hydrogen bonding solubility parameter components. The latter allows to assume that capsules made of PU have the lowest water permeability, making PU the best candidate.

According to the first requirement, the oil phase should consist of isocyanate prepolymer (reactive monomer) and ODTMS. These two components are immiscible liquids and require therefore implementation of cosolvent, which would possess the homogeneity of the mixture, which basically means that it should be miscible with both isocyanate prepolymer and ODTMS. At the same time the addition of the cosolvent should ensure the accomplishment of the fourth requirement. The latter means that the cosolvent should be hydrophilic. The hydrophilic substance, however, is not a good solvent for the highly hydrophobic ODTMS. A compromise was found by usage of a mixture of alkoxy silanes with hydrophobic tail of different length. Short-chain reagent (MTOS containing C<sub>8</sub> hydrocarbon tail) being not as effective as MTODS will provide homogeneity of the system, while the alkoxy silane with a long tail (MTODS) will provide the mixture with high hydrophobizing capability. The introduction of inert cosolvent (DEPh), however, was still necessary; introduction of MTOS only allows to reduce the volume fraction of the inert cosolvent necessary for homogenization from 0.5 (the case with TMOS) to 0.3 (without TMOS), allowing to achieve the encapsulation efficiency of 40% vol. instead of 20% vol. (without TMOS).

In order to check the satisfaction of the fourth requirement spontaneous spreading of the liquid core material (DEPh, ODTMS and TMOS mixture, containing the amount of each component expected in the capsule core after solidification of the prepolymer isocyanate) on the surface of polished aluminium substrate was verified in 100% humidity.

The efficiency of the core component mixture for the aluminium alloy surface hydrophobization was tested. For that a drop of the mixture was placed on a freshly polished aluminium surface and allowed to spread. After that the plate was either kept under water or in 100% humidity overnight. The rest of the unreacted material was washed away from the surface either with ethanol or a big amount of water under pressure (the way of washing did not influence the result). The plates were dried, the contact angles were measured. The plates treated with the mixture representing the core material of the capsules showed a dramatic change in wetting behavior: after treatment the contact angle changed from 60 to 130 degrees (**fig.33**). The latter allowed us to consider the mixture as a promising candidate for the encapsulation.



**Fig.33.** Contact angle on aluminium alloy plates after the standard cleaning procedure (left) and after treatment (right) with solution of alkoxy silanes in DEPh (the composition of the mixture is the same as the core of the microcontainers).

The next step for the capsule preparation is to ensure the core-shell morphology of the resulting capsules. For this the HSP of each component of the mixture should be estimated. The HSP of DEPh are 17.6, 9.6, 4.5; the phase separation between PU and DEPh was already proven (see Chapter V.3.2.). The HSP database does not contain HSP for ODTMOS and TMOS. The HSP for these substances can be, however, roughly estimated. HSP for vinyltrimethoxysilane are 9.7, 4.3, 1.2. Increase of the hydrocarbon tail length would usually lead to increase of the  $\delta_D$  parameter with simultaneous decrease of  $\delta_P$  and  $\delta_H$ . According to the solubility map (**fig.34**) vinyltrimethoxysilane in combination with PU is expected to give

core-shell particles. For TMOS and especially ODTMOS the core-shell morphology is also expected, since their coordinates on the solubility sphere are expected to be out of the solubility sphere of PU.

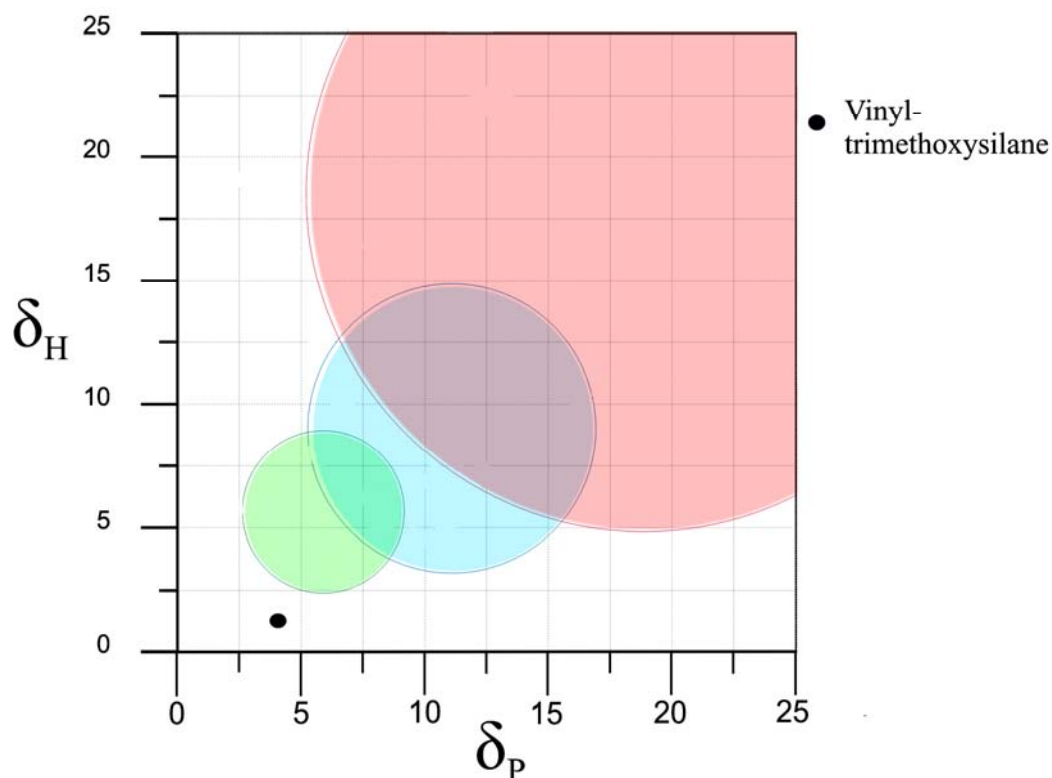


**Fig.34.** HSP solubility graph for PU (green), PUa (blue) and PA (red) with HSP for vinyltrimethoxysilane.

The PU capsules containing the mixture of DEPh and two alkoxy silanes are expected to have core-shell morphology, since each of the components is a “poor” solvent for PU.

### VI.1.3. Synthesis of capsules

PU-microcapsules containing the mixture of alkoxy silanes were prepared as follows: 1 ml of the homogeneous mixture of TMDOC, TMOS, DEPh and isocyanate prepolymer (with the volume fractions 0.2/0.2/0.3/0.3, correspondingly) was mixed with 10 ml 2wt.% aqueous PVA solution using an ULTRA-TURRAX<sup>®</sup> high-speed homogenizer (IKA<sup>®</sup> Werke, Staufen, Germany) for 3 minutes (the speed was varied within 11000-22000 min<sup>-1</sup>). The resulting emulsion was added to the buffer solution (6 ml) containing DABCO (200 mg) and glycerol (4 ml). This mixture was left for 1 hour at 65 °C under stirring. After 1 hour, heating was stopped and the solution was left without stirring overnight. The

suspension of containers was dialyzed in order to remove residual glycerol and PVA (membrane with the pore size of 12-18 KDa was used). Capsules with PU-shells containing the mixture of alkoxy silanes (PU-AlkSi) were precipitated by centrifugation. After decantation of supernatant the paste of capsules was collected. The mass weight of capsules in the paste was estimated as 65 %wt. The paste was used further for the modification of the coating.

#### VI.1.4. Characterization

For the further characterization the paste was dried on air during two days. The powder was free-flowing. The capsules could be easily redispersed in water. The optical microscope observations showed no agglomeration of capsules after redispersion. The outer appearance of the capsule powder is an indication of the successful encapsulation of the liquid material.

The mean size of the resulting capsules can be varied simply by changing the speed of the stirring on the emulsification step (**Fig.35**)

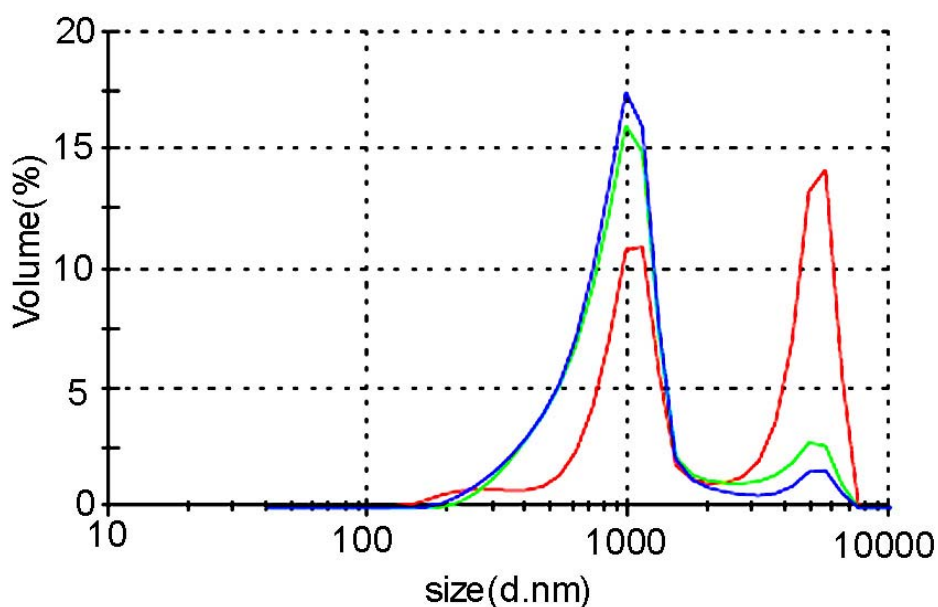


**Fig.35.** The size distribution by volume of capsules synthesized at different speed of the stirrer:  $11000 \text{ min}^{-1}$  (red),  $16000 \text{ min}^{-1}$  (green),  $22000 \text{ min}^{-1}$  (blue).

The size distribution by volume in all cases is quite broad, but one can clearly see that the average diameter of the containers decreases with the increase of the stirring speed. Irrespective of the stirring speed there are two populations of capsules: with the average

size of 1  $\mu\text{m}$  and 8 $\mu\text{m}$ . Application of high-speed homogenizers for emulsification typically leads to a comparatively broad size distribution of the emulsion droplets and consequently of the resulting containers. Nevertheless, the broad size distribution is not a problem itself, because the upper limit of the particle size is the only parameter, determining the possibility to embed them into the coating. If the containers have the diameter much smaller than the thickness of the coating, its integrity should not be noticeably affected by the incorporation of the particles. In all cases (using different rotor speeds) the upper limit of the container size was roughly 10  $\mu\text{m}$ , while the thickness of the coating was at least 30  $\mu\text{m}$ .

SEM images of the capsules synthesized at different stirring speed are presented in **fig.36**.

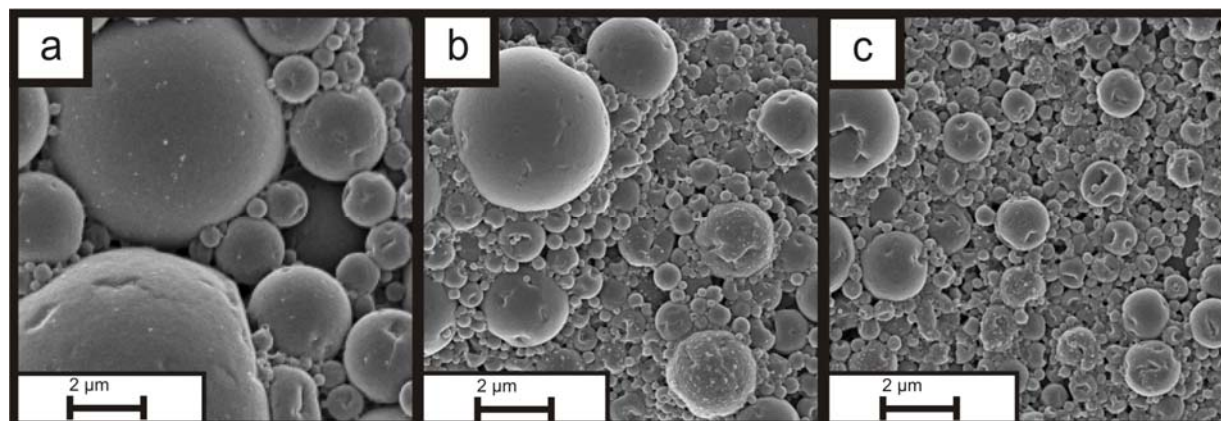


**Fig.36.** SEM image of microcontainers synthesized at different speed of the stirrer: **(a)** 11000  $\text{min}^{-1}$  **(b)** 16000  $\text{min}^{-1}$  and **(c)** 22000 $\text{min}^{-1}$

SEM images also demonstrate a substantial decrease of the capsules size with stirring speed increase. The capsules show a smooth surface and mostly spherical shape with some concavities and folds on the surface.

To determine whether the capsules have the desired core-shell morphology or not, they were crushed with the razor blade. SEM images clearly demonstrate that the morphology is core-shell. The inner part of the capsule wall is not smooth showing sponge-like structure. The structure of the inner part is attributed to the fact that, after the nascent shell is formed, the polymerization reaction takes place on the side of the organic phase, leading to the formation of extended structures on the inner side of the capsule wall.

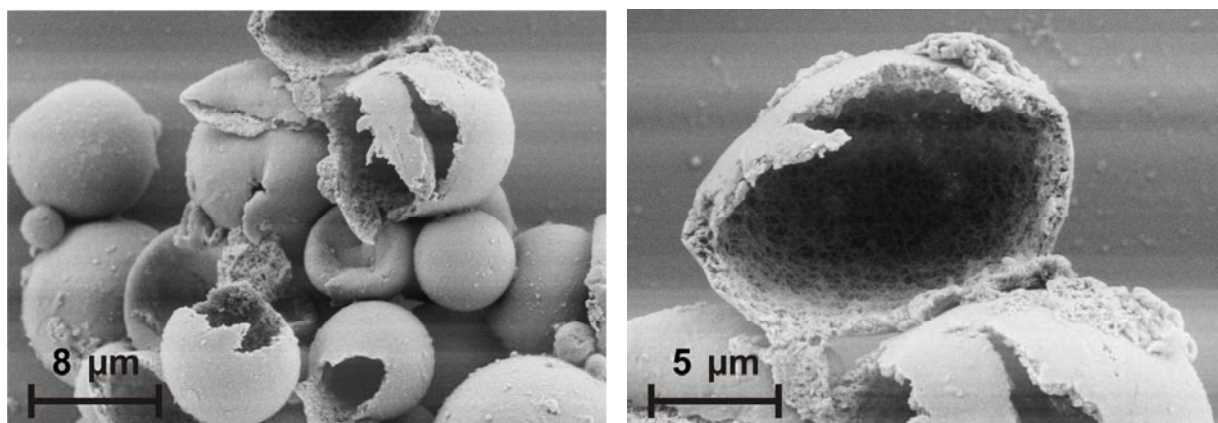


**Fig.37.** SEM images of crushed PU-AlkSi capsules.

The completion of the polycondensation reaction in the container shells was confirmed by FTIR spectroscopy (**fig.38**). A drastic decrease of the peak intensity at  $2276\text{ cm}^{-1}$  typical for the isocyanate group indicates that practically all  $\text{-NCO}$  groups were reacted.

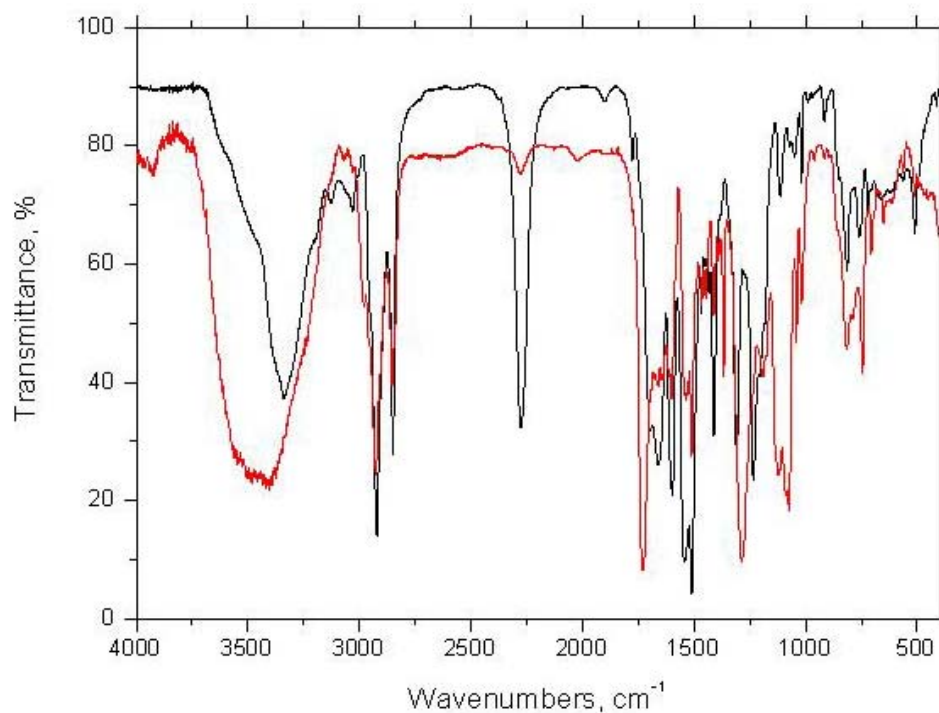


**Fig.38.** FT-IR spectra of isocyanate prepolymer (black) and resulting capsules loaded with a mixture of alkoxy silanes. Absence of the typical peak for the isocyanate group at  $2276\text{ cm}^{-1}$  for the resulting microcapsules indicates that the reaction of  $\text{-NCO}$  group with alcohol or/and water was complete. Reprinted from <sup>163</sup>

### VI.1.5 Performance of the coating modified with PU-AlkSi capsules

Synthesized PU-AlkSi capsules were introduced into the model water-based epoxy coating in the form of a paste. The curing of the resulting modified coating was performed in the same way as for the unmodified coating.

The mechanical properties of the capsules play a crucial role for the protection efficiency of the final “smart” coating. If the container shell is too hard or adhesion between it and the coating is not good enough, the containers may simply slide out from the path of the mechanical stress propagation. Therefore one should make sure that disruption of containers indeed takes place when the coating is damaged. **Fig.39** represents the cut of the coating with a high content of the containers (about 40% wt.) and clearly demonstrates that the container shells are fragile enough. The adhesion of container shell material to the coating is good: the vast majority of containers remain in the coating matrix even in the crushed state.

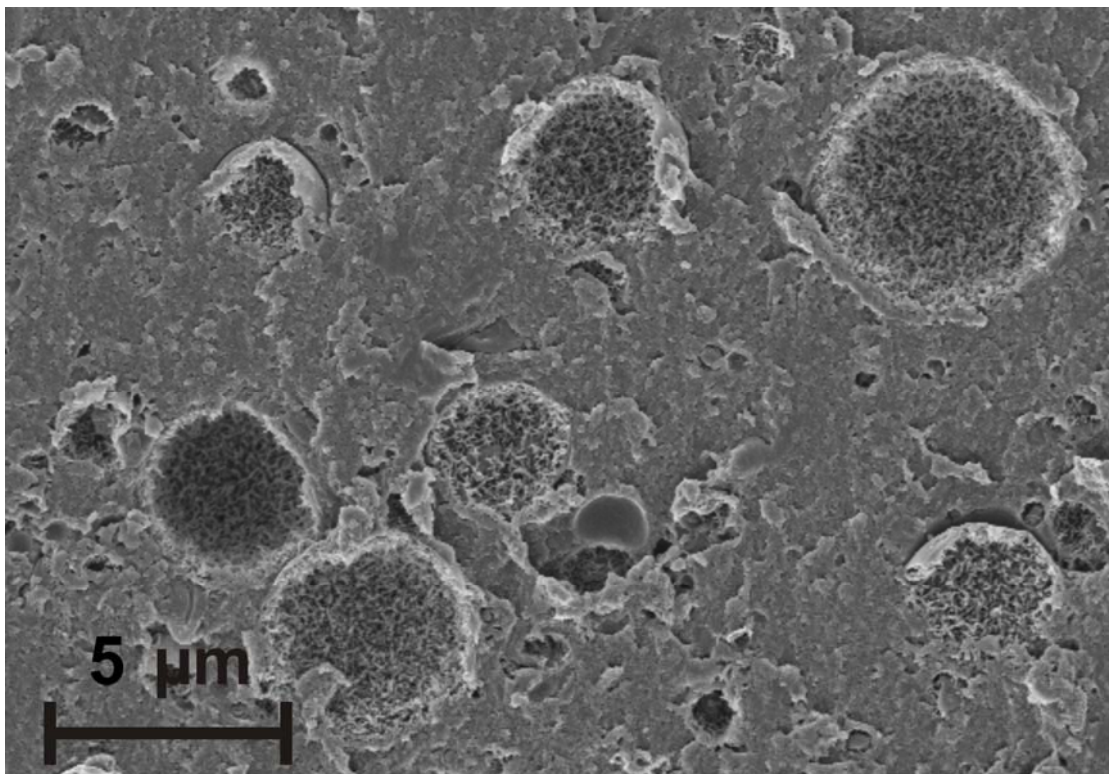


**Fig.39.** SEM image of the cut of the coating with high content of microcontainers incorporated. Reprinted from <sup>163</sup>

The investigation of corrosion-protection ability of the developed “smart” anticorrosion coating loaded with PU-AlkSi capsules was carried out via SVET. The aluminium alloy plates were covered with the model coating (control sample) and model coating loaded

with 6% wt. PU-AlkSi capsules. Damage was induced by manual scratching through the  $\sim 30 \mu\text{m}$  thick coating and into the substrate using a razor blade. The current density distribution near the metal surface was measured as a function of time. Before the SVET measurements scratched samples were left to cure for 12 hours at 100% humidity.

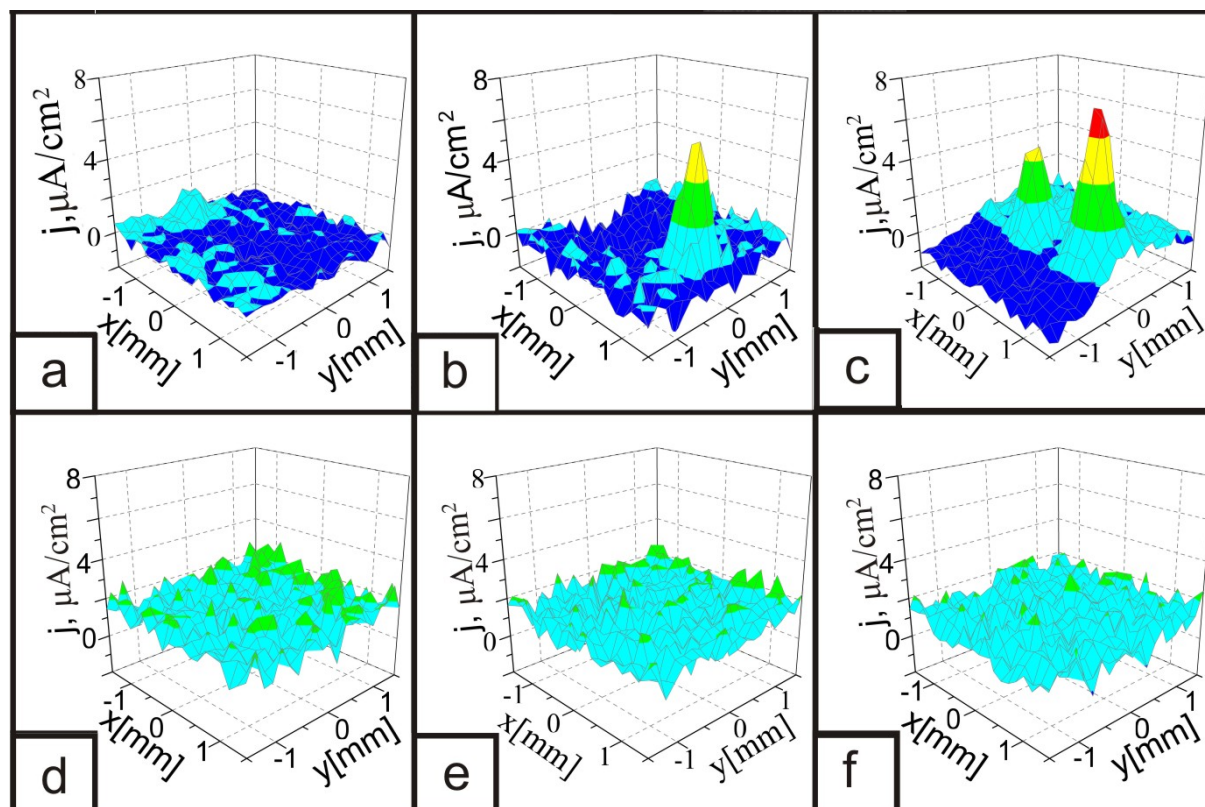


**Fig.40.** Current density maps measured via SVET after 0 (a,d), 1 (b,e) and 12 (c,f) hours of immersion in 0.1 M NaCl for control sample (model coating, a-c) and self-healing system (model coating doped by 6%wt. PU-Alk-Si microcapsules, d-f) correspondingly. Reprinted from <sup>163</sup>

The current density maps immediately, 1 and 12 hours after immersion in 0.1 M NaCl are presented for a control sample and a sample covered with epoxy film containing 6%wt. capsules (**fig.40**). Fast increase of the current density with time in the case of the control sample is observed. At the same time significant suppression of the corrosion process for samples with embedded capsules is detected.

The visual corrosion test also confirms the effectiveness of the proposed self-healing system. All control samples showed the corrosion onset already 6 hours after immersion in 0.1 M NaCl solution (the process starts with the blackening of the defect surface followed by appearance of white fluffy precipitate within the groove of the scratched

regions). In contrast, samples modified with PU-AlkSi capsules show no visual evidence of corrosion even 3 days after exposure (the surface of the scratch remains shiny).

Electrochemical impedance measurements of the aluminium plates covered with the unmodified and PU-AlkSi modified coating were performed (**fig.41**) in order to verify whether the barrier properties of the coating were disturbed by the introduction of the capsules. The Bode plot shows slight suppression of the average complex impedance of the modified coating compared to unmodified one. Nevertheless the reproducibility of the measurements is insufficient, which is probably the result of the inhomogeneity of the model coating. The model coating is a water-born two-component system; the two components should be mixed immediately before the coating application giving a suspension of epoxy component in the hardener solution. The homogenization of the coating happens due to water evaporation and dissolution of the epoxy-component followed by polymer crosslinking. Local non-ideality of the mixture can lead to the formation of defects. Since the formation of the defects is a local event, the measured properties of the system become spot-dependent, leading to the low reproducibility. The Nyquist plot shows the features of the mass-transfer processes in the unmodified coating (an increase of the  $Z'$  component in the region of the high  $Z''$ ). This is the evidence of the presence of defects, allowing electrolyte penetration.

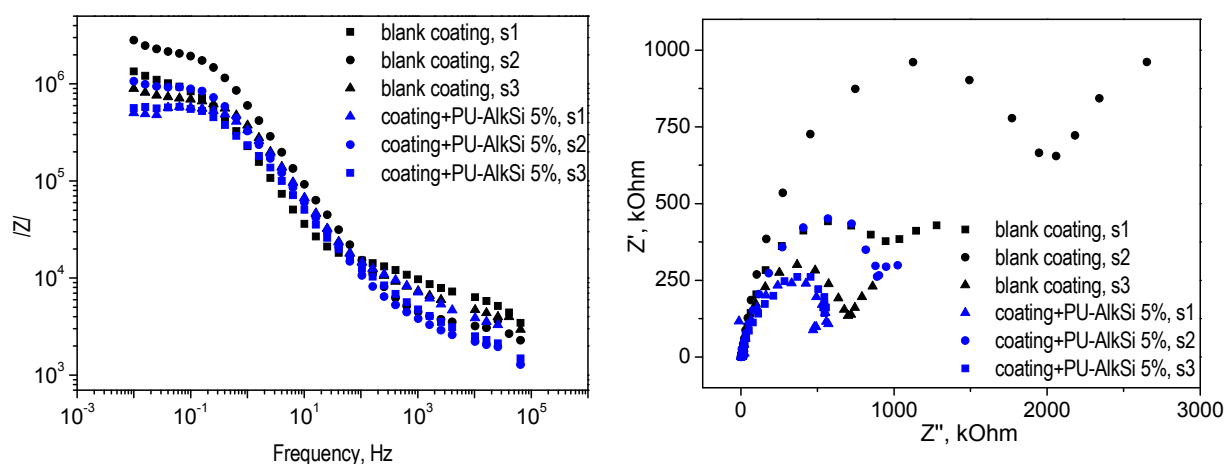


**Fig.41.** EIS measurements for the pure model coating and model coating modified with 5%wt. PU-AlkSi capsules. The Bode plot (left) represents the modulus of the complex resistivity versus frequency. The Nyquist plot (right) represents the relation between real and imaginary parts of the complex electrical impedance. Black symbols correspond to pure coating; blue ones – to the modified coating. S1,2,3 correspond to different samples.

Taking into account average impedance values, slight suppression of the coating resistivity and consequently the barrier properties due to capsule introduction can be deduced. Suppression of the coating resistivity can be due to lower resistivity of the introduced capsules compared to the overall matrix resistivity as well as due to the insufficient adhesion of the capsules to the coating matrix.

A 300 hours long salt-spray chamber test was performed in order to simulate the real corrosion behavior of the steel plates covered with unmodified coating, coating modified with PU-AlkSi capsules and model coating doped with the capsule core components directly. The SVET and electrochemical impedance measurements were performed on aluminium, since alkoxy silanes are expected to be more effective on aluminium than on steel due to the stronger Si-O-Me bond for aluminium. The standard salt-spray chamber test for aluminium, however, would take 3000 hours, which was not possible in the frame of the present work. Since the efficiency of the organofunctional silanes for the steel surface modification is expected to be lower than for aluminium, an improvement of the corrosion behavior of steel would include the improvement of the aluminium corrosion behavior as well. In case of positive salt-spray chamber test results for steel, the salt-spray chamber test for aluminium should be made.

**Fig.42** gives the comparison of the outer appearance of the plates after 300 hours exposure in the salt-spray chamber. The thickness of the darkened area around the scratch, which is an evidence of the underlying corrosion propagation, is higher for the pure PU samples than for the other two samples. At the same time the amount of pits is higher for the modified coatings than for the unmodified one. This fact is in a good correlation with the electrical impedance measurements and probably indicates that the integrity of the coating is disturbed by the capsule incorporation. Surprisingly the coating doped directly shows even better performance than the one with PU-AlkSi capsules. Usually an introduction of comparatively hydrophobic liquid would lead to a serious damage of a coating (see further the case with MeBT-doped coating) due to the phase separation of the components. In the particular case the phase separation probably did not happen, either due to the dissolution of the organofunctional silanes or due to the formation of a stable emulsion of the components in the coating formulation. The emulsion can be stabilized by the epoxy particles present in the formulation on the first steps of coating drying.

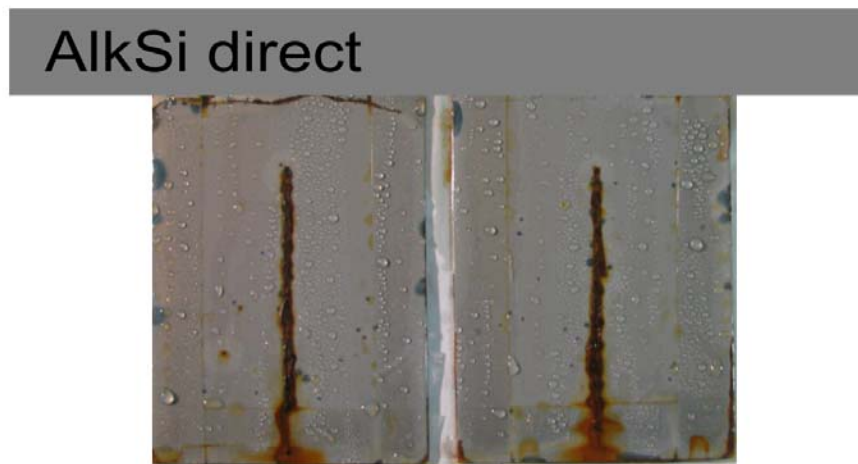
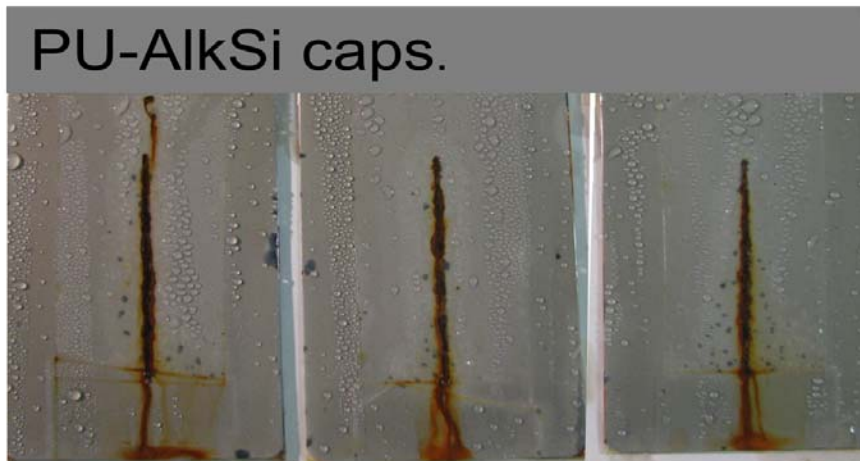
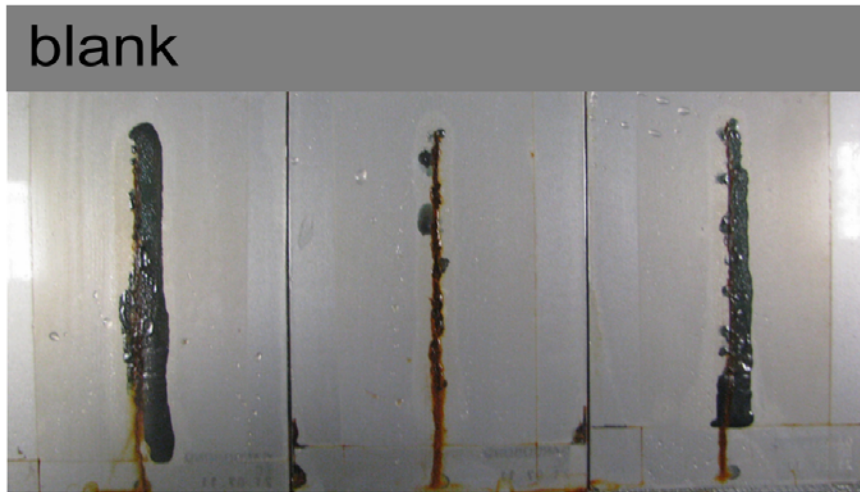


**Fig.42.** The outer appearance of 3 and 2 samples of steel plates covered with model coating (blank), coating modified with 5%wt. PU-AlkSi capsules and coating doped directly by core material of the capsules after 300 hours in the salt-spray chamber. A deep scratch (until the metal surface) was introduced before placing the plates into the chamber.

## VI.1.6 Conclusions

In general it can be concluded that the performance of the PU-AlkSi capsules is promising. The SVET measurements demonstrate sufficient local corrosion suppression. The salt-spray chamber test on steel shows sufficient reduction of the underlying corrosion for samples modified with the mixture of alkoxysilanes directly and in encapsulated state. The pitting corrosion was less pronounced in the case of unmodified coating, indicating bad distribution of capsules in the coating confirmed by the electrochemical impedance measurements. Since the performance of the modified coating on steel was good, salt spray chamber tests for the aluminium samples coated with the modified coatings definitely should be performed. Redispersion of the capsules in the coating formulation should be performed with particular care. The better or comparable performance of the directly doped coating in the particular coating case indicates that encapsulation of the material was not necessary. The same result, however, can not be expected for every coating. The encapsulation is therefore necessary in order to make the approach of organofunctional silane application coating-independent.

## VI.2. PA capsules loaded with cerium diethylhexyl phosphate

A relatively recent line of research has dealt with the development of new inhibitor compounds, designed according to the principles of green chemistry<sup>38</sup>. This research has been focused on the use of rare-earth metal compounds as an alternative for chromates. Cerium salts have been shown to provide protection for magnesium and aluminium alloys against corrosion<sup>164-168</sup>. In addition, many organic compounds that are benign to the environment are currently being investigated as potential corrosion inhibitors for aluminium alloys, in particular using combinations of organic anions and inorganic anodic inhibitors to create hybrid inhibitors<sup>169-171</sup>. A recent concept developed by Forsyth and co-workers<sup>169,172-174</sup> envisages the coupling of a rare-earth metallic element with an organic inhibitor containing multiple functional groups, in order to produce a multifunctional inhibitor with potential synergism effects between the two components. In<sup>175</sup> cerium dibutyl phosphate (Ce(DBuPh)<sub>3</sub>) was tested as a hybrid inhibitor with mixed inhibition functions and a low critical inhibitor concentration for protection of aluminium alloys. This organophosphate was chosen with the idea that phosphates and phosphonates have been employed in corrosion inhibition formulations for aluminium alloys. It was found that Ce(DBuPh)<sub>3</sub> offers superior protection when compared to CeCl<sub>3</sub>, with no discernable corrosion products, significant pitting, or evidence of replaced copper on the surface. Toxicity testing suggested that cerium

dibutylphosphate is able to fulfill the basic requirements for consideration as an environmentally friendly corrosion inhibitor.

For further application cerium dibutylphosphate has to be introduced into a coating. Direct doping of the coating is, however, problematic due to the sticky, wax-like texture of the substance. Homogeneous dispersion of the substance in a coating would meet complications, while high hydrophobicity would lead to weak adhesion of the particles to a coating matrix leading to the degradation of the barrier properties of the latter. Further, the salt-spray chamber tests results will be demonstrated in order to illustrate the failure of the direct doping. In order to improve the colloidal properties and adhesion to a coating cerium phosphate salt was encapsulated in PA.

### **VI.2.1. Synthesis of the cerium phosphate salt derivation**

The inhibitor analogous to  $\text{Ce}(\text{DBuPh})_3$  was synthesized. Diethylhexyl phosphate (DEtHePh) instead of dibutyl phosphate (DBuPh) organic substitution was used. The substance synthesis was performed according to the procedure described in <sup>176</sup>.

Cerium chloride heptahydrate was dissolved in a 100 ml ethanol-water mixture (equal volumes). 12 ml DEtHePh was dissolved in 12 ml Ethanol. The second solution was added to the first solution slowly under mechanical stirring. Formation of white flakes of precipitate was observed. The mixture was stirred over one hour to ensure the completion of the reaction. The white precipitate was collected and washed first with 500 ml of water followed by washing with 100 ml of ethanol and 100 ml of acetone in order to remove the rest of the unreacted components. The washed precipitate was dried under vacuum overnight and stored in desiccator.

### **VI.2.2. The choice of the components**

The requirements for the capsules to be satisfied:

- The content of the active material should be maximal in order to achieve high efficiency of the resulting capsules.
- The morphology of capsules should be core-shell in order to ensure good adhesion of the capsule walls to a coating matrix.

To satisfy the first requirement a solvent that would dissolve high amount of cerium salt and would not react with the oil-soluble reactive monomer (either isocyanate prepolymer or TPhCl) should be selected. A number of conventional solvents were tested; none of the solvents was able to dissolve more than 5 wt. % of the cerium salt due to the hybrid

structure of the salt represented by inorganic( $\text{Ce}^{3+}$ ) and organic components (DEtHePh anion). Even THF, well known as an effective solvent for metal-organic compounds, provided solubility less than 10% wt.

Finally DBuPh was chosen as the solvent. DBuPh has a structure, similar to the synthesized cerium salt, leading to the comparatively high solubility of the latter. The solubility of the cerium salt in the DBuPh was estimated as 20 %wt.

Usage of DEtHePh allowed to dissolve even higher amounts of cerium salt. Mixing of the final solution with TPhCl, however, led to the precipitation of some component, which was probably formed due to a cross-esterification reaction between the components. Usage of dibutyl phosphate allowed to avoid the precipitation.

In order to satisfy the second condition, an appropriate shell material should be chosen. The HSP of DBuPh are not in the HSP database, but can be estimated on the basis of HSP of DEtHePh (16.2, 6.7, 7.4) (see **fig. 43**). DBuPh is less hydrophobic than DETHePh, which would yield higher values of  $\delta_P$  and  $\delta_H$ . The cerium salt, however, contains three hydrophobic substituents (DEtHePh), which would yield higher hydrophobicity and lower  $\delta_P$  and  $\delta_H$  as the result. Therefore the solvency of the mixture was estimated to be close to the one of DEtHePh. Formation of the core-shell particles, needed for the second requirement satisfaction, is expected in combination with PA.

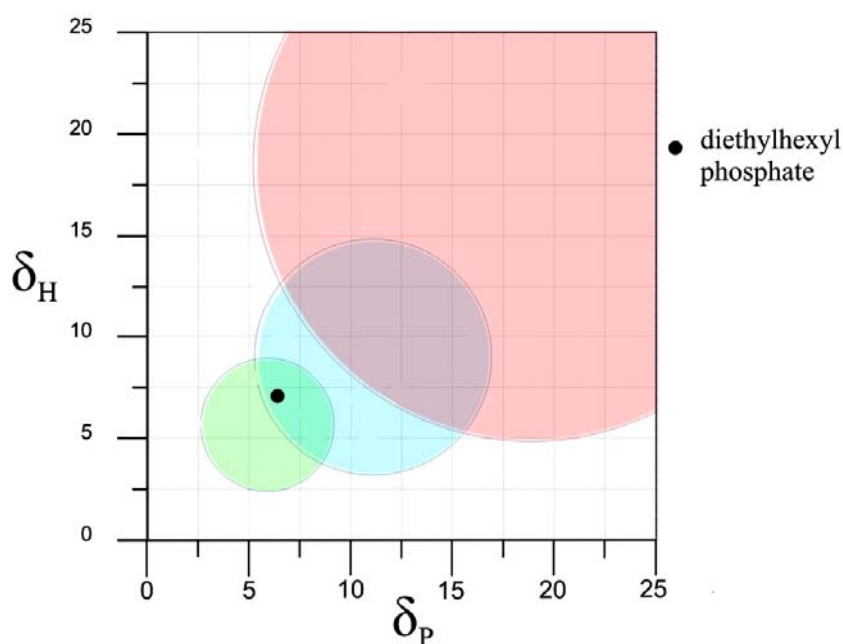


**Fig.43.** HSP solubility graph for PU (green), PUa (blue) and PA (red) with HSP for DEtHePh.

### VI.2.3. Encapsulation of cerium diethylhexyl phosphate

The organic phase for the capsule synthesis consisted of 200 mg cerium DEtHePh, 200 mg TPhCl and 1 ml of DBuPh. The mixture was transparent and stayed transparent at least for one hour after mixing (usage of soft ultrasonic bath was necessary).

The oil phase was emulsified in 10 ml 2 %wt. PVA solution by Ultraturrax at  $16000 \text{ min}^{-1}$  for one minute. The resulting emulsion was slowly added to the 20 ml of amine solution (EDA (0.91 g) and TEPA (0.4 ml) in water. The mixture was stirred for 3 hours without heating. After the stirring was stopped, the capsules (PA-Ce capsules) were centrifuged and washed three times with water in order to remove the rest of the PVA. In absence of PVA the dispersion of capsules in water needed an effort, the usage of a soft ultrasonic bath, however, allowed to obtain a homogeneous suspension. Optical microscopy showed relatively small agglomerates consisting of 3-7 capsules. After washing and centrifugation, the supernatant was decanted; the paste of capsules was used further for the coating modification. The colloidal stability of the dried paste was not excellent, like in the case of PU-AlkSi capsules, it was judged, however, as acceptable.

### VI.2.4. Characterization

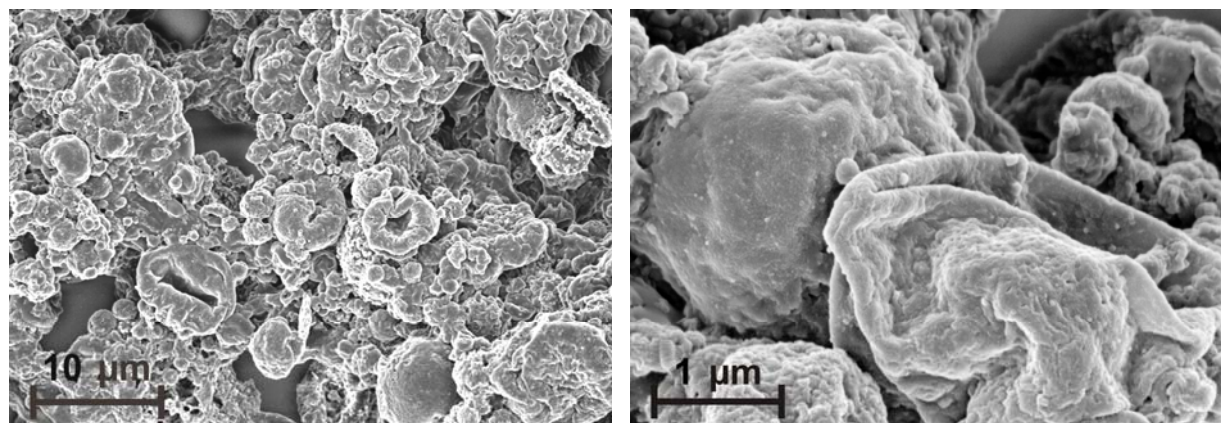
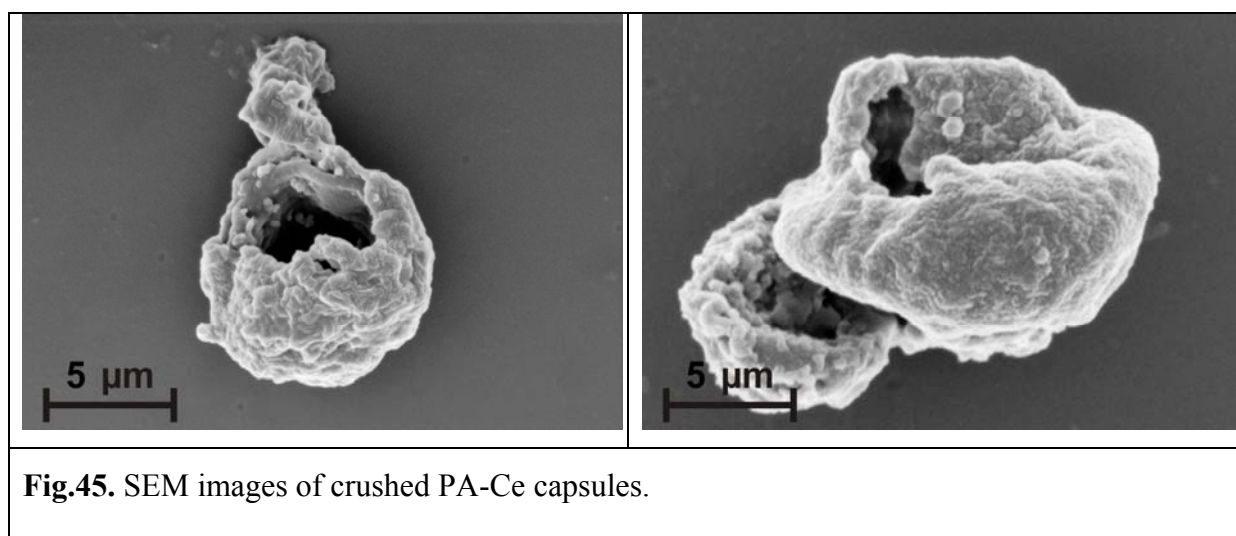


**Fig.44.** SEM images of PA-Ce capsules made with smaller (left) and higher (right) magnification.

The SEM images in **fig.44** show that the capsules have mainly irregular shape with many folds. Discrete capsules can be, however, distinguished. The walls are elastic and not destroyed during the drying procedure. The latter allows to use the capsules for further modification of the coating.

The mechanical properties of the resulting capsules were found to be strongly dependent on the type of amine used and the conditions of the synthesis. Different amines, bifunctional (EDA), trifunctional (DETA), tetrafunctional (TETA) and pentafunctional (TEPA), were tested separately and in various combinations and at different concentrations. In general it was found that usage of the combination of bifunctional and pentafunctional amines leads to the formation of capsules with the best mechanical properties. The mechanical properties were not tested directly, but were estimated by the appearance of the final dry powder (free-flowing/sticky) and by the shape of the capsules under SEM. The order and speed of solution and suspension mixing influenced the mechanical properties of the resulting capsules as well. Systematic investigation of the amine nature and synthesis conditions influencing the mechanical properties of PA capsules is necessary. The empirically found combination of the amine nature and content as well as other synthesis conditions were found satisfactory for the further application of capsules as the active part of the “smart” anticorrosion coating. The core-shell structure of the capsules was verified by SEM of crushed capsules (**fig.45**).



The SEM images show a well distinguished inner cavity. The structure of the capsule wall, however, is rather uncommon with comparatively dense and smooth inner part and bulky outer part. The reason of such wall structure is not clear.

### **VI.2.5. Performance of the coating modified with PA-Ce capsules**

An appropriate amount of the capsules paste was mixed into the model coating. The performance of the resulting hybrid “smart” anticorrosion coating was evaluated by means of impedance and salt-spray chamber test.

The bad colloidal stability of the resulting capsules is reflected in the electrochemical

impedance measurements for modified model coating. The values of the complex impedance modulus for all unmodified samples are higher than for modified ones. Even the performance of the pure coating is not very reproducible, the data can be an evidence of the bad influence of container incorporation on the barrier properties of the coating. On the Nyquist plot all curves representing modified coating lie under the worst-performing sample of unmodified coating. This is the evidence that the resistivity of the model coating is sufficiently suppressed by the introduction of the capsules. The effect is probably due to agglomeration of the particles which leads to pore formation and electrolyte penetration.

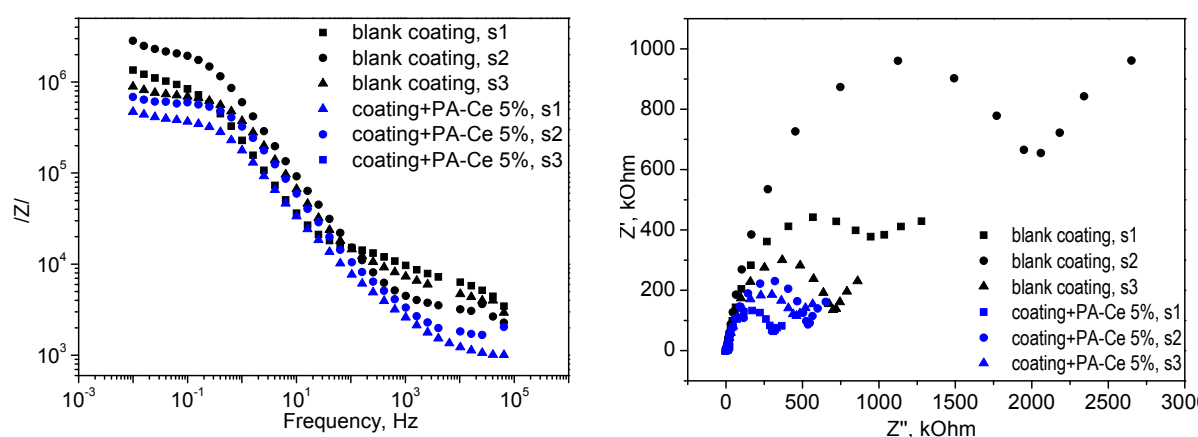


**Fig.46.** Electrical impedance measurements for the pure model coating and model coating modified with 5%wt. PA-Ce capsules. The Bode plot (left) represents the modulus of the complex resistivity versus frequency. The Nyquist plot (right) represents the relation between real and imaginary parts of complex electrical impedance. Black symbols correspond to pure coating; blue ones – to the modified coating. S1,2,3 correspond to different samples.

In order to correlate the impedance measurements with the real corrosion behavior of the modified coating the salt-spray chamber test (**fig.47**) was performed for the unmodified coating, coating modified with the PA-Ce capsules and coating modified with free cerium salt.

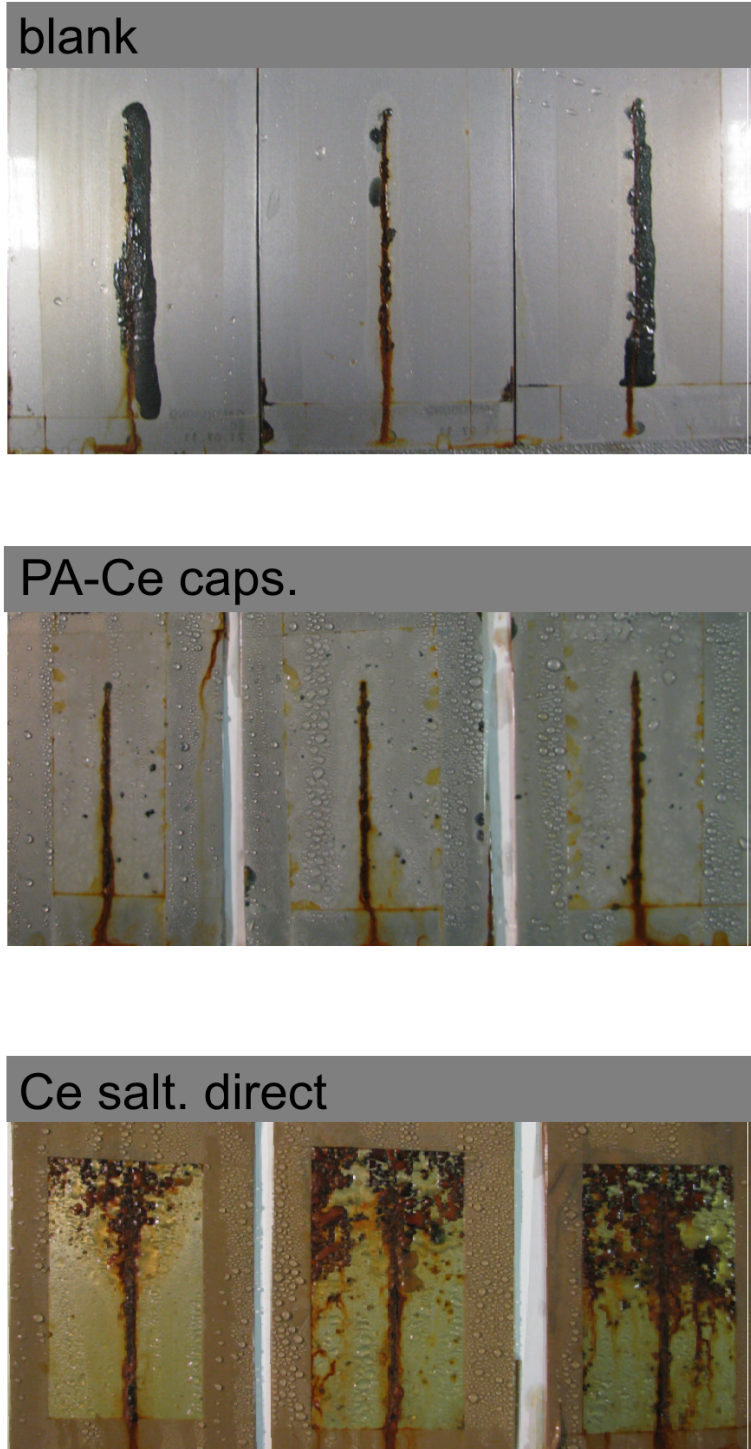


**Fig.47.** The result of 300 h long Salt-spray chamber test for the steel plates covered with unmodified model coating (blank), model coating doped with 3% wt. cerium salt and model coating modified with 5% wt. PA-Ce capsules.

As it was expected, the performance of the coating directly doped with the cerium salt can

not be characterized as acceptable. Multiple pitting covering almost 50% of the sample area can be seen. These results show that direct doping of the coating with the cerium salt causes serious destruction of the coating integrity and total deterioration of coatings barrier properties. The performance of the coating modified with the PA-Ce capsules is better, which shows that encapsulation can sufficiently improve the final coating properties. Colloidal stability of the fabricated PA-Ce capsules should be, however, further improved, since the samples covered with capsule-modified coating demonstrate a substantial amount of pits.

### V.2.6. Conclusions

Both electrochemical impedance and salt-spray chamber tests showed that the colloidal stability of the resulting capsules should be improved. For this systematic investigation of the synthesis parameters influencing the mechanical properties of the PA capsule shells should be made. Until then no further conclusions about capsule effectiveness can be made.

### VI.3. PU capsules loaded with biocide



**Fig.48.** Illustration of bio-fouling.

Microbiologically induced corrosion (MIC) is brought about by the presence of bacteria or other microbes in the environment (**fig.48**). Corrosion induced by bacteria is a recognized problem in the gas and oil industries, pipelines, municipal sewage treatment systems, the pulp and paper industry, and a variety of industrial applications. Sulfate-reducing bacteria can convert noncorrosive water into highly corrosive water through the conversion of sulfate to

sulfide. Other microorganisms can also increase the corrosivity of the environment by a variety of mechanisms<sup>177</sup>.

The most common method of prevention of fouling on ship hulls and other underwater structures uses copper or organotin containing paints. Although organotin containing coatings are highly effective, they are also dangerous to the marine environment in which they are used, because they can poison non-target organisms such as fish, vegetation, and marine mammals. Because of the increased evidence of ecosystem damage in areas close to concentrated use of tin-containing paints, application of these antifouling paints is being restricted and in some cases prohibited. Fouling release coating technologies are currently under development in response to the need for a nontoxic coating alternative to antifouling paints.

### **VI.3.1. Active material**

4,5-Dichloro-2-octyl-2H-isothiazol-3-one (DCOIT), the active component of the commercially available PARMETOL® S 15, controls a wide range of microorganisms, including fungi, algae and bacteria. As far as fungi are concerned, this isothiazolinone product inhibits the growth of many species at low use levels. Its efficiency against *Aureobasidium pullulans* (the fungus predominantly responsible for the development of mildew in exterior paints) is particularly noteworthy. Equally important from the stand point of in-can protection, this biocide also is very effective against bacteria, especially the *Pseudomonas* species that attack paints, joint compounds, roof coatings, exterior insulating and finishing systems, and clear finishes. In addition to its impressive antimicrobial capabilities, DCOIT has a number of other appealing features for formulators. Because of its isothiazolinone chemistry, it is non-persistent in the environment, breaking down readily into harmless compounds.

In practice antifouling protection is realized by direct doping of the coating with biocide. The efficiency of the antifouling protection is achieved by continuous diffusion of biocide to the coating surface. The diffusion kinetics should ensure constant concentration of the antifouling agent on the coating surface. The concentration should be high enough to terminate bacteria and fungi growth, but low enough to provide long-term efficiency of the antifouling agent. The control of the diffusion rate can be realized by the encapsulation of the antifouling agent. Variation of the capsule wall thickness and wall material would allow to control the release behavior of the substance. Encapsulation also protects the active material from the reaction with coating components.

### VI.3.2. The coise of the components

The requirements for the capsules to be satisfied:

- The content of the active material in the capsule should be maximal in order to achieve high efficiency.
- The morphology of capsules should be core-shell in order to provide the control of the release kinetics of the active component.
- The capsule wall should be only partially permeable for the active agent, which means that DCOIT should be concentrated in the liquid core.

The liquid component of the PARMETOL® S 15 is represented by a mixture of benzene derivatives similar to heptylbenzene (the chain length of the substituent varies from five to eight carbon atoms). The concentration of DCOIT in PARMETOL® S 15 is 10 wt%.

PARMETOL® S 15 was encapsulated in a PU. The choice of the polymeric shell component was performed on the basis of HSP of the components according to the second requirement for the capsules. Since the main component of the core is a benzene derivative, the morphology of the capsules will be mainly determined by its phase behavior with the chosen polymer. HSP parameters of the mixture components are listed in **Table 3**.

Pentylbenzene	17,6	2,2	2,4
Hexylbenzene	17,5	2,1	2,4
Heptylbenzene	17,4	2,6	2,9
Octylbenzene	17,2	1,8	1,9

**Table.3.** HSP parameters of benzene derivatives (see in the text)

The HSP parameters vary only slightly for the components. The average HSP for the mixture of the components can be therefore estimated as 17.4, 2.2, 2.4. The HSP map of polymers with HSP of the liquid component of PARMETOL® S 15 shows (**fig.49**) that any of the polymers can be used as the shell material, when the core-shell structure of capsules is desired.

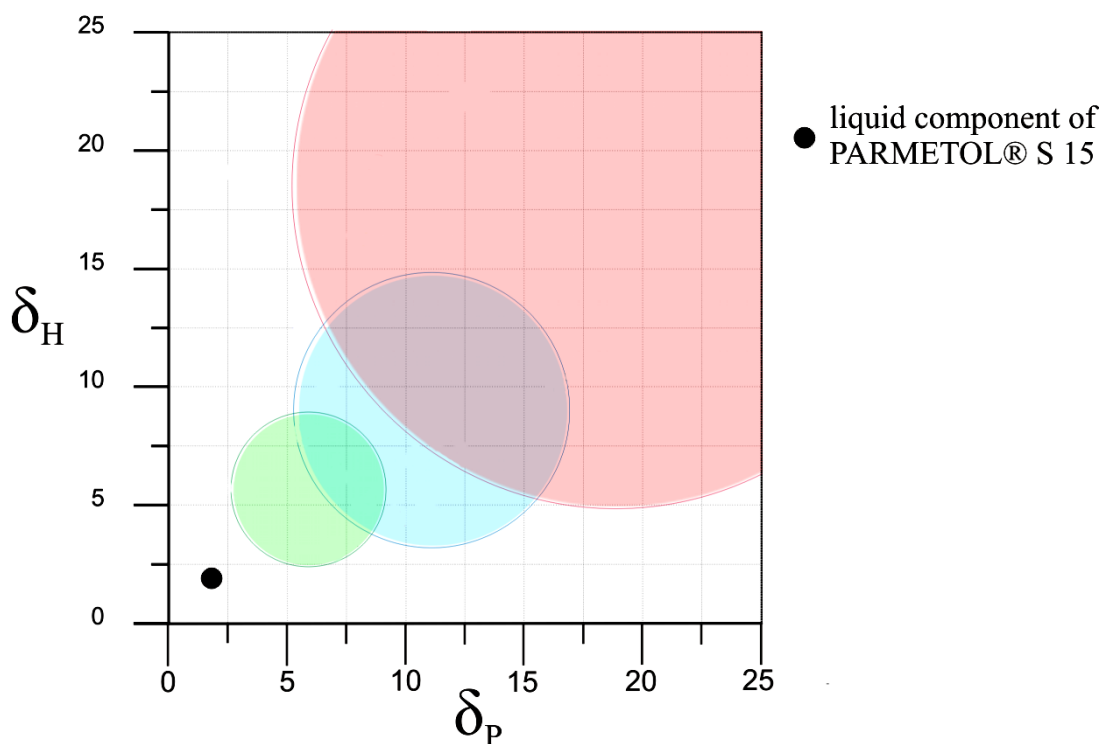


**Fig.49.** The HSP map of PU(green), PUa (blue) and PA (red) with HSP of the liquid component of PARMETOL® S 15

The HSP parameters of DCOIT are not available, presence of two chloride substituents in the molecule (**fig.50**) can lead to comparatively high values of  $\delta_P$  and  $\delta_H$ . The latter can induce the situation when core-shell particles are formed, but the active material, due to the high affinity to the polymer matrix, will be mainly concentrated in the shell. Such situation would

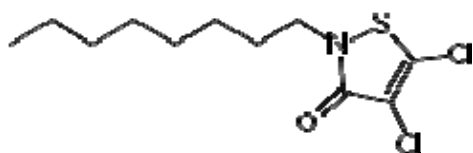


**Fig.50.** Structure of DCOIT, the active component of PARMETOL® S 15

be unfavorable, since the polymer wall should be only partially permeable for the active molecule. The distribution of the component between core and shell is hard to predict. High solubility of the biocide in the main component of the core material, however, allows to expect the favorable development of the process.

PARMETOL® S 15 is not miscible with isocyanate prepolymer. Therefore DEPh was used as the cosolvent for two components.

### VI.3.3. Synthesis of PU-biocide capsules

The composition of the oil phase for the capsule synthesis was 700  $\mu\text{l}$  of PARMETOL® S 15, 300  $\mu\text{l}$  of isocyanate prepolymer and 200  $\mu\text{l}$  of DEPh as cosolvent. The concentration of cosolvent in the capsule is therefore 17 %wt., which is comparatively low allowing satisfaction the first requirement for the capsules. 10 ml of 2 %wt. PVA water solution was used for the oil phase emulsification as usual. The oil phase was emulsified by Ultraturrax at 16000  $\text{min}^{-1}$ . After one minute stirring was stopped and the solution of glycerine (4 ml) and DABCO (200 mg) in water (6 ml) was added slowly to the emulsion. This mixture was left for one hour at 65°C under stirring. Then, heating was stopped and the solution was left without stirring overnight. The low density of the resulting capsules (PU-biocide) allowed avoiding the time and water consuming dialysis procedure. The separation and washing of capsules was performed by following centrifugation and redispersion of the suspension for three times. The paste of the capsules was collected for the further modification of the coating. A part of the paste was dried in air overnight in order to estimate the colloidal stability. The powder was excellent to handle; the redispersion of the capsules was absolutely effortless.

### VI.3.4. Characterization

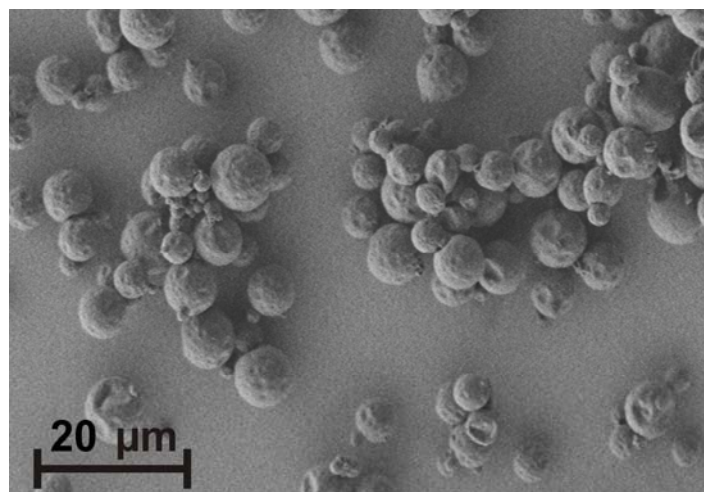


**Fig.51.** SEM image of PU-biocide capsules

The SEM image in **fig.51** shows that the capsules have mostly spherical shape; the amount of concavities and folds is minor. The surface is smooth.

In order to estimate the morphology of capsules they were introduced (about 40% wt.) into the polymer matrix (equal to the model coating). The polymer matrix was cut into slices which were analyzed by means of SEM (**fig.52**).

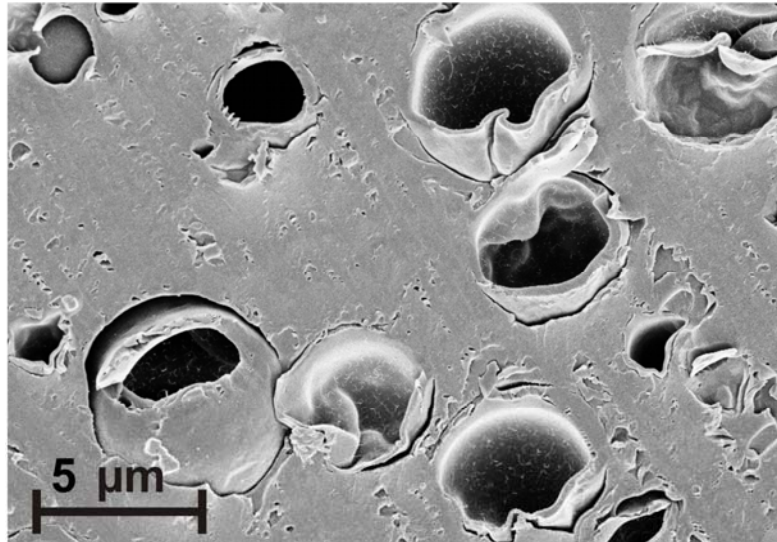


**Fig.52.** SEM images of a polymeric matrix cut with introduced PU-biocide capsules

The morphology of the capsules is core-shell. The inner side of the capsule walls is smooth. The thickness of the capsule walls is nonuniform. Folding of the capsule walls mainly happens on the thinner side of the capsules. The folding of capsules at least in the present case is probably the consequence of the nonuniform stress distribution due to the nonuniform wall thickness. The latter may be the case also for other capsules. The wall thickness is comparatively large, which can be a hint for the DCOIT presence in the polymeric shell. The latter would mean that the last requirement for the capsules is not satisfied. In order to check whether DCOIT is present in the capsule wall, elemental mapping by means of energy dispersive X-ray spectroscopy (EDXS) in combination with TEM was carried out. Detection of DCOIT can be performed only by detection of chlorine and sulfur, since they are the only elements special for the DCOIT.

In the TEM analysis, strong deformation of the particles was observed, which is an indicator that the material is not stable under the high-energetic electron beam (200 kV). A representative TEM image of polymeric capsules is shown in **fig.53** in order to illustrate uselessness of TEM for the morphology analysis in case of polymeric capsules. Even the core-shell morphology of capsules is clear from the SEM analysis (**fig.52**), TEM images show

particles with homogeneous electron density distribution. Similar results were obtained for other types of capsules.

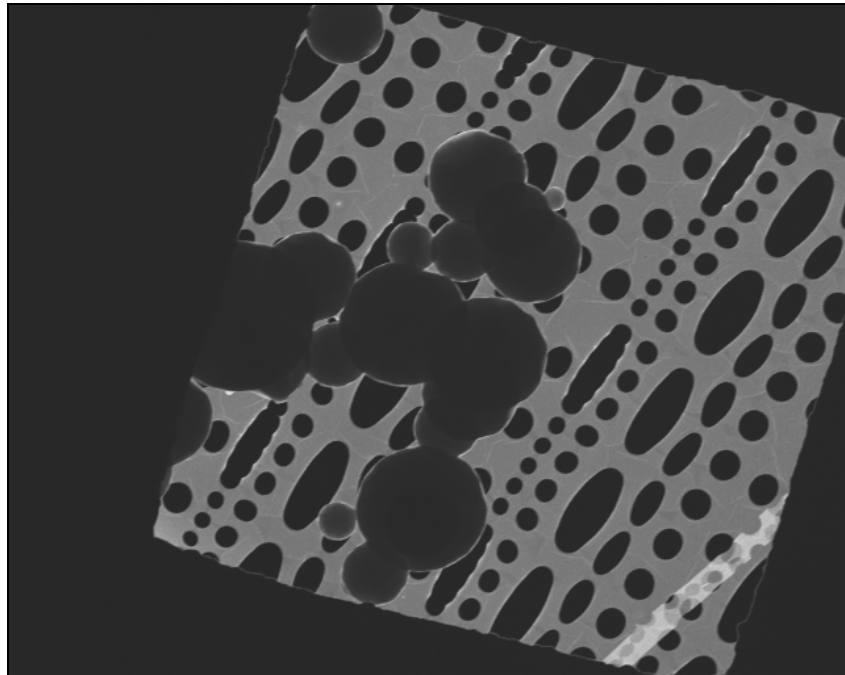


**Fig.53.** Representative TEM images of the polymeric capsules.

Analysis with SEM was possible, but limited by specimen charging and specimen damaging under the electron beam (**fig.54**).

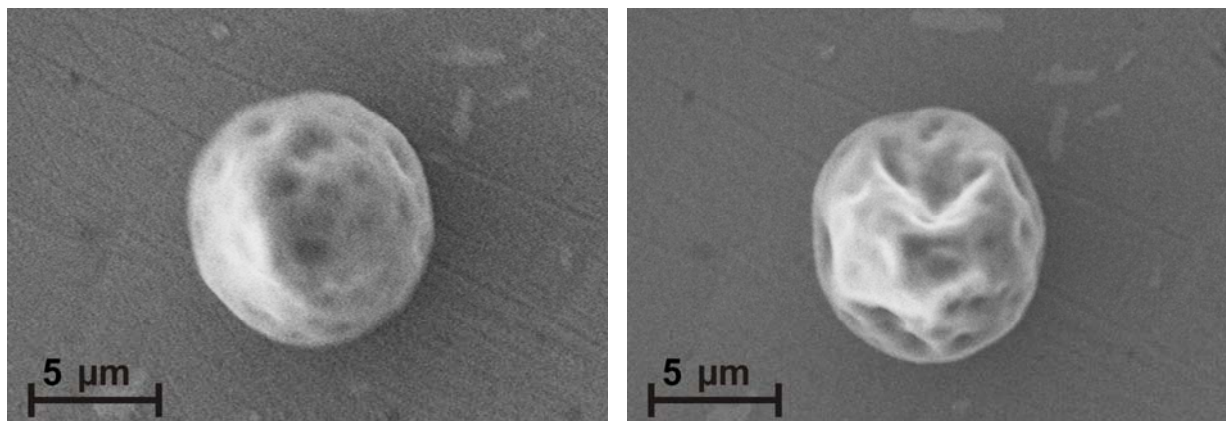


**Fig.54.** Illustration of polymeric capsule damage by the electron beam. SEM image of the PU-biocide capsule immediately (left) and after one minute of electron beam irradiation (right).

By means of EDXS analysis the elements nitrogen, carbon and oxygen from the polymer substrate were detected (**fig.55**). The element chlorine was found in a concentration, which is too small to estimate local variations by elemental mapping. The element sulfur was not found at all. Al and Cu signals are due to the specimen holder. According to the initial content of the

oil phase the concentration of DCOIT in the capsule is 7 %wt., which corresponds to 1,25 %wt. of chlorine and 0,56 %wt. of sulfur. The concentration of both chlorine and sulfur is probably close to the lower limit of EDX detection limit.

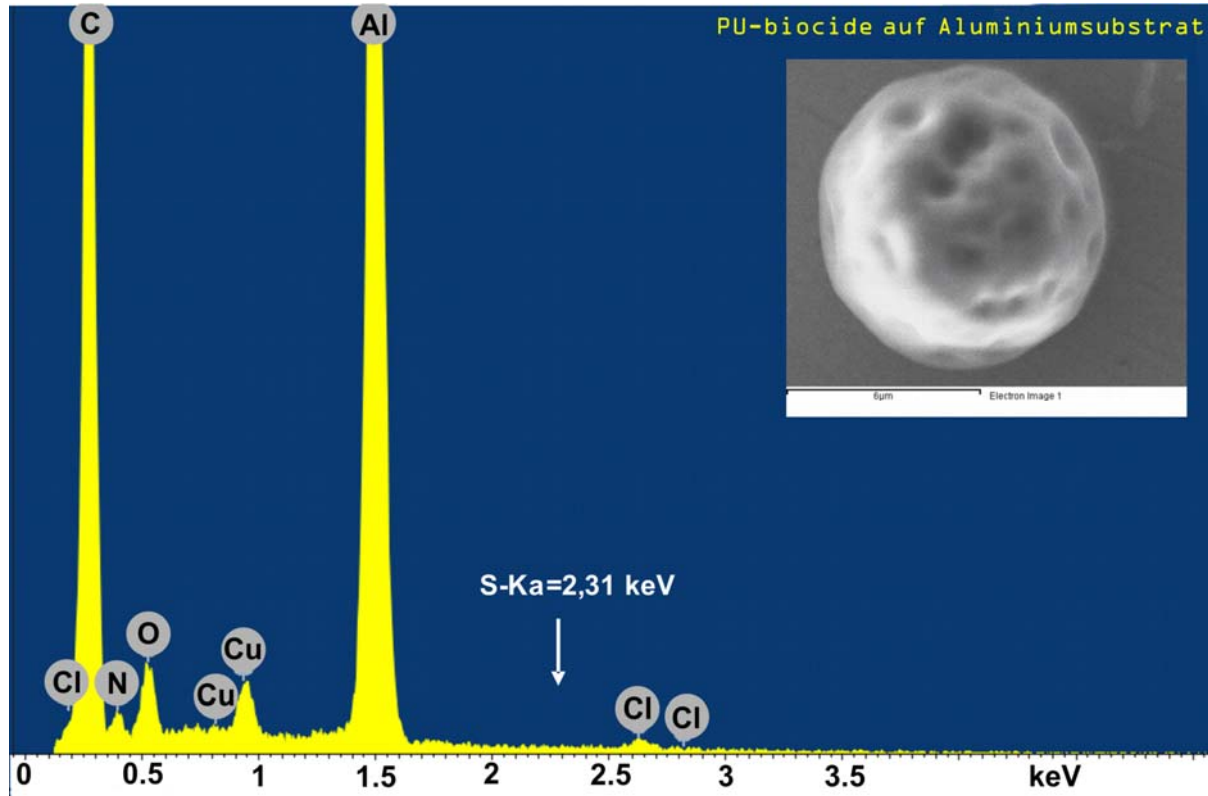


**Fig.55.** EDX analysis results for the area represented in the upper right corner by the SE micrograph. The elements carbon, nitrogen and oxygen from the PU substrate material are found. In a small concentration the element chlorine is found ( $\text{Cl-K}\alpha=2,62 \text{ keV}$ ). The element sulfur was not found (see the arrow). Al and Cu signals are due to the specimen holder.

The elemental distribution (see **fig.56**) of carbon correlates with the PU sphere (see SE micrograph). The element distribution of nitrogen correlates not completely with the PU sphere. The reason is signal suppression by topography effects.

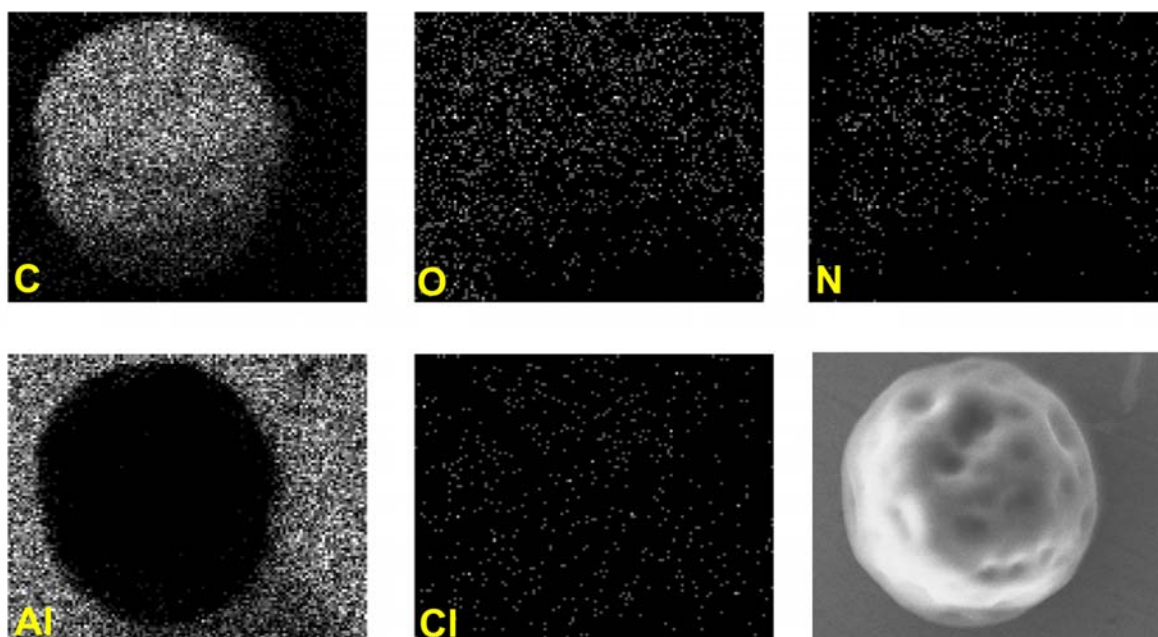


**Fig.56** EDXS elemental maps of the area represented in the down right corner by SE micrograph.

### **VI.3.5. Conclusions**

PU-biocide capsules with polymeric shell and liquid core were successfully synthesized. However, the partition of the DCOIT between core and shell material could not be evaluated by means of the performed EDX analysis. The condition of the DCOIT location in the liquid core was one of the main conditions to be satisfied. Without the information on the DCOIT partition further development and application of capsules for coating modification can not be performed.

TEM images presented in this chapter (**fig.53**) demonstrate that the morphology of polymeric capsules can not be determined by means of this method. Even the core-shell morphology of capsules is clearly demonstrated by SEM, TEM does not show any contrast between core and shell material. Similar results were found for the other core-shell capsules described in the thesis. SEM images (**fig.54**) show that the topography of capsules can be significantly changed by the electron beam. Therefore when the topography of polymeric capsules is of interest, SEM should be applied with caution.

#### **VI.4. Compact and core-shell capsules loaded with MeBT**

In <sup>178</sup> the efficiency of indoles of different structures was tested as corrosion inhibitors for the 3003 aluminium alloy in trichloroacetic acid solutions. The efficiency was decreasing in the following order: indole, 2-methylbenzothiazole, 1,2,3-benzotriazole and 2-mercaptobenzothiazole. By the same authors it was shown that in neutral media the order is basically reverse <sup>179</sup>. All mentioned compounds were found efficient against aluminium corrosion with the efficiency coefficient between 94 and 99 %.

From the substances mentioned above MeBT is the only one, which is liquid at room temperature. Direct doping of a coating, especially a water-based one, with MeBT can be problematic due to the liquid state of the substance. An attempt to introduce MeBT into a water-based coating can cause phase separation of two components and lead to bad wetting conditions and consequently bad adhesion of a coating to the metal substrate. In order to avoid this situation, an introduction of additional emulsifiers would be needed, which would lead to substantial changes in a coating formulation. Degradation of the barrier properties of the coating could be a result. Introduction of MeBT in the form of capsules of micrometer size would solve the problem of the dispersion.

When only colloidal stability is the aim, the morphology of the capsules is not very important. The release behavior of capsules with different morphology would be, however, different. Core-shell morphology of capsules would lead to the immediate release of the liquid capsule content, once the capsules are broken. The release from the capsules with compact morphology is mainly determined by the mobility of the liquid component in the capsule matrix and in general would be slower than in the case of the core-shell morphology.

For anticorrosion coating introduction of capsules with both types of morphologies is essential. When the integrity of a coating is damaged the core-shell capsules would immediately release the encapsulated active material and ensure protection of the metal substrate on the first moments of the corrosion attack. With time deterioration of the protective component from the local spot of the defect would happen. Introduction of compact particles would provide slow release of the corrosion inhibitor, which would ensure the replenishment of the inhibitor concentration in the local spot with high risk of corrosion. Combination of both types of capsules should therefore provide superior corrosion protective capabilities of the resulting hybrid coating.

Another good reason for MeBT encapsulation is to use the resulting capsules as the basis for their further modification. Since MeBT is the liquid substance, it can be used as solvent for solid corrosion inhibitors. The usage of inert cosolvent in this case is not needed. Usage of

liquid inhibitor instead of cosolvent would allow to increase substantially the loading efficiency of capsules. The efficiency of the capsules containing simultaneously two corrosion inhibitors would be superior to the ones with just one type of inhibitor. Right combination of the inhibitors could lead to synergistic effects.

As it was shown in Chapter V.3.2 formation of capsules with core-shell morphology is possible when PA is used as polymeric component of the capsules. In case of PU and PUa, capsules with compact morphology were obtained. See solubility map (**fig.30**).

#### VI.4.1. Characterization

SEM images were already presented earlier in the Chapter V.3.1. and repeated here for more convenience (**fig.57**).

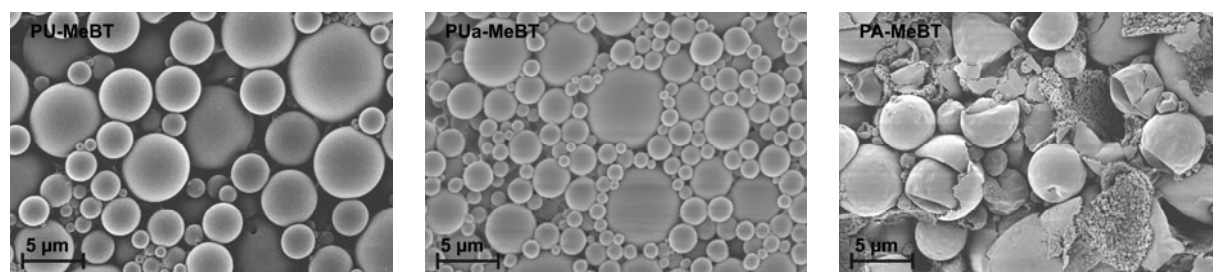


**Fig. 57.** SEM images of PU, PUa and PA capsules with MeBT encapsulated.

PA-MeBT capsules can not be used for the further coating modification due to their utmost fragility. Even being handled very carefully, capsules break on one of the stages of powder preparation. Dispersion of the capsules in the viscous coating would imply application of high-speed homogenizers or mechanical stirring which would inevitably lead to the capsules collapse.

An attempt to improve the mechanical stability of capsules was made. Different variations of amine solutions were tested. The functionality (bi-, tri-, tetra-, penta- and polyfunctional amines were tried), the temperature, concentration of amines in the solution as well as oil soluble monomer/water soluble monomer ratio and other parameters were varied. The mechanical properties were found to be dependent on the mentioned parameters, but no clear correlation was found. All tried variants lead to the formation of PA capsules with insufficient mechanical stability. The problem of the control of the mechanical properties of the PA core-shell particles was already addressed in the literature <sup>102,112,125</sup>, a reasonable solution of the

problem to the best knowledge of the author was not found. Further attempts to improve the strength of the capsule walls could be related to the change of the oil-soluble reactive monomer (TPhCl). A candidate should introduce certain plasticity into the polymer structure. For this purpose “soft” monomers with big hydrocarbon fillers should be used. This possibility was not realized within the framework of the present work due to the time limitations.

Compact PU and PUa particles were considered as the candidates for further coating modification. One of the customary requirements for any kind of capsules is their colloidal stability. In order to estimate it, the PU-MeBT and PUa-MeBT capsules were dried. The flowability of the powders and simplicity of capsules redispersion was compared. According to both named parameters, the PUa capsules were found better for further application. The PUa-MeBT powder was free-flowing, the redispersion of capsules in water was easy and did not need application of ultrasonic bath etc.

#### VI.4.2. Performance of the coating modified with PUa-MeBT capsules

The paste of capsules prepared as usual was introduced into the model coating. The impedance measurements and salt spray chamber tests of the model coating and coating modified with 3.5 %wt. capsules were performed.

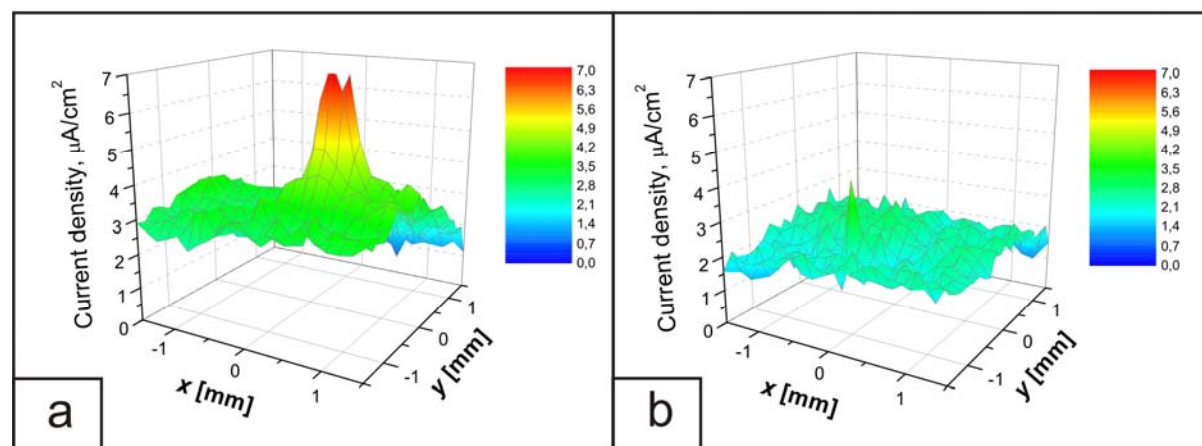


**Fig.58.** Graphical representation of the current density distribution for aluminium substrates covered with (a) unmodified model coating and (b) model coating modified with 5% PUa-MeBT capsules after 12 hours of immersion in 0.1 M NaCl solution. The current density was measured 300  $\mu\text{m}$  above the sample surface.

The current density maps after 12 hours of immersion in 0.1 M NaCl are presented for control sample (unmodified coating) (**Fig.58**) and modified coating. Significant suppression of the corrosion process for samples with embedded capsules is detected, which is the evidence of the MeBT corrosion inhibition efficiency.

Impedance measurements of the modified coatings (**fig.59**) showed even better performance than the unmodified ones. The average value of the complex impedance modulus is higher for the modified coating, which means that the barrier properties of the coating, containing encapsulated MeBT, are better than of unmodified coating. This behavior was first attributed to the plasticizing effect of the MeBT on the coating polymer. Partial leakage of the encapsulated MeBT can lead to the situation, when the homogeneity of the system is improved by the presence of good solvent (MeBT).

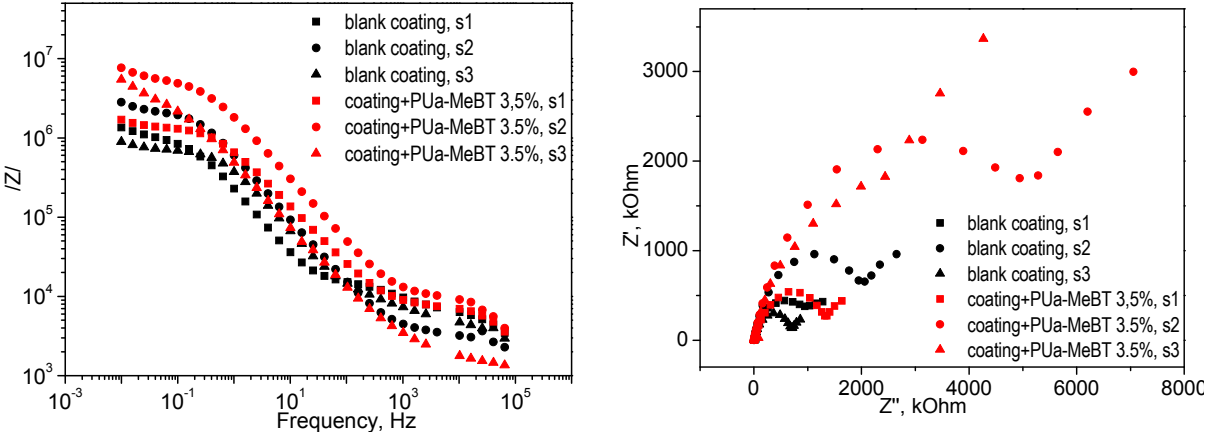


**Fig.59.** Effect of the PUa-MeBT capsule incorporation on the electrical impedance of the model coating. Concentration of the PUa-MeBT coapsules in the modified coating is 3.5%wt. Black symbols represent model coating, red ones – coating modified with the capsules.

Salt-spray chamber tests (**Fig.60**), however, did not confirm this hypothesis, showing very bad performance of the coating doped directly with the MeBT. Therefore the plasticizing effect is probably not the reason of the shown behavior. The salt-spray chamber test on steel substrates showed substantial suppression of the underlying corrosion and no pitting for the samples modified with PUa-MeBT capsules, which is in good agreement with electrochemical impedance measurements. MeBT is, however, an inhibitor for aluminium, not for steel. Therefore positive performance on the steel substrates can not be explained by active corrosion suppression, but only by the coating integrity improvement. The question about the origin of the positive PUa-MeBT capsules performance is still open.

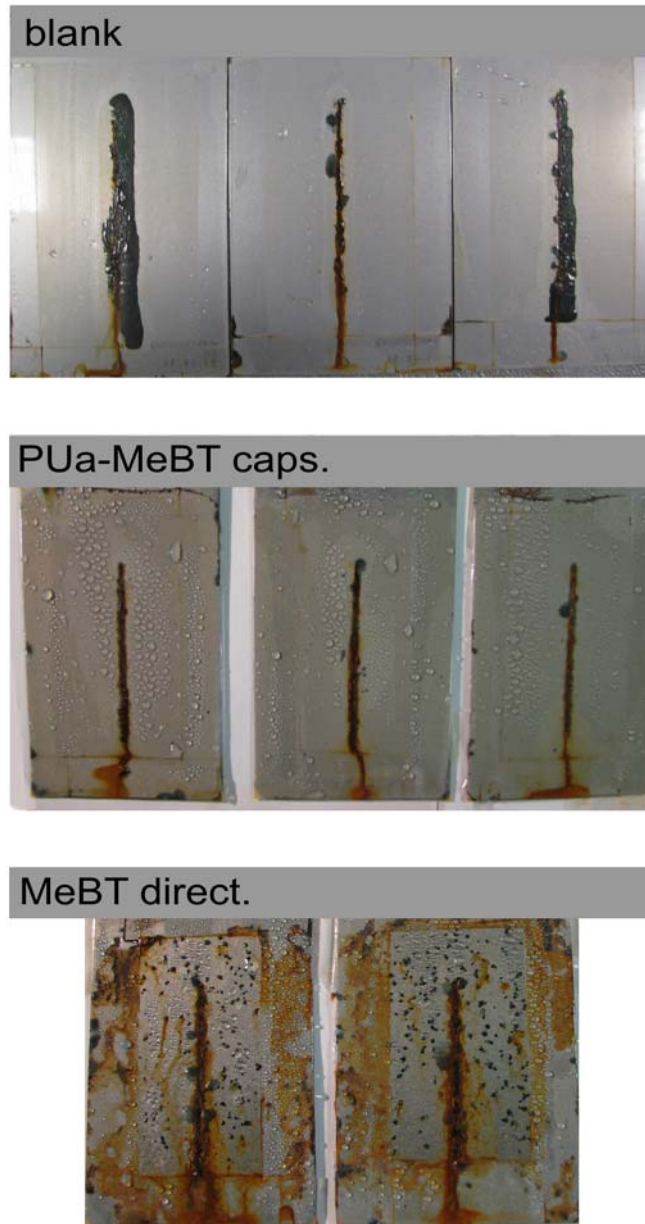


**Fig.60.** The result of 300 h long salt-spray chamber tests for the steel plates covered with unmodified model coating (blank), model coating directly doped with 3 %wt. MeBT and model coating modified with 5% wt. PUa-MeBT capsules.

### **VI.4.3. Conclusions**

The suppression of aluminum corrosion in case of modified coating (comparing to the unmodified one) was confirmed by SVET. Surprisingly the barrier properties of the modified coating were improved by introduction of the capsules, which was in agreement with salt-

spray chamber tests on steel. Further salt-spray tests on aluminium substrates definitely should be performed.

### VI.5. When in-situ loading is not possible

Interfacial polymerization allows in-situ loading of capsules. This fact makes the method very attractive for the application, since fabrication of capsules includes fewer steps. This approach, however, is not applicable for some substances due to the possible reaction of the oil-soluble monomer with the material to be encapsulated. In the particular case of isocyanate prepolymer and TPhCl in-situ encapsulation of substances carrying groups with mobile hydrogen atoms is impossible; such groups react readily with isocyanate and acid chloride groups leading to deactivation of both encapsulated material and reactive monomer. In acid-, alcohol-, mercapto- and aminogroups the hydrogen atom is mobile, which means that all compounds carrying these groups can not be encapsulated in PU, PUa and PA via interfacial polymerization due to the possible reactions. At the same time very often these groups are the ones that determine the functionality of the active material to be encapsulated. For example benzotriazole (BTA) and 8-hydroxyquinoline (8-HQ) are highly effective corrosion inhibitors for both steel and aluminium alloys<sup>180-183</sup>. Encapsulation of these compounds and further application of capsules as an active part of smart coatings would be very promising. Their chemical structure (see **fig.61**) contains, however, groups (amino group for BTA and alcohol group for 8-HQ) that would readily react with both isocyanate prepolymer and TPhCl.



**Fig.61.** 8-HQ and BTA chemical structures

For the encapsulation of these substances other methods should be used, that do not imply the polymerization reaction simultaneously with capsule formation. One method would be for example solvent evaporation (or extraction), when preformed linear polymer is precipitated on the surface of oil droplets leading to the formation of capsules.

### VI.5.1. Exploitation of swelling for capsule loading

In the case of crosslinked polymers the loading procedure can in principle follow the formation of the capsules. In this case due to the polymerization reaction the reactive monomer is neutralized and can not react with the material to be encapsulated. Since the molding of the capsules, consisting of crosslinked polymer, happens on the stage of capsule formation, the loading procedure does not influence the morphology of final capsules.

The loading of preformed capsules is realized by exploitation of the swelling ability of the crosslinked polymers. Evaluation of swelling conditions is therefore a critical factor determining the whole process. Application of the HSP approach is useful for this purpose as well.

Loading of capsules with both compact and core-shell morphologies is possible. In both cases the solvent appropriate for the loading procedure should be found. The requirements for the solvent are:

--Solvent should be a “good” solvent for the polymer. The better the swelling ability of the polymer the higher values of loading can be achieved.

--Solvent should dissolve substantial amount of the substance to be encapsulated. The higher the solubility the higher is the loading efficiency of the method.

--Solvent should be volatile in order to be easy to remove. Other methods to remove the solvent can be also used (for example extraction).

The process of compact particle loading is illustrated schematically in **fig.62**.

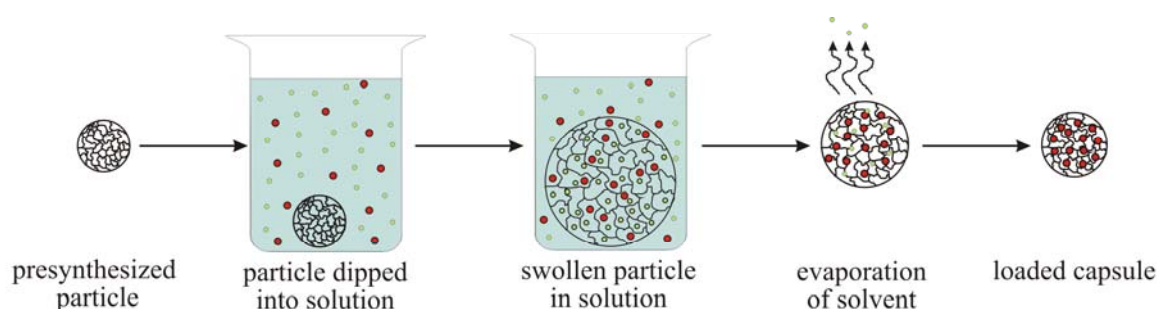


**Fig.62.** Scheme of compact particle loading by the swelling mechanism

First, particles with appropriate morphology should be synthesized. A solvent matching the mentioned conditions should be found (HSP approach can be used). Solution of material to be

encapsulated in the solvent should be prepared. Polymer particles should be left in contact with the solvent for the amount of time necessary for swelling. Swollen capsules should be removed from the solution; the solvent should be let to evaporate. Since the material to be encapsulated is nonvolatile, it will stay entrapped inside the capsules.

### VI.5.2. Calculation of loading

To estimate the loading efficiency of the method a simple calculation can be made. If  $\alpha$  – the swelling ability of polymer (the mass of solvent in swollen capsule divided by mass of polymer) and  $C$  is the concentration of active material in the solvent (%wt.),  $Z$  gram of capsules absorb  $Z \times \alpha$  gram of solvent.  $Z \times \alpha$  gram of solvent contain  $Z \times C \times \alpha / 100$  gram of active material. If the distribution of the active material does not depend on the local surrounding, which means that the concentration of the active material in the free solvent and solvent inside the polymeric net is equal, the final loading can be calculated as

$$L = \frac{Z \times C \times \alpha}{Z \times 100} \times 100\% = C \times \alpha$$

For  $\alpha=3$  and  $C=20$  %wt. loading would be 60 %wt., which is a relatively high value.

In reality the concentration of the active material inside the polymer matrix is not equal to its concentration in the free solvent. The difference would be determined by the affinity of the substance to the polymer matrix, degree of crosslinking, the size of the active material molecule and so on. The scheme presented here, however suffices for the preliminary estimation of the loading efficiency. Exact loading should be determined by an independent method.

For capsules with core-shell structure loading is also possible (**fig. 63**).

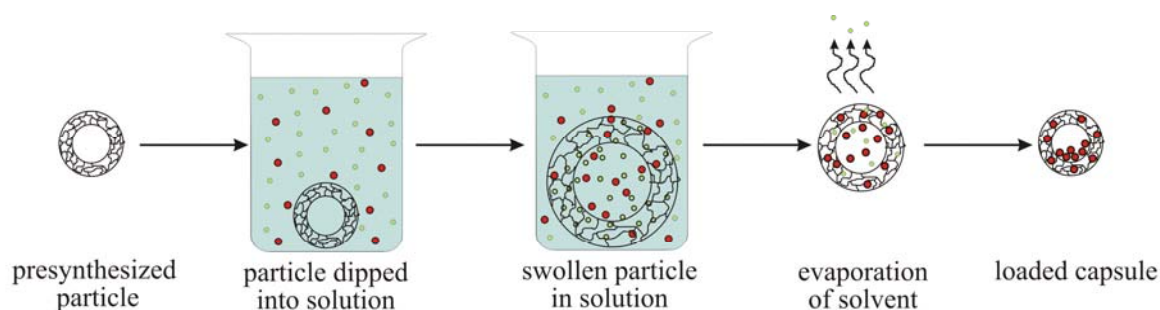


**Fig.63.** Scheme of core-shell particle loading by the swelling mechanism

The distribution of the active material between core and shell is mainly determined by the affinity of the active material to the polymer matrix. If the affinity is low the concentration of the active material inside the capsule cavity instead of homogeneous distribution is theoretically possible.

### VI.5.3. PUa capsules loaded with BTA and 8HQ

The inhibitors BTA and 8-HQ, highly effective against both steel and aluminium corrosion, were encapsulated via the procedure described above.

Acetone was chosen as the solvent for loading due to the high solubility of the inhibitors and the high swelling ability of PUa in acetone. The pure polymer PUa particles were used as polymeric carrier. 20%wt. solution of inhibitor was prepared. 1 gram of polymeric particles was dipped into the 3 ml inhibitor solution in acetone for 1 week. The amount of acetone was selected in such a way that the polymer can absorb the whole amount of solvent. In this way the procedure of separation of swollen capsules from solution can be avoided, however the loading efficiency of capsules can vary from fraction to fraction. After 1 week the capsules were dried under vacuum in order to remove the solvent. Expected loading of capsules was estimated as 60%wt. according to the scheme presented above.

The resulting powder demonstrated good colloidal stability: capsules could be redispersed in water only by shaking without using ultrasonic bath.

#### VI.5.3.a Characterization

SEM images (**fig.64**) demonstrate the outer appearance of the resulting capsules.

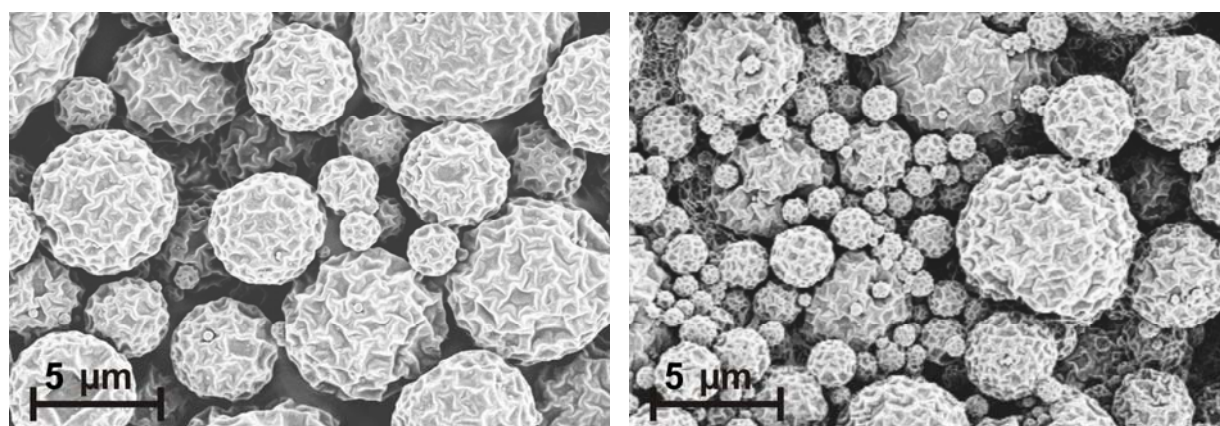


**Fig.64.** Compact PUa capsules loaded with 8-HQ and BTA by the swelling mechanism.

Capsules have mainly spherical shape. The surface is not smooth, but consists of many folds. The appearance of the capsule surface is probably due to the significant expansion and following contraction of the capsule surface due to the swelling and further solvent evaporation.

### VI.5.3.b Performance of the coating modified with PUa-BTA and PUa-8-HQ capsules

In order to simplify the distribution of capsules in the coating, a paste containing 60 %wt. of capsules and 40 %wt. of water was prepared. The resulting paste was further used for the coating modification. Coatings containing 3.5 %wt. of capsules loaded with 8-HQ and BTA were prepared. The anticorrosion efficiency of the modified coatings was compared to the unmodified one.

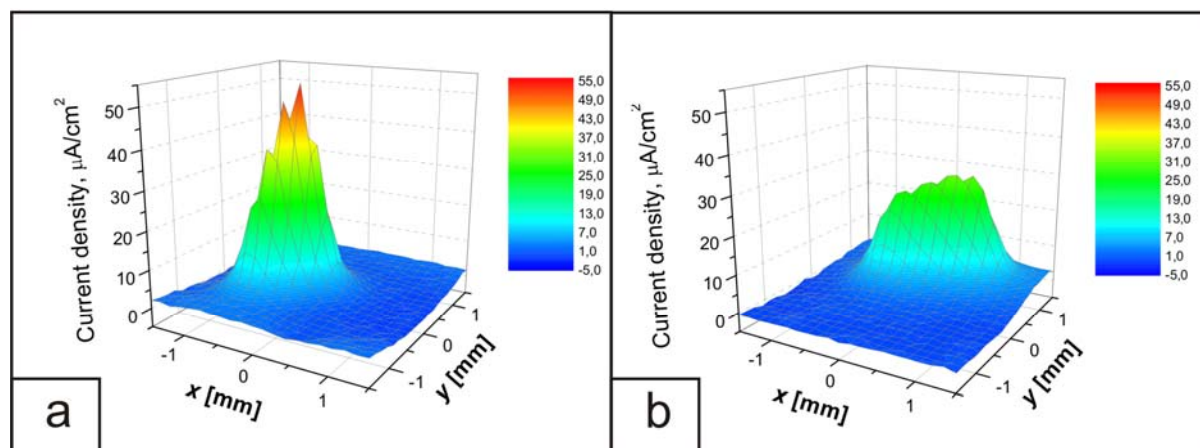


**Fig.65.** Graphical representation of the current density distribution for steel samples covered with (a) unmodified model coating and (b) model coating modified with 5% PUa-8-HQ capsules after 12 hours of immersion in 1 M NaCl solution.

The active anticorrosion capability of the coating modified with PUa-8HQ and PUa-BTA was demonstrated by means of SVET analysis (fig.65, 66). The current density graphs for two modified systems show similar results: the current density above the scratched coating was suppressed almost two times compared to unmodified coating. This result is not quite satisfactory, since total suppression of corrosion at least in the first 12 hours is desired. However, the demonstrated performance shows that the whole concept is perspective. The loading of capsules as well as the capsule concentration in the coating probably should be increased in order to improve the performance.

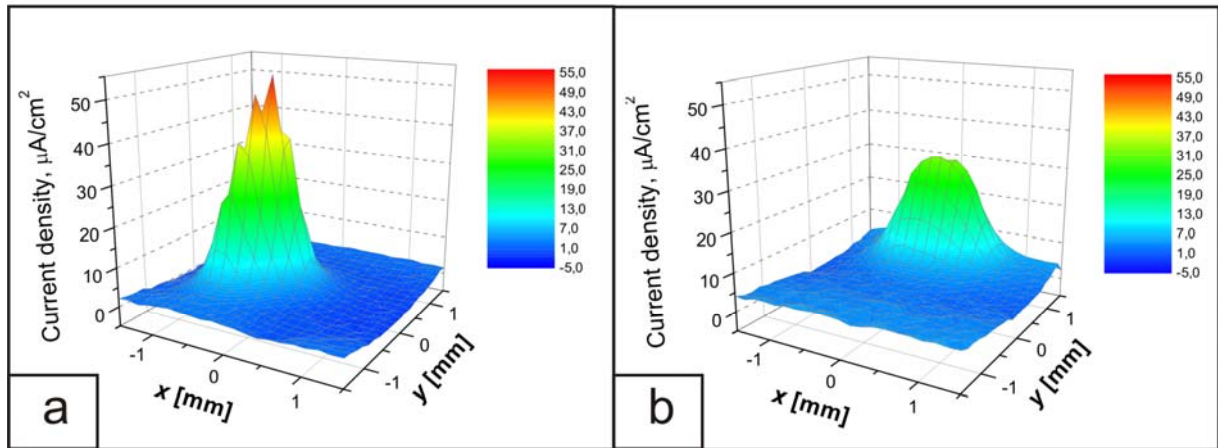


**Fig.66.** Graphical representation of the current density distribution for steel samples covered with (a) unmodified model coating and (b) model coating modified with 5% PUa-8-HQ capsules after 12 hours of immersion in 1 M NaCl solution.

Impedance measurements of the system do not look very promising (**fig.67**). Both complex impedance modulus and resistivity are considerably higher for the unmodified coating than for the modified ones. However one of three samples of PUa-8HQ modified coating demonstrate the impedance characteristics very similar to the best performing sample of unmodified coating. This can be an evidence that suppression of the barrier properties of the coating is due to the bad distribution of the capsules in the coating. In the case of good distribution (PUa-8HQ sample3) the performance is good.

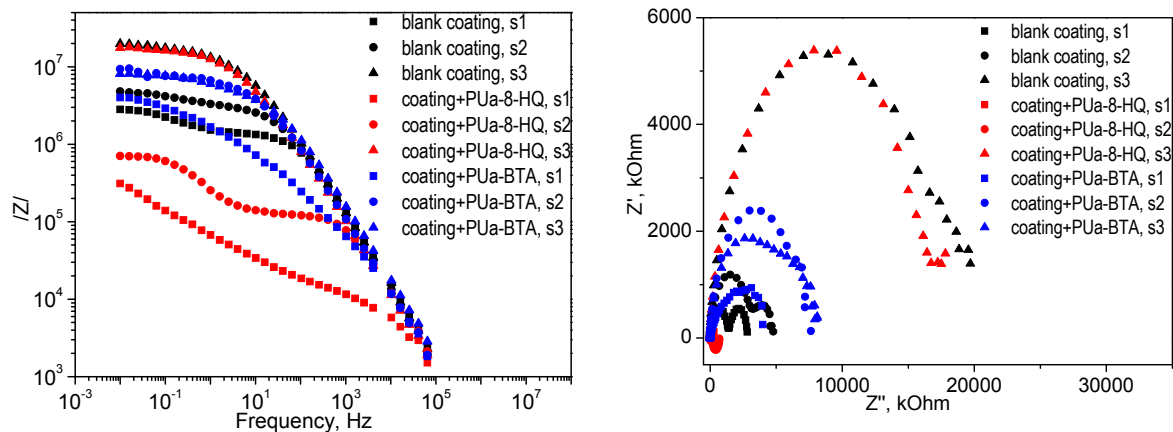


**Fig.67.** Impedance measurements for blank model coating (black symbols) and coating modified with 3.5%wt. PUa-8HQ capsules (blue symbols) and 3.5%wt. PUa-BTA capsules (red symbols). Measurements were performed on steel.

Salt-spray chamber tests (**fig.68**) showed that direct introduction of inhibitors into a coating destroys it. The situation is significantly better in the case of BTA direct doping; the result is however not acceptable. Coating can not be doped with the named inhibitors directly.

Introduction of the inhibitor in encapsulated state leads to much better results. The black area around the scratch is smaller for the samples containing capsules than for unmodified coating. The amount of pitting corrosion of the modified samples is comparable to the pure sample; however, delamination of the coating happens (see the white areas around the scratch). The corrosion under the delaminated areas does not take place, but such a behavior of the coating is unacceptable, since adhesion is too bad. Being disturbed by any mechanical impact delaminated parts of the coating will fall apart opening big spots of the bare metal for the corrosion attack. Probably the bad adhesion of the modified coating is the reason for the low electrochemical resistivity of the modified samples.

### **VI.5.3.c Conclusions**

The performance of coating modified with capsules containing corrosion inhibitors show way better results than systems doped with inhibitors directly. According to this encapsulation of inhibitors sufficiently improves performance of the coating. Nevertheless some properties of the coating such as adhesion to metal can be spoiled by capsule incorporation.

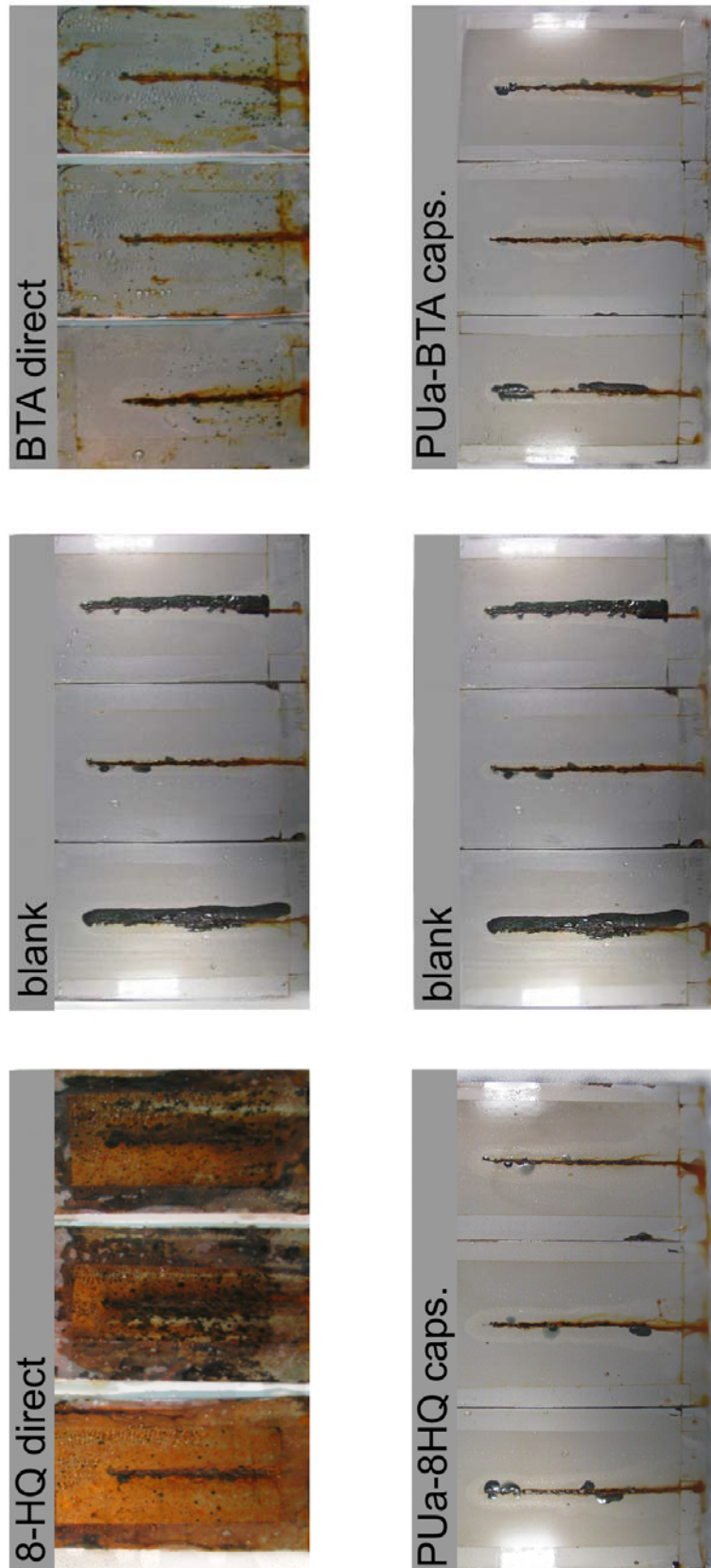


**Fig.68.** The result of salt-spray chamber tests for steel plates covered with unmodified model coating (blank), model coating doped with 3 % wt. 8-HQ and BTA (8-HQ direct and BTA direct) and model coating modified with 5 % wt. PUa-8HQ and PUa-BTA capsules.

## VII. Conclusions

In the first part of this work, it was shown that the morphology of capsules consisting of a crosslinked polymer and a solvent can be predicted. Formation of compact morphology happens if the solvent is a “good” solvent for the polymer. If the solvent is “poor” either core-shell or multicompartment morphology will be formed.

The quality of the solvent can be estimated on the basis of the swelling behavior of the polymer in the solvent. In this case swelling experiment should be performed for every polymer-solvent pair. It was shown, however, that due to the different reasons swelling behavior and morphology of capsules in some cases do not correlate.

HSP approach was shown to be more convenient for the capsule morphology prediction, since it allows consideration of the inherent parameters of single components in stead of a pair of components, which significantly facilitates the components choice. In HSP approach the “solubility sphere”, unique for every polymer, is constructed according to the swelling behavior of the polymer in a set of solvents with different polarity. The “good” solvents are located inside the sphere; the “poor” ones are outside. Further the mixing behavior of the polymer, estimated on the basis of swelling behavior in the limited number of solvents, can be approximated to any solvent (or even solid substance) with known (or possible-to estimate) HSP. Fabrication of capsules with desired morphology should be performed according to the solubility sphere of the polymer: all solvents located inside the “solubility sphere” will give capsules with compact morphology, formation of capsules with core-shell or multicompartment morphology will happen, if the coordinates of solvent on the HSP graph lay outside of the polymers “solubility sphere”.

The application of the described approach was demonstrated in the second part of the present work. Capsules with on-demand morphology containing different corrosion inhibitors were successfully fabricated. The choice of the polymer, solvents and cosolvents was done on the basis of HSP approach. The morphology of the resulting capsules was always in agreement with the one predicted by the HSP.

Further the fabricated capsules were introduced into the model coating resulting in new coatings with the self-healing capabilities. The efficiency of the new self-healing coatings against corrosion in comparison to the original unmodified coating was investigated by means of SVET, EIS and salt-spray chamber tests. The EIS experiments showed that in almost all

cases the barrier properties of the coating were somewhat disturbed by the introduction of the capsules. However the SVET experiments showed essential suppression of the corrosion activity, which was the evidence, that encapsulation of the corrosion inhibitor does not lead to its deactivation. The salt-spray chamber test, which reflects the effectiveness of both passive and active parts of the coating, showed that in most cases the performance of the capsule-modified coatings was better than the performance of original model coating and model coating directly doped with the inhibitor. The latter allows to conclude, that the approach, presented here, is an effective one and can be considered as the perspective for further industrial application.

## VIII. References

- (1) Ghosh, S. K.: *Self-healing Materials: Fundamentals, Design Strategies, and Applications*; Wiley-VCH, Weinheim 2008.
- (2) Feng, W.; Patel, S. H.; Young, M. Y.; Zunino, J. L., III; Xanthos, M.: Smart polymeric coatings - Recent advances. *Advances in Polymer Technology* **2007**, *26*, 1-13.
- (3) Blaiszik, B. J.; Kramer, S. L. B.; Olugebefola, S. C.; Moore, J. S.; Sottos, N. R.; White, S. R.: Self-Healing Polymers and Composites. In *Annual Review of Materials Research, Vol 40*; Clarke, D. R. R. M. Z. F., Ed., 2010; Vol. 40; pp 179-211.
- (4) Bergman, S. D.; Wudl, F.: Mendable polymers. *Journal of Materials Chemistry* **2008**, *18*, 41-62.
- (5) Murphy, E. B.; Bolanos, E.; Schaffner-Hamann, C.; Wudl, F.; Nutt, S. R.; Auad, M. L.: Synthesis and characterization of a single-component thermally remendable polymer network: Staudinger and Stille revisited. *Macromolecules* **2008**, *41*, 5203-5209.
- (6) Park, J. S.; Takahashi, K.; Guo, Z.; Wang, Y.; Bolanos, E.; Hamann-Schaffner, C.; Murphy, E.; Wudl, F.; Hahn, H. T.: Towards Development of a Self-Healing Composite using a Mendable Polymer and Resistive Heating. *Journal of Composite Materials* **2008**, *42*, 2869-2881.
- (7) Murphy, E. B.; Wudl, F.: The world of smart healable materials. *Progress in Polymer Science* **2010**, *35*, 223-251.
- (8) Zhang, Y.; Broekhuis, A. A.; Picchioni, F.: Thermally Self-Healing Polymeric Materials: The Next Step to Recycling Thermoset Polymers? *Macromolecules* **2009**, *42*, 1906-1912.
- (9) Davis, D. A.; Hamilton, A.; Yang, J.; Cremar, L. D.; Van Gough, D.; Potisek, S. L.; Ong, M. T.; Braun, P. V.; Martinez, T. J.; White, S. R.; Moore, J. S.; Sottos, N. R.: Force-induced activation of covalent bonds in mechanoresponsive polymeric materials. *Nature* **2009**, *459*, 68-72.
- (10) Luo, X.; Ou, R.; Eberly, D. E.; Singhal, A.; Viratyaporn, W.; Mather, P. T.: A Thermoplastic/Thermoset Blend Exhibiting Thermal Mending and Reversible Adhesion. *Acs Applied Materials & Interfaces* **2009**, *1*, 612-620.
- (11) Hayes, S. A.; Jones, F. R.; Marshiya, K.; Zhang, W.: A self-healing thermosetting composite material. *Composites Part a-Applied Science and Manufacturing* **2007**, *38*, 1116-1120.
- (12) Varley, R. J.; van der Zwaag, S.: Towards an understanding of thermally activated self-healing of an ionomer system during ballistic penetration. *Acta Materialia* **2008**, *56*, 5737-5750.
- (13) Kalista, S. J., Jr.: Self-healing of poly(ethylene-co-methacrylic acid) copolymers following projectile puncture. *Mechanics of Advanced Materials and Structures* **2007**, *14*, 391-397.
- (14) Kalista, S. J., Jr.; Ward, T. C.: Thermal characteristics of the self-healing response in poly (ethylene-co-methacrylic acid) copolymers. *Journal of the Royal Society Interface* **2007**, *4*, 405-411.
- (15) Cordier, P.; Tournilhac, F.; Soulie-Ziakovic, C.; Leibler, L.: Self-healing and thermoreversible rubber from supramolecular assembly. *Nature* **2008**, *451*, 977-980.
- (16) Montarnal, D.; Tournilhac, F.; Hidalgo, M.; Couturier, J.-L.; Leibler, L.: Versatile One-Pot Synthesis of Supramolecular Plastics and Self-Healing Rubbers. *Journal of the American Chemical Society* **2009**, *131*, 7966-+.

- (17) White, S. R.; Sottos, N. R.; Geubelle, P. H.; Moore, J. S.; Kessler, M. R.; Sriram, S. R.; Brown, E. N.; Viswanathan, S.: Autonomic healing of polymer composites. *Nature* **2001**, *409*, 794-797.
- (18) Kumar, A.; Stephenson, L. D.; Murray, J. N.: Self-healing coatings for steel. *Progress in Organic Coatings* **2006**, *55*, 244-253.
- (19) Suryanarayana, C.; Rao, K. C.; Kumar, D.: Preparation and characterization of microcapsules containing linseed oil and its use in self-healing coatings. *Progress in Organic Coatings* **2008**, *63*, 72-78.
- (20) Sauvant-Moynot, V.; Gonzalez, S.; Kittel, J.: Self-healing coatings: An alternative route for anticorrosion protection. *Progress in Organic Coatings* **2008**, *63*, 307-315.
- (21) Cho, S. H.; White, S. R.; Braun, P. V.: Self-Healing Polymer Coatings. *Advanced Materials* **2009**, *21*, 645-+.
- (22) Sugama, T.; Gawlik, K.: Self-repairing poly(phenylenesulfide) coatings in hydrothermal environments at 200 degrees C. *Materials Letters* **2003**, *57*, 4282-4290.
- (23) Toohey, K. S.; Hansen, C. J.; Lewis, J. A.; White, S. R.; Sottos, N. R.: Delivery of Two-Part Self-Healing Chemistry via Microvascular Networks. *Advanced Functional Materials* **2009**, *19*, 1399-1405.
- (24) Davis, J. R.: *Corrosion: understanding the basics*; ASM International, 2000.
- (25) Clark, W. J.; Ramsey, J. D.; McCreery, R.L.; Frankel, G. S.: A galvanic corrosion approach to investigating chromate effects on aluminum alloy 2024-T3. *Journal of the Electrochemical Society* **2002**, *149*, B179-B185.
- (26) Brett, C. M. A.; Gomes, I. A. R.; Martins, J. P. S.: THE ELECTROCHEMICAL-BEHAVIOR AND CORROSION OF ALUMINUM IN CHLORIDE MEDIA - THE EFFECT OF INHIBITOR ANIONS. *Corrosion Science* **1994**, *36*, 915-&.
- (27) Brett, C. M. A.; Gomes, I. A. R.; Martins, J. P. S.: INHIBITION OF ALUMINUM CORROSION IN CHLORIDE MEDIA - AN IMPEDANCE STUDY. *Journal of Applied Electrochemistry* **1994**, *24*, 1158-1163.
- (28) Pryor, M. J.; Cohen, M.: The Inhibition of the Corrosion of Iron by Some Anodic Inhibitors. *Journal of the Electrochemical Society* **1953**, *100*, 203-215.
- (29) Sinko, J.: Challenges of chromate inhibitor pigments replacement in organic coatings. *Progress in Organic Coatings* **2001**, *42*, 267-282.
- (30) Zheludkevich, M. L.; Serra, R.; Montemor, M. F.; Yasakau, K. A.; Salvado, I. M. M.; Ferreira, M. G. S.: Nanostructured sol-gel coatings doped with cerium nitrate as pre-treatments for AA2024-T3 - Corrosion protection performance. *Electrochimica Acta* **2005**, *51*, 208-217.
- (31) Rudd, W. J.; Scully, J. C.: THE FUNCTION OF THE REPASSIVATION PROCESS IN THE INHIBITION OF PITTING CORROSION ON ALUMINUM. *Corrosion Science* **1980**, *20*, 611-631.
- (32) Aramaki, K.: The inhibition effects of chromate-free, anion inhibitors on corrosion of zinc in aerated 0.5 M NaCl. *Corrosion Science* **2001**, *43*, 591-604.
- (33) Gonzalez, Y.; Lafont, M. C.; Pebere, N.; Chatainier, G.; Roy, J.; Bouissou, T.: A CORROSION INHIBITION STUDY OF A CARBON-STEEL IN NEUTRAL CHLORIDE SOLUTIONS BY ZINC SALT PHOSPHONIC ACID ASSOCIATION. *Corrosion Science* **1995**, *37*, 1823-1837.
- (34) Mu, G. N.; Li, X. H.; Qu, Q.; Zhou, J.: Molybdate and tungstate as corrosion inhibitors for cold rolling steel in hydrochloric acid solution. *Corrosion Science* **2006**, *48*, 445-459.
- (35) Powell, S. M.; McMurray, H. N.; Worsley, D. A.: Use of the scanning reference electrode technique for the evaluation of environmentally friendly, nonchromate corrosion inhibitors. *Corrosion* **1999**, *55*, 1040-1051.

- (36) Robertson, W. D.: MOLYBDATE AND TUNGSTATE AS CORROSION INHIBITORS AND THE MECHANISM OF INHIBITION. *Journal of the Electrochemical Society* **1951**, 98, 94-100.
- (37) Gao, L. J.; Conway, B. E.: POISONING EFFECTS OF ARSENIC SPECIES ON H ADSORPTION AND KINETIC-BEHAVIOR OF THE H-2 EVOLUTION REACTION AT PT IN KOH SOLUTION. *Journal of Electroanalytical Chemistry* **1995**, 395, 261-271.
- (38) Bethencourt, M.; Botana, F. J.; Calvino, J. J.; Marcos, M.; Rodriguez-Chacon, M. A.: Lanthanide compounds as environmentally-friendly corrosion inhibitors of aluminium alloys: A review. *Corrosion Science* **1998**, 40, 1803-1819.
- (39) Mansfeld, F.; Smith, T.; Parry, E. P.: BENZOTRIAZOLE AS CORROSION INHIBITOR FOR COPPER. *Corrosion* **1971**, 27, 289-&.
- (40) Armstrong, R. D.; Peggs, L.; Walsh, A.: BEHAVIOR OF SODIUM-SILICATE AND SODIUM-PHOSPHATE (TRIBASIC) AS CORROSION-INHIBITORS FOR IRON. *Journal of Applied Electrochemistry* **1994**, 24, 1244-1248.
- (41) Salvarezza, R. C.; Demele, M. F. L.; Videla, H. A.: MECHANISMS OF THE MICROBIAL CORROSION OF ALUMINUM-ALLOYS. *Corrosion* **1983**, 39, 26-32.
- (42) Shchukin, D. G.; Moehwald, H.: Surface-engineered nanocontainers for entrapment of corrosion inhibitors. *Advanced Functional Materials* **2007**, 17, 1451-1458.
- (43) Shchukin, D. G.; Zheludkevich, M.; Yasakau, K.; Lamaka, S.; Ferreira, M. G. S.; Moehwald, H.: Layer-by-layer assembled nanocontainers for self-healing corrosion protection. *Advanced Materials* **2006**, 18, 1672-+.
- (44) Khramov, A.; Voevodin, N. N.; Balbyshev, V. N.; Mantz, R. A.: Sol-gel-derived corrosion-protective coatings with controllable release of incorporated organic corrosion inhibitors. *Thin Solid Films* **2005**, 483, 191-196.
- (45) Khramov, A. N.; Voevodin, N. N.; Balbyshev, V. N.; Donley, M. S.: Hybrid organo-ceramic corrosion protection coatings with encapsulated organic corrosion inhibitors. *Thin Solid Films* **2004**, 447, 549-557.
- (46) Zheludkevich, M. L.; Serra, R.; Montemor, M. F.; Ferreira, M. G. S.: Oxide nanoparticle reservoirs for storage and prolonged release of the corrosion inhibitors. *Electrochemistry Communications* **2005**, 7, 836-840.
- (47) Montemor, M. E.; Fefreira, M. G. S.: Cerium salt activated nanoparticles as fillers for silane films: Evaluation of the corrosion inhibition performance on galvanised steel substrates. *Electrochimica Acta* **2007**, 52, 6976-6987.
- (48) Cook, R. L.: Releasable corrosion inhibitor compositions. *Pat. 6933046* **2005**.
- (49) Schmidt, C.: Anti-corrosive coating including a filler with a hollow cellular structure. *US Pat. 6383271* **2002**.
- (50) Eckler, E. P. a. F., L.M.: nti-corrosive protective coatings. *US Pat. 4738720* **1988**.
- (51) McMurray, H. N.; Williams, D.; Williams, G.; Worsley, D.: Inhibitor pretreatment synergies demonstrated using a scanning Kelvin probe technique. *Corrosion Engineering Science and Technology* **2003**, 38, 112-118.
- (52) Bohm, S.; McMurray, H. N.; Powell, S. M.; Worsley, D. A.: Novel environment friendly corrosion inhibitor pigments based on naturally occurring clay minerals. *Materials and Corrosion-Werkstoffe Und Korrosion* **2001**, 52, 896-903.
- (53) Wang, H.; Presuel, F.; Kelly, R. G.: Computational modeling of inhibitor release and transport from multifunctional organic coatings. *Electrochimica Acta* **2004**, 49, 239-255.
- (54) Buchheit, R. G.; Guan, H.; Mahajanam, S.; Wong, F.: Active corrosion protection and corrosion sensing in chromate-free organic coatings. *Progress in Organic Coatings* **2003**, 47, 174-182.

- (55) Poznyak, S. K.; Tedim, J.; Rodrigues, L. M.; Salak, A. N.; Zheludkevich, M. L.; Dick, L. F. P.; Ferreira, M. G. S.: Novel Inorganic Host Layered Double Hydroxides Intercalated with Guest Organic Inhibitors for Anticorrosion Applications. *Acs Applied Materials & Interfaces* **2009**, *1*, 2353-2362.
- (56) Yang, H.; van Ooij, W. J.: Plasma-treated triazole as a novel organic slow-release paint pigment for corrosion control of AA2024-T3. *Progress in Organic Coatings* **2004**, *50*, 149-161.
- (57) Decher, G.; Hong, J. D.; Schmitt, J.: BUILDUP OF ULTRATHIN MULTILAYER FILMS BY A SELF-ASSEMBLY PROCESS .3. CONSECUTIVELY ALTERNATING ADSORPTION OF ANIONIC AND CATIONIC POLYELECTROLYTES ON CHARGED SURFACES. *Thin Solid Films* **1992**, *210*, 831-835.
- (58) Grigoriev, D. O.; Koehler, K.; Skorb, E.; Shchukin, D. G.; Moehwald, H.: Polyelectrolyte complexes as a "smart" depot for self-healing anticorrosion coatings. *Soft Matter* **2009**, *5*, 1426-1432.
- (59) Shchukin, D. G.; Moehwald, H.: Self-repairing coatings containing active nanoreservoirs. *Small* **2007**, *3*, 926-943.
- (60) Zheludkevich, M. L.; Shchukin, D. G.; Yasakau, K. A.; Moehwald, H.; Ferreira, M. G. S.: Anticorrosion coatings with self-healing effect based on nanocontainers impregnated with corrosion inhibitor. *Chemistry of Materials* **2007**, *19*, 402-411.
- (61) Andreeva, D. V.; Skorb, E. V.; Shchukin, D. G.: Layer-by-Layer Polyelectrolyte/Inhibitor Nanostructures for Metal Corrosion Protection. *Acs Applied Materials & Interfaces* **2010**, *2*, 1954-1962.
- (62) Shchukin, D. G.; Zheludkevich, M.; Moehwald, H.: Feedback active coatings based on incorporated nanocontainers. *Journal of Materials Chemistry* **2006**, *16*, 4561-4566.
- (63) Borisova, D.; Moehwald, H.; Shchukin, D. G.: Mesoporous Silica Nanoparticles for Active Corrosion Protection. *Acs Nano* **2011**, *5*, 1939-1946.
- (64) Hollamby, M. J.; Fix, D.; Doench, I.; Borisova, D.; Moehwald, H.; Shchukin, D.: Hybrid Polyester Coating Incorporating Functionalized Mesoporous Carriers for the Holistic Protection of Steel Surfaces. *Advanced Materials* **2011**, *23*, 1361-1365.
- (65) Kartsonakis, I.; Daniilidis, I.; Kordas, G.: Encapsulation of the corrosion inhibitor 8-hydroxyquinoline into ceria nanocontainers. *Journal of Sol-Gel Science and Technology* **2008**, *48*, 24-31.
- (66) Kartsonakis, I. A.; Danilidis, I. L.; Pappas, G. S.; Kordas, G.: Encapsulation and Release of Corrosion Inhibitors into Titania Nanocontainers. *Journal of Nanoscience and Nanotechnology* **2010**, *10*, 5912-5920.
- (67) Kartsonakis, I. A.; Kordas, G.: Synthesis and Characterization of Cerium Molybdate Nanocontainers and Their Inhibitor Complexes. *Journal of the American Ceramic Society* **2010**, *93*, 65-73.
- (68) Mekeridis, E. D.; Kartsonakis, I. A.; Pappas, G. S.; Kordas, G.: Release studies of corrosion inhibitors from cerium titanium oxide nanocontainers. *Journal of Nanoparticle Research* **2011**, *13*, 541-554.
- (69) Kartsonakis, I. A.; Balaskas, A. C.; Kordas, G. C.: Influence of cerium molybdate containers on the corrosion performance of epoxy coated aluminium alloys 2024-T3. *Corrosion Science* **2011**, *53*, 3771-3779.
- (70) Snihirova, D.; Lamaka, S. V.; Taryba, M.; Salak, A. N.; Kallip, S.; Zheludkevich, M. L.; Ferreira, M. G. S.; Motemor, M. F.: Hydroxyapatite Microparticles as Feedback-Active Reservoirs of Corrosion Inhibitors. *Acs Applied Materials & Interfaces* **2010**, *2*, 3011-3022.
- (71) Abdullayev, E.; Price, R.; Shchukin, D.; Lvov, Y.: Halloysite Tubes as Nanocontainers for Anticorrosion Coating with Benzotriazole. *Acs Applied Materials & Interfaces* **2009**, *1*, 1437-1443.

- (72) Fix, D.; Andreeva, D. V.; Lvov, Y. M.; Shchukin, D. G.; Moehwald, H.: Application of Inhibitor-Loaded Halloysite Nanotubes in Active Anti-Corrosive Coatings. *Advanced Functional Materials* **2009**, *19*, 1720-1727.
- (73) Lvov, Y.; Price, R.; Gaber, B.; Ichinose, I.: Thin film nanofabrication via layer-by-layer adsorption of tubule halloysite, spherical silica, proteins and polycations. *Colloids and Surfaces a-Physicochemical and Engineering Aspects* **2002**, *198*, 375-382.
- (74) Lvov, Y. M.; Shchukin, D. G.; Moehwald, H.; Price, R. R.: Halloysite clay nanotubes for controlled release of protective agents. *Acs Nano* **2008**, *2*, 814-820.
- (75) Shchukin, D. G.; Sukhorukov, G. B.; Price, R. R.; Lvov, Y. M.: Halloysite nanotubes as biomimetic nanoreactors. *Small* **2005**, *1*, 510-513.
- (76) Veerabadrán, N. G.; Mongayt, D.; Torchilin, V.; Price, R. R.; Lvov, Y. M.: Organized Shells on Clay Nanotubes for Controlled Release of Macromolecules. *Macromolecular Rapid Communications* **2009**, *30*, 99-103.
- (77) Luca, V.; Thomson, S.: Intercalation and polymerisation of aniline within a tubular aluminosilicate. *Journal of Materials Chemistry* **2000**, *10*, 2121-2126.
- (78) Shchukin, D. G.; Lamaka, S. V.; Yasakau, K. A.; Zheludkevich, M. L.; Ferreira, M. G. S.; Moehwald, H.: Active anticorrosion coatings with halloysite nanocontainers. *Journal of Physical Chemistry C* **2008**, *112*, 958-964.
- (79) Kuang, F.; Shi, T.; Wang, J.; Jia, F.: Microencapsulation technology for thiourea corrosion inhibitor. *Journal of Solid State Electrochemistry* **2009**, *13*, 1729-1735.
- (80) Park, J. H.; Kim, K. Y.; Park, J. M.: Polymer hollow particles: Encapsulation of phosphoric acid partial esters and morphology manipulation. *Polymer* **2010**, *51*, 3014-3022.
- (81) Haase, M. F.; Grigoriev, D.; Moehwald, H.; Tiersch, B.; Shchukin, D. G.: Encapsulation of Amphoteric Substances in a pH-Sensitive Pickering Emulsion. *Journal of Physical Chemistry C* **2010**, *114*, 17304-17310.
- (82) Szabo, T.; Molnar-Nagy, L.; Bogнар, J.; Nyikos, L.; Telegdi, J.: Self-healing microcapsules and slow release microspheres in paints. *Progress in Organic Coatings* **2011**, *72*, 52-57.
- (83) Mookhoek, S. D.: Novel routes to liquid-based self-healing polymer systems. *PhD thesis* **2010**.
- (84) Mao, S.; Xu, J.; Cai, C.; Germershaus, O.; Schaper, A.; Kissel, T.: Effect of WOW process parameters on morphology and burst release of FITC-dextran loaded PLGA microspheres. *International Journal of Pharmaceutics* **2007**, *334*, 137-148.
- (85) Sah, H.; Toddywala, R.; Chien, Y. W.: CONTINUOUS RELEASE OF PROTEINS FROM BIODEGRADABLE MICROCAPSULES AND IN-VIVO EVALUATION OF THEIR POTENTIAL AS A VACCINE ADJUVANT. *Journal of Controlled Release* **1995**, *35*, 137-144.
- (86) Sah, H. K.; Toddywala, R.; Chien, Y. W.: BIODEGRADABLE MICROCAPSULES PREPARED BY A W/O/W TECHNIQUE - EFFECTS OF SHEAR FORCE TO MAKE A PRIMARY W/O EMULSION ON THEIR MORPHOLOGY AND PROTEIN RELEASE. *Journal of Microencapsulation* **1995**, *12*, 59-69.
- (87) Youan, B. B. C.; Jackson, T. L.; Dickens, L.; Hernandez, C.; Owusu-Ababio, G.: Protein release profiles and morphology of biodegradable microcapsules containing an oily core. *Journal of Controlled Release* **2001**, *76*, 313-326.
- (88) Barat, A.; Ruskin, H. J.; Crane, M.: 3D multi-agent models for protein release from PLGA spherical particles with complex inner morphologies. *Theory in Biosciences* **2008**, *127*, 95-105.
- (89) Shulkin, A.; Stover, H. D. H.: Microcapsules from styrene-maleic anhydride copolymers: study of morphology and release behavior. *Journal of Membrane Science* **2002**, *209*, 433-444.

- (90) Dong, Z.; Ma, Y.; Hayat, K.; Jia, C.; Xia, S.; Zhang, X.: Morphology and release profile of microcapsules encapsulating peppermint oil by complex coacervation. *Journal of Food Engineering* **2011**, *104*, 455-460.
- (91) Cai, C.; Mao, S.; Germershaus, O.; Schaper, A.; Rytting, E.; Chen, D.; Kissel, T.: Influence of morphology and drug distribution on the release process of FITC-dextran-loaded microspheres prepared with different types of PLGA. *Journal of Microencapsulation* **2009**, *26*, 334-345.
- (92) Yow, H. N.; Routh, A. F.: Formation of liquid core-polymer shell microcapsules. *Soft Matter* **2006**, *2*, 940-949.
- (93) Barsoukov, E.; Macdonald, J. R.: *Impedance spectroscopy: theory, experiment, and applications*; Wiley-Interscience, 2005.
- (94) Antonietti, M.; Landfester, K.: Polyreactions in miniemulsions. *Progress in Polymer Science* **2002**, *27*, 689-757.
- (95) Mathiowitz, E.; Cohen, M. D.: POLYAMIDE MICROCAPSULES FOR CONTROLLED RELEASE .1. CHARACTERIZATION OF THE MEMBRANES. *Journal of Membrane Science* **1989**, *40*, 1-26.
- (96) Mathiowitz, E.; Cohen, M. D.: POLYAMIDE MICROCAPSULES FOR CONTROLLED RELEASE .2. RELEASE CHARACTERISTICS OF THE MICROCAPSULES. *Journal of Membrane Science* **1989**, *40*, 27-41.
- (97) Mathiowitz, E.; Cohen, M. D.: POLYAMIDE MICROCAPSULES FOR CONTROLLED RELEASE .5. PHOTOCHEMICAL RELEASE. *Journal of Membrane Science* **1989**, *40*, 67-86.
- (98) Mathiowitz, E.; Cohen, M. D.: POLYAMIDE MICROCAPSULES FOR CONTROLLED RELEASE .3. SPONTANEOUS RELEASE OF AZOBENZENE. *Journal of Membrane Science* **1989**, *40*, 43-54.
- (99) Mathiowitz, E.; Cohen, M. D.: POLYAMIDE MICROCAPSULES FOR CONTROLLED RELEASE .4. EFFECTS OF SWELLING. *Journal of Membrane Science* **1989**, *40*, 55-65.
- (100) Alexandridou, S.; Kiparissides, C.: PRODUCTION OF OIL-CONTAINING POLYTERTEREPHTHALAMIDE MICROCAPSULES BY INTERFACIAL POLYMERIZATION - AN EXPERIMENTAL INVESTIGATION OF THE EFFECT OF PROCESS VARIABLES ON THE MICROCAPSULE SIZE DISTRIBUTION. *Journal of Microencapsulation* **1994**, *11*, 603-614.
- (101) Alexandridou, S.; Kiparissides, C.; Mange, F.; Foissy, A.: Surface characterization of oil-containing polyterephthalamide microcapsules prepared by Interfacial polymerization. *Journal of Microencapsulation* **2001**, *18*, 767-781.
- (102) Toubeli, A.; Kiparissides, C.: Synthesis and characterization of polyterephthalamide membranes for encapsulation use: Effect of the amine type and composition on the membrane permeability. *Journal of Membrane Science* **1998**, *146*, 15-29.
- (103) Frere, W.; Danicher, L.; Gramain, P.: Preparation of polyurethane microcapsules by interfacial polycondensation. *European Polymer Journal* **1998**, *34*, 193-199.
- (104) Hong, K.; Park, S.: Preparation of polyurethane microcapsules with different soft segments and their characteristics. *Reactive & Functional Polymers* **1999**, *42*, 193-200.
- (105) Kim, I. H.; Seo, J. B.; Kim, Y. J.: Preparation and characterization of polyurethane microcapsules containing functional oil. *Polymer-Korea* **2002**, *26*, 400-409.
- (106) Kwon, J. Y.; Kim, H. D.: Preparation and application of polyurethane-urea microcapsules containing phase change materials. *Fibers and Polymers* **2006**, *7*, 12-19.
- (107) Su, J.-F.; Wang, L.-X.; Ren, L.; Huang, Z.; Meng, X.-W.: Preparation and characterization of polyurethane microcapsules containing n-octadecane with styrene-maleic

anhydride as a surfactant by interfacial polycondensation. *Journal of Applied Polymer Science* **2006**, *102*, 4996-5006.

(108) Suzuki, S.; Kondo, T.; Mason, S. G.: STUDIES ON MICROCAPSULES .I. PREPARATION OF POLYURETHANE AND POLYPHENOLESTER MICROCAPSULES. *Chemical & Pharmaceutical Bulletin* **1968**, *16*, 1629-&.

(109) Cho, J. S.; Kwon, A.; Cho, C. G.: Microencapsulation of octadecane as a phase-change material by interfacial polymerization in an emulsion system. *Colloid Polym. Sci.* **2002**, *280*, 260-266.

(110) Soto-Portas, M. L.; Argillier, J. F.; Mechin, F.; Zydowicz, N.: Preparation of oily core polyamide microcapsules via interfacial polycondensation. *Polymer International* **2003**, *52*, 522-527.

(111) Brown, E. N.; Kessler, M. R.; Sottos, N. R.; White, S. R.: In situ poly(urea-formaldehyde) microencapsulation of dicyclopentadiene. *Journal of Microencapsulation* **2003**, *20*, 719-730.

(112) Laguecir, A.; Louhaichi, M. R.; Burgard, M.: Influence of the monomers type on the morphology of polyamide microcapsules. *Current Drug Delivery* **2004**, *1*, 111-117.

(113) Persico, P.; Carfagna, C.; Danicher, L.; Frere, Y.: Polyamide microcapsules containing jojoba oil prepared by inter-facial polymerization. *Journal of Microencapsulation* **2005**, *22*, 471-486.

(114) Kim, M. D.; Iskakov, R. M.; Batyrbekov, E. O.; Zhubanov, B. A.; Perichaud, A.: Segmented polyurethane-based microparticles: Synthesis, properties, and isoniazid encapsulation and kinetics of release. *Polymer Science Series A* **2006**, *48*, 1257-1262.

(115) Janssen, L.; Boersma, A.; Tenijenhuis, K.: ENCAPSULATION BY INTERFACIAL POLYCONDENSATION .3. MICROENCAPSULATION, THE INFLUENCE OF PROCESS CONDITIONS ON WALL PERMEABILITY. *Journal of Membrane Science* **1993**, *79*, 11-26.

(116) Janssen, L.; Tenijenhuis, K.: ENCAPSULATION BY INTERFACIAL POLYCONDENSATION .1. THE CAPSULE PRODUCTION AND A MODEL FOR WALL GROWTH. *Journal of Membrane Science* **1992**, *65*, 59-68.

(117) Janssen, L.; Tenijenhuis, K.: ENCAPSULATION BY INTERFACIAL POLYCONDENSATION .2. THE MEMBRANE WALL STRUCTURE AND THE RATE OF THE WALL GROWTH. *Journal of Membrane Science* **1992**, *65*, 69-75.

(118) Torini, L.; Argillier, J. F.; Zydowicz, N.: Interfacial polycondensation encapsulation in miniemulsion. *Macromolecules* **2005**, *38*, 3225-3236.

(119) Johnsen, H.; Schmid, R. B.: Preparation of polyurethane nanocapsules by miniemulsion polyaddition. *Journal of Microencapsulation* **2007**, *24*, 731-742.

(120) Takahashi, T.; Taguchi, Y.; Tanaka, M.: Preparation of polyurea microcapsules containing pyrethroid insecticide with hexamethylene diisocyanate uretidione and isocyanurate. *Journal of Chemical Engineering of Japan* **2005**, *38*, 929-936.

(121) Li, G.; Feng, Y. Q.; Li, X. G.; Gao, P.; Wang, J.; Xie, J. Y.: Preparation and characterization of polyurea microcapsules containing colored electrophoretic responsive fluid. *Journal of Materials Science* **2007**, *42*, 4838-4844.

(122) Yang, J.; Keller, M. W.; Moore, J. S.; White, S. R.; Sottos, N. R.: Microencapsulation of Isocyanates for Self-Healing Polymers. *Macromolecules* **2008**, *41*, 9650-9655.

(123) Pascu, O.; Garcia-Valls, R.; Giamberini, M.: Interfacial polymerization of an epoxy resin and carboxylic acids for the synthesis of microcapsules. *Polymer International* **2008**, *57*, 995-1006.

(124) Zhang, H.; Wang, X.: Fabrication and performances of microencapsulated phase change materials based on n-octadecane core and resorcinol-modified melamine-

formaldehyde shell. *Colloids and Surfaces a-Physicochemical and Engineering Aspects* **2009**, *332*, 129-138.

(125) Essawy, H.; Tauer, K.: Polyamide capsules via soft templating with oil drops- I. Morphological studies of the capsule wall. *Colloid Polym. Sci.* **2010**, *288*, 317-331.

(126) Hong, K.; Park, S.: Characterization of ovalbumin-containing polyurethane microcapsules with different structures. *Polymer Testing* **2000**, *19*, 975-984.

(127) Crespy, D.; Stark, M.; Hoffmann-Richter, C.; Ziener, U.; Landfester, K.: Polymeric nanoreactors for hydrophilic reagents synthesized by interfacial polycondensation on miniemulsion droplets. *Macromolecules* **2007**, *40*, 3122-3135.

(128) HernandezBarajas, J.; Hunkeler, D.: Heterophase water-in-oil polymerization of acrylamide by a hybrid inverse-emulsion/inverse-microemulsion process. *Polymer* **1997**, *38*, 5623-5641.

(129) Shukla, P. G.; Sivaram, S.: Microencapsulation of the water-soluble pesticide Monocrotophos by an oil in oil interfacial polyaddition method. *Journal of Microencapsulation* **1999**, *16*, 517-521.

(130) Mueller, K.; Klapper, M.; Muellen, K.: Preparation of high molecular weight polyurethane particles by nonaqueous emulsion polyaddition. *Colloid Polym. Sci.* **2007**, *285*, 1157-1161.

(131) Klapper, M.; Nenov, S.; Haschick, R.; Mueller, K.; Muellen, K.: Oil-in-oil emulsions: A unique tool for the formation of polymer nanoparticles. *Accounts of Chemical Research* **2008**, *41*, 1190-1201.

(132) Kobaslija, M.; McQuade, D. T.: Polyurea microcapsules from oil-in-oil emulsions via interfacial polymerization. *Macromolecules* **2006**, *39*, 6371-6375.

(133) Shukla, P. G.; Kalidhass, B.; Shah, A.; Palaskar, D. V.: Preparation and characterization of microcapsules of water-soluble pesticide monocrotophos using polyurethane as carrier material. *Journal of Microencapsulation* **2002**, *19*, 293-304.

(134) Bouchemal, K.; Briancon, S.; Chaumont, P.; Fessi, H.; Zydowicz, N.: Microencapsulation of dehydroepiandrosterone (DHEA) with poly(ortho ester) polymers by interfacial polycondensation. *Journal of Microencapsulation* **2003**, *20*, 637-651.

(135) Matyjaszewski, K.; Gnanou, Y.; Leibler, L.: *Macromolecular engineering: precise synthesis, materials properties, applications. Elements of macromolecular structural control*; WILEY-VCH, 2007.

(136) Landfester, K.: Polyreactions in miniemulsions. *Macromolecular Rapid Communications* **2001**, *22*, 896-936.

(137) Dubey, R.; Shami, T. C.; Rao, K. U. B.; Yoon, H.; Varadan, V. K.: Synthesis of polyamide microcapsules and effect of critical point drying on physical aspect. *Smart Materials & Structures* **2009**, *18*.

(138) Flory, P. J.; Rehner, J.: Statistical mechanics of cross-linked polymer networks II Swelling. *Journal of Chemical Physics* **1943**, *11*, 521-526.

(139) Ulrich, H.: *Chemistry and technology of isocyanates*; J. Wiley & Sons, 1996.

(140) Patai, S.: *The chemistry of acyl halides*; Interscience, 1972.

(141) <http://www.hansen-solubility.com>.

(142) Flory, P. J.: PHASE EQUILIBRIA IN SOLUTIONS OF ROD-LIKE PARTICLES. *Proceedings of the Royal Society of London Series a-Mathematical and Physical Sciences* **1956**, *234*, 73-89.

(143) Flory, P. J.: Molecular size distribution in three dimensional polymers. I. Gelation. *Journal of the American Chemical Society* **1941**, *63*, 3083-3090.

(144) Favre, E.; Nguyen, Q. T.; Schaetzel, P.; Clement, R.; Neel, J.: SORPTION OF ORGANIC-SOLVENTS INTO DENSE SILICONE MEMBRANES .1. VALIDITY AND LIMITATIONS OF FLORY-HUGGINS AND RELATED THEORIES. *Journal of the Chemical Society-Faraday Transactions* **1993**, *89*, 4339-4346.

- (145) Hildebrand, J. H.: *Solubility of non-electrolytes*; Reinhold Pub. Corp., 1936.
- (146) Barton, A. F. M.: *CRC handbook of solubility parameters and other cohesion parameters*; CRC Press, 1991.
- (147) Hansen, C. M.: The Three Dimensional Solubility Parameter - Key to Paint Component Affinities I. - Solvents, Plasticizers, Polymers, and Resins. *J. Paint Techn.* **1967**, *39*, 104-117.
- (148) Hansen, C. M.: The Three Dimensional Solubility Parameter - Key to Paint Component Affinities II. - Dyes, Emulsifiers, Mutual Solubility and Compatibility, and Pigments. *J. Paint Techn.* **1967**, *39*, 505-510.
- (149) Hansen, C. M., and Skaarup, K.: The Three Dimensional Solubility Parameter - Key to Paint Component Affinities III. - Independent Calculation of the Parameter Components. *J. Paint Techn.* **1967**, *39*, 511-514.
- (150) Hansen, C. M.: Doctoral Dissertation, The Three Dimensional Solubility Parameter and Solvent Diffusion Coefficient, Their Importance in Surface Coating Formulation. *Danish Technical Press, Copenhagen* **1967**.
- (151) Hansen, C. M.: Hansen Solubility Parameters: A User's Handbook, Second Ed. *CRC Press, Boca Raton, FL* **2007**.
- (152) Plueddemann, E. P.: *Silane coupling agents*; Plenum Press, 1982.
- (153) Arkles, B.: Silane Coupling Agents: Connecting Across Boundaries. <http://www.gelest.com/goods/pdf/couplingagents.pdf>.
- (154) Child, T. F.; Van Ooij, W. J.: Application of silane technology to prevent corrosion of metals and improve paint adhesion. *Transactions of the Institute of Metal Finishing* **1999**, *77*, 64-70.
- (155) Franquet, A.; De Laet, J.; Schram, T.; Terryn, H.; Subramanian, V.; van Ooij, W. J.; Vereecken, J.: Determination of the thickness of thin silane films on aluminium surfaces by means of spectroscopic ellipsometry. *Thin Solid Films* **2001**, *384*, 37-45.
- (156) Franquet, A.; Le Pen, C.; Terryn, H.; Vereecken, J.: Effect of bath concentration and curing time on the structure of nonfunctional thin organosilane layers on aluminium. *Electrochimica Acta* **2003**, *48*, 1245-1255.
- (157) Hu, J.-M.; Liu, L.; Zhang, J.-Q.; Cao, C.-N.: Electrodeposition of silane films on aluminum alloys for corrosion protection. *Progress in Organic Coatings* **2007**, *58*, 265-271.
- (158) Subramanian, V.; van Ooij, W. J.: Silane based metal pretreatments as alternatives to chromating. *Surface Engineering* **1999**, *15*, 168-172.
- (159) Van Schaftinghen, T.; Le Pen, C.; Terryn, H.; Horzenberger, F.: Investigation of the barrier properties of silanes on cold rolled steel. *Electrochimica Acta* **2004**, *49*, 2997-3004.
- (160) Frignani, A.; Zucchi, F.; Trabanelli, G.; Grassi, V.: Protective action towards aluminium corrosion by silanes with a long aliphatic chain. *Corrosion Science* **2006**, *48*, 2258-2273.
- (161) Zucchi, F.; Frignani, A.; Grassi, V.; Balbo, A.; Trabanelli, G.: Organo-silane coatings for AZ31 magnesium alloy corrosion protection. *Materials Chemistry and Physics* **2008**, *110*, 263-268.
- (162) Zucchi, F.; Grassi, V.; Frignani, A.; Trabanelli, G.: Inhibition of copper corrosion by silane coatings. *Corrosion Science* **2004**, *46*, 2853-2865.
- (163) Latnikova, A.; Grigoriev, D. O.; Hartmann, J.; Moehwald, H.; Shchukin, D. G.: Polyfunctional active coatings with damage-triggered water-repelling effect. *Soft Matter* **2011**, *7*, 369-372.
- (164) Arenas, M. A.; Bethencourt, M.; Botana, F. J.; de Damborenea, J.; Marcos, M.: Inhibition of 5083 aluminium alloy and galvanised steel by lanthanide salts. *Corrosion Science* **2001**, *43*, 157-170.

- (165) Brunelli, K.; Dabala, M.; Calliari, I.; Magrini, M.: Effect of HCl pre-treatment on corrosion resistance of cerium-based conversion coatings on magnesium and magnesium alloys. *Corrosion Science* **2005**, *47*, 989-1000.
- (166) Dabala, M.; Armelao, L.; Buchberger, A.; Calliari, I.: Cerium-based conversion layers on aluminum alloys. *Applied Surface Science* **2001**, *172*, 312-322.
- (167) Fahrenholtz, W. G.; O'Keefe, M. J.; Zhou, H. F.; Grant, J. T.: Characterization of cerium-based conversion coatings for corrosion protection of aluminum alloys. *Surface & Coatings Technology* **2002**, *155*, 208-213.
- (168) Rudd, A. L.; Breslin, C. B.; Mansfeld, F.: The corrosion protection afforded by rare earth conversion coatings applied to magnesium. *Corrosion Science* **2000**, *42*, 275-288.
- (169) Deacon, G. B.; Forsyth, C. M.; Behrsing, T.; Konstas, K.; Forsyth, M.: Heterometallic Ce-III-Fe-III-salicylate networks: models for corrosion mitigation of steel surfaces by the 'Green' inhibitor, Ce(salicylate)(3). *Chemical Communications* **2002**, 2820-2821.
- (170) Hughes, A. E.; Ho, D.; Forsyth, M.; Hinton, B. R. W.: Towards replacement of chromate inhibitors by rare earth systems. *Corrosion Reviews* **2007**, *25*, 591-605.
- (171) Li, X.; Deng, S.; Mu, G.; Qu, Q.: The synergistic inhibition effect of rare earth cerium(IV) ion and iso-vanillin on the corrosion of cold rolled steel in 1.0 M H<sub>2</sub>SO<sub>4</sub> solution. *Materials Letters* **2007**, *61*, 2514-2517.
- (172) Birbilis, N.; Buchheit, R. G.; Ho, D. L.; Forsyth, M.: Inhibition of AA2024-T3 on a phase-by-phase basis using an environmentally benign inhibitor, cerium dibutyl phosphate. *Electrochemical and Solid State Letters* **2005**, *8*, C180-C183.
- (173) Blin, F.; Leary, S. G.; Wilson, K.; Deacon, G. B.; Junk, P. C.; Forsyth, M.: Corrosion mitigation of mild steel by new rare earth cinnamate compounds. *Journal of Applied Electrochemistry* **2004**, *34*, 591-599.
- (174) Markley, T. A.; Forsyth, M.; Hughes, A. E.: Corrosion protection of AA2024-T3 using rare earth diphenyl phosphates. *Electrochimica Acta* **2007**, *52*, 4024-4031.
- (175) Ho, D.; Brack, N.; Scully, J.; Markley, T.; Forsyth, M.; Hinton, B.: Cerium dibutylphosphate as a corrosion inhibitor for AA2024-T3 aluminum alloys. *Journal of the Electrochemical Society* **2006**, *153*, B392-B401.
- (176) Behrsing, T.: *Ph.D. Dissertation* **2003**, Monash University, School of Chemistry, Melbourne, Australia.
- (177) Yebra, D. M.; Kiil, S.; Dam-Johansen, K.: Antifouling technology - past, present and future steps towards efficient and environmentally friendly antifouling coatings. *Progress in Organic Coatings* **2004**, *50*, 75-104.
- (178) R. K. Shah, B. B. P. a. N. K. P.: Influence of Azoles as Corrosion Inhibitor towards 3003 Aluminium in Trichloroacetic Acid Solutions. *Werkstoffe und Korrosion* **10/1974**, *25. Jahrg. Heft*
- (179) Vora, J. C.; Makwana, S. C.; Koshel, K. C.; Potel, N. K.: Corrosion inhibitors for aluminium and its alloys in neutral media. *Materials and Corrosion* **1974**, *25*, 753-756.
- (180) Khaled, K. F.: Molecular simulation, quantum chemical calculations and electrochemical studies for inhibition of mild steel by triazoles. *Electrochimica Acta* **2008**, *53*, 3484-3492.
- (181) Abdel-Aal, M. S.; Morad, M. S.: Inhibiting effects of some quinolines and organic phosphonium compounds on corrosion of mild steel in 3M HCl solution and their adsorption characteristics. *British Corrosion Journal* **2001**, *36*, 253-260.
- (182) Tang, L. B.; Li, X. M.; Si, Y. S.; Mu, G.; Liu, G. H.: The synergistic inhibition between 8-hydroxyquinoline and chloride ion for the corrosion of cold rolled steel in 0.5 M sulfuric acid. *Materials Chemistry and Physics* **2006**, *95*, 29-38.

(183) Zheludkevich, M. L.; Yasakau, K. A.; Bastos, A. C.; Karavai, O.; Ferreira, M. G. S.: On the application of electrochemical impedance spectroscopy to study the self-healing properties of protective coatings. *Electrochemistry Communications* **2007**, *9*, 2622-2628.